POLITECNICO DI TORINO

Master's Degree in Civil Engineering

MASTER'S DEGREE THESIS

Nonlinear FEM Analysis of Prestressed Gerber Beam Bridges: Shear assessment of A Highway Infrastructure Case Study

Supervisor:

Prof. Marco Domaneschi

Co-supervisor:

PhD Candidate Leonardo Zunino

Candidate:

Lorenzo Foti

Thesis developed in collaboration with:

SINA S.p.A. (ASTM Group)

DECEMBER 2025 - A.Y. 2024/2025

Abstract

This thesis, developed in collaboration with SINA S.p.A. of the ASTM Group, investigates the structural adequacy of prestressed Gerber beam bridges constructed during Italy's 1970s highway infrastructure expansion. The research focuses on the critical shear assessment of girder beam end half-joints, which exhibit insufficient transverse reinforcement according to contemporary design standards. A comprehensive comparative analysis between 1970s design codes and current Italian technical standards (NTC2018, DM 578 - Linee Guida Ponti) reveals significant discrepancies in shear reinforcement requirements, with conventional verification procedures indicating substantial structural deficiencies for many existing bridges.

The study develops advanced nonlinear finite element methodologies using ANSYS software to accurately simulate the complex stress distribution patterns within these critical structural elements. This modeling approach is fully compliant with current Italian (NTC2018) and European (Eurocode 2) structural design codes, which explicitly permit nonlinear analysis methods for structural verification. Particular attention is devoted to disturbed regions (D-regions) where geometric discontinuities create stress concentrations, employing strut-and-tie modeling principles integrated within a sophisticated computational framework.

The local finite element model is validated through three stages: analytical verification using a simplified LUSAS model for global load distribution, an extended beam model investigating size effects and deep beam behavior, and an alternative boundary condition model verifying support reactions and crack patterns. Results demonstrate that nonlinear analysis, accounting for material plastic capacity and stress redistribution, confirms adequate shear structural capacity under design loads, contradicting deficiencies predicted by conventional linear elastic assessments. The findings suggest that many bridges flagged for strengthening may possess sufficient structural capacity, supporting development of optimized assessment procedures that could substantially reduce strengthening interventions and enable more cost-effective infrastructure management strategies.

Contents

Chapter 1

Introduction

1.1 Overview of 20th century Italian infrastructures

Italy, a country renowned for its rich historical and architectural heritage, also possesses an extensive network of reinforced concrete (RC) bridges that serve as crucial links within its national infrastructure. These structures play a fundamental role in connecting regions, supporting transportation, and facilitating economic development. However, over time, prolonged exposure to harsh environmental conditions has led to significant structural deterioration in many of these bridges. Common issues include cracking, material degradation, and a progressive reduction in load-carrying capacity [1]. Starting in the 1950s, Italian transportation culture underwent a radical shift from a train-based system to one centered around cars. This transformation was driven by political strategies that strongly favored public works, promoting road expansion and improvement with the goal of creating a more modern, connected, and faster nation. In fact, between 1926 and 1950, over 13,000 kilometers of roads were built. One of the most iconic achievements of this era was the construction of the Autostrada del Sole in 1964, a landmark national highway stretching 755 kilometers and linking Milan, Bologna, Florence, Rome, and Naples.

Figure 1.1: Italian Highway: Autostrada del Sole

Italy's diverse and complex geography put the creativity and daring of engineers and builders to the test. The route had to cross varying terrains, from the flat plains of the north, through the Apennine mountain range, and into the rolling green hills of Tuscany. The segment between Bologna and Florence alone spans 90 kilometers and includes 67 bridges and viaducts, along with 24 tunnels. To accelerate construction through the challenging Apennine section, each company was assigned a single lot, allowing multiple firms to work simultaneously. In total, 27 different designers contributed to this stretch, resulting in a rich variety of structural solutions: bridges and viaducts made from steel, reinforced concrete, prestressed concrete, and composite materials [2]. Each bridge represents a unique prototype, shaped by its specific boundary conditions, material selection, construction methodology, and traffic loads. The service life expectancy established in design codes serves as a probabilistic reference for load evaluation and structural detailing aimed at enhancing durability but does not necessarily correspond to the actual lifespan of the infrastructure. Italy's rich infrastructure heritage includes Roman bridges, medieval structures, and steel and reinforced concrete bridges over a century old, all main-

tained in excellent condition, demonstrating that longevity depends on consistent evolutionary design aligned with realistic loads and boundary conditions, systematic maintenance throughout the structure's lifecycle, and continuous monitoring to ensure compatibility between actual and designed loads. Contemporary infrastructure development faces the challenge of cost reduction while maintaining safety standards, creating sustainability requirements but also introducing hidden risks such as inadequate assessment of boundary conditions, underestimation of applied loads, poor attention to critical details like rainwater drainage, deficient construction practices, and insufficient long-term maintenance. A fundamental distinction exists between ancient and modern structural approaches: historical bridges relied exclusively on compression stress flows, eliminating tensile reinforcement and inherently providing greater durability, while modern engineering exploits steel's tensile capacity to achieve more ambitious geometries. In steel structures, profiles can be effectively protected through systematic painting programs, making maintenance straightforward and visible, whereas reinforced and prestressed concrete structures embed steel reinforcement within concrete's alkaline environment, theoretically reducing maintenance requirements but creating vulnerabilities where reinforcement is hidden from inspection, local exposure to aggressive agents requires specialized treatment, and the protective concrete environment can be compromised without visible warning signs .

Figure 1.2: Bridges and viaducts maintained by RFI: several typologies made of masonry, r/c, p/c and steel

[3]

The major risk associated with cement-based structures was significantly amplified during Italy's economic boom period when construction knowledge was limited, and while this knowledge gap has largely been addressed today, its legacy persists in existing infrastructure. The contrasting conditions of roadway and railway bridges in Italy illustrate the importance of systematic maintenance practices, as the superior condition of railway bridges results from long-term adherence to structured maintenance protocols, while problems observed in roadway bridges stem from the absence of such systematic approaches, emphasizing that durability design must be coupled with meticulous construction detailing, rigorous quality control, comprehensive maintenance manuals, and clear identification of critical monitoring points throughout the structure's lifecycle [3].

Figure 1.3: Different structural damages in (a) Typical PRC viaduct, (b) steel span of a viaduct and (c) circular piers with cap beam.

[4]

1.2 Bridges with half-joint Gerber beams

European countries feature extensive infrastructure networks, predominantly constructed during the 1960s and 1970s. During this era, prefabrication processes were gaining success, with reinforced and prestressed concrete decks becoming one of the most widely adopted and researched bridge typologies. However, the design and construction practices of that period quickly became outdated, while understanding of detailing effects significantly improved. A particularly common structural element was the half-joint, valued for its prefabrication advantages and strategic importance. The rapid post-World War II growth period drove the design and construction of most European infrastructure networks. Half-joints were frequently employed in reinforced concrete structures during this time, consisting of reduced beam ends (Gerber joints) supported by complementary half-joints or pier caps, forming suspended spans or Gerber beams. These suspended spans were popular due to their straightforward prefabrication process and optimized stress distribution resulting from a static structural scheme that remained insensitive to differential settlement and thermal variations. Nevertheless, the geometry of these joints leads to accelerated material deterioration, including premature corrosion and concrete spalling, with the most severely damaged areas remaining inaccessible for visual inspection. Water and de-icing salts from road surfaces can easily penetrate the nib and accumulate within the supporting half-joint. These inherent characteristics of half-joints compromise their reliability and generate skepticism when assessments must comply with current codes and loading requirements [5]. Gerber beams capitalize on the advantages of both systems: joints permit rotations and can be modelled as hinges, strategically positioned at points where bending moments are zero. This creates a simply supported static scheme with the moment distribution characteristics of a continuous beam. Joint forces consist of horizontal and vertical reactions, with minimal bending moments.

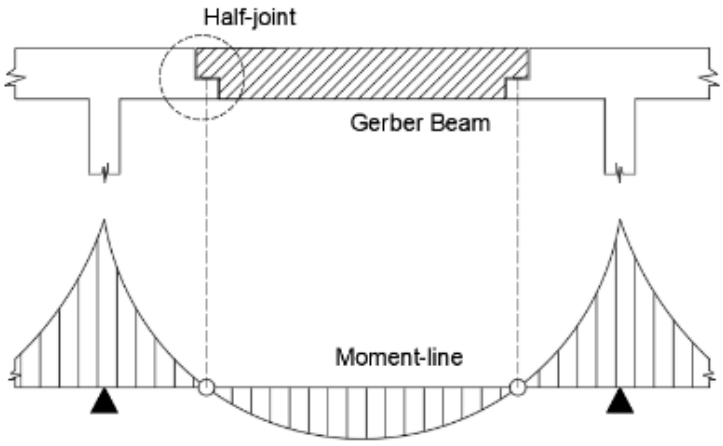

Figure 1.4: Half-joint element in a Gerber beam and its bending moment distribution under service load configuration [6]

However, the joint geometry itself presents several critical disadvantages that require consideration and resolution:

- Inspections are impossible in the most problematic joint regions where water readily infiltrates and accumulates, increasing vulnerability to chloride-induced corrosion from road surface sealant seepage.
- Reinforcement layouts in existing joints lack standardized configurations, exhibiting numerous geometric variations.

This diversity complicates efforts to establish uniform assessment criteria or identify critical joint regions. On one hand, there exists non-compliance with current standards and questionable design and construction practices. On the other hand, problems affect all structures, including those with sound design principles: traffic loads have increased beyond 1960s reference values, many existing structures approach end-of-life, and environmental effects cause inevitable material degradation. Consequently, control and maintenance planning for an enormous number of elements becomes increasingly urgent. Technologies, theories, and strategies must be updated and adapted to address current structural problems, ensuring adequate monitoring and repair programs while preventing catastrophic failures [7] [8]. Furthermore, design codes specifically addressing half-joint dimensioning were neither available nor universally recognized, resulting in existing elements with varying re-

inforcement configurations and design assumptions. Some researches demonstrated that reinforcement layout directly influences crack patterns at the Ultimate Limit State:

• When reinforcement includes diagonal, horizontal, and vertical bars in both the nib and adjacent areas, critical cracks develop within the nib's interior, accompanied by distributed secondary cracks throughout the beam.

• With reinforcement limited to inclined and vertical bars, critical cracks cut subvertically through the nib.

• When reinforcement consists only of vertical and horizontal bars, structural failure occurs with minimal deformation.

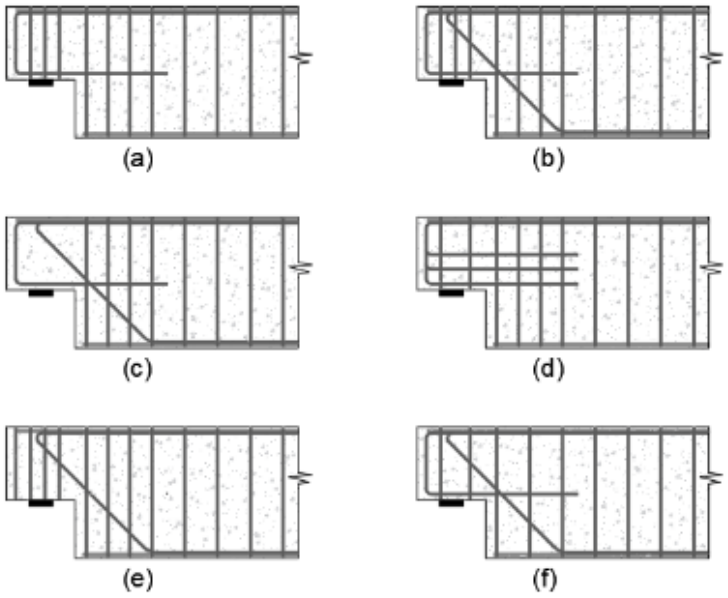

Figure 1.5: Different reinfrocements' layouts for half-joints elements

Several test campaigns confirmed that inclined reinforcement proves highly effective for crack control. The selection of structural scheme directly influences stress magnitudes and sensitivity to actions such as differential settlements or thermal variations. Simply supported schemes enable straightforward force calculations for individual elements and do not generate internal forces from settlements and thermal variations. However, mid-span moments are higher compared to continuous beams, which redistribute moments to the supports. The final moment distribution in continuous beams, depending on span count, approaches that of a beam fixed at

both ends. While continuous beams achieve superior moment distribution, they are intolerant of differential settlements or thermal variations, causing beam deflection and additional internal stresses [5].

1.2.1 Collapse of Polcevera viaduct

One of the most significant bridge collapses in modern engineering history, which has profoundly marked the contemporary infrastructure landscape, is that of the Polcevera Viaduct (Morandi Bridge) that occurred on August 14, 2018, in Genoa. This dramatic event, involving a viaduct characterized by the use of Gerber systems for connections between the main cable-stayed structure and adjacent spans, has catalyzed the attention of the international scientific community and constituted a fundamental turning point for regulatory evolution in the infrastructure sector. The collapse has indeed accelerated the implementation of new guidelines for risk classification and management of existing bridges, leading to significant modifications in inspection protocols, monitoring procedures, and structural safety assessment at both national and European levels. The viaduct over the Polcevera Valley in Genoa, Italy, constructed between 1963 and 1967, was a 1100-meter-long, 18-meter-wide structure supported by twelve intermediate piers positioned between two end abutments. The bridge's distinctive design featured three balanced cable-stayed systems to span the Polcevera River and two railway lines, each consisting of 90-meter-tall A-shaped concrete towers connected to the main girder extremities through prestressed concrete stays, with the deck elevated approximately 45 meters above the river level.

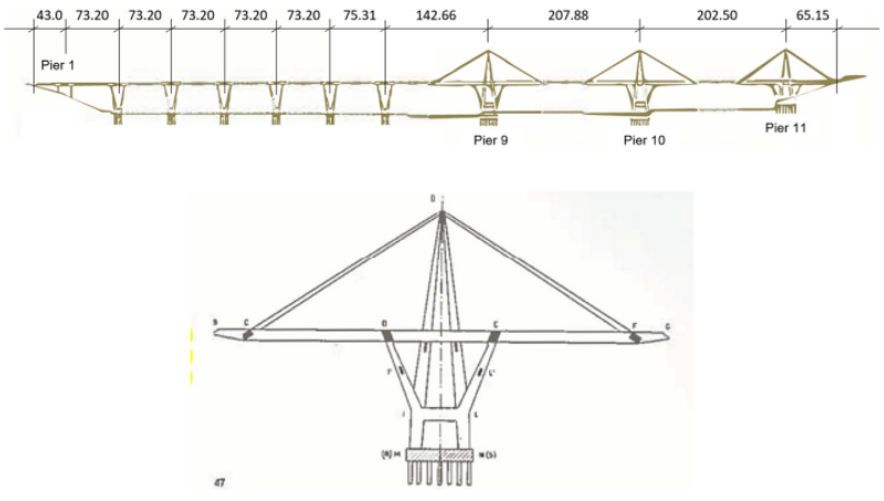

Figure 1.6: Polcevera Viaduct Layout and Pier 9 detail

Over its operational lifespan, the four-lane bridge experienced significant traffic growth, from an initial daily count of 20,000 vehicles to 150,000 vehicles during its final years of service. On August 14, 2018, Pier #9 catastrophically failed, causing a 250-meter section of the deck to collapse into the river and railway infrastructure below, with the only significant loading at the time of failure being a 44-ton truck passing near the failed pier. The collapse resulted in forty-three fatalities and nine injuries among motorists and municipal waste company workers operating beneath the bridge, while displacing six hundred residents from nearby homes. Although comprehensive structural assessments were conducted following the collapse, critical deterioration had been documented decades earlier through visual inspections performed between 1991 and 1992 on stays in Piers #9 and #11, which revealed that most ducts lacked the grout injection intended during construction, extensive strand corrosion was present, and several cables exhibited loose strands. Inspections of Pier #11 stays at the tower summit indicated severely deteriorated strands with significant corrosion, numerous broken elements, and missing grout injection, conditions that were confirmed to have further deteriorated during subsequent 2015 inspections. Dynamic testing of the balanced systems in 2017 revealed asymmetric response patterns in the mode shapes, indicating structural irregularities that prompted the development of a maintenance program scheduled for 2017, which included retrofitting the stays in Piers #9 and #10 using external cable reinforcement similar to previous interventions on Pier #11, but the bridge collapsed before these critical repairs could be implemented [9]. After this event, the Superior Council of Public Works, as part of the Italian Ministry of Infrastructure and Transport (MIT) developed specific Guidelines on risk classification and management, safety assessment and the monitoring of existing bridges (LG20). The Guidelines were approved as a technical code through the Ministry of Infrastructure Decree n. 578 (17 December 2020) which is examined in depth in the next chapter.These guidelines aimed to define and standardize the criteria for monitoring, assessing structural safety, and classifying the risk of existing bridges through a multi-risk approach. The Guidelines LG20 can be considered a specialized standard, in agreement with the provisions of the Standards for Construction (NTC 2018) and Application Circular (Circolare 2019), conceived to consider the bridge vulnerability, the environmental hazards (e.g., seismic, landslide, flooding), and the exposure (e.g., traffic loads, etc.)

to evaluate the infrastructural risk. The guidelines aim at a quick identification of the road infrastructure to prioritize for intervention to be performed, thus ensuring savings in terms of human, economic, and time resources. On the other hand, Italian bridges are owned and managed by various local and national bodies that use in-house management systems with different levels of complexity [4].

Chapter 2

Evolution of Bridge Design Standards

The design and construction of Italy's highway infrastructure during the 1960s and early 1970s represented a pivotal period in the nation's civil engineering history, driven by ambitious economic growth and the massive expansion of the Autostrada network. This era was characterized by innovative structural solutions and rapid construction methodologies that successfully created the backbone of Italy's modern transportation system. However, the structural assessment of aging infrastructure has revealed significant discrepancies between historical design practices and contemporary safety requirements, particularly regarding shear reinforcement provisions in critical structural elements such as Gerber beam half-joints. This chapter presents a comprehensive comparative analysis between the design standards employed during the original construction period and the current Italian Technical Standards for Construction (NTC2018), supplemented by the recent Guidelines for Risk Classification and Management, Safety Assessment and Monitoring of Existing Bridges (DM 578 17/12/20). The development of these new guidelines was significantly accelerated following the catastrophic collapse of the Polcevera Viaduct in Genoa in August 2018, which highlighted the urgent need for systematic assessment and management protocols for Italy's aging bridge infrastructure. The evolution of design philosophies, load specifications, and reinforcement detailing requirements over the past

five decades has created a challenging scenario where numerous existing structures, despite being structurally sound under their original design criteria, no longer satisfy contemporary verification procedures. Understanding this regulatory evolution is essential for developing appropriate assessment methodologies and intervention strategies that balance structural safety with the practical constraints of managing Italy's extensive highway bridge inventory, enabling infrastructure owners to make informed decisions regarding maintenance, strengthening, or replacement of critical structural elements.

2.1 Current Regulatory Framework: Bridge Assessment Guidelines DM 578/2020

[10]The Guideline outlines a procedure for the safety management of existing bridges, with the objective of preventing unacceptable levels of damage and maintaining risk within acceptable thresholds. It is structured into three main parts, dealing respectively with the inventory and risk classification of bridges, the assessment of structural safety, and the surveillance and monitoring of existing bridges and viaducts (hereinafter referred to simply as "bridges" or "structures"). The term "bridge" refers to any structure with an overall span greater than 6.0 meters, designed to span a depression in the terrain or an obstacle such as a river, body of water, canal, transportation route, or any other natural or artificial discontinuity. The document illustrates how risk classification — or more precisely, the assignment of an "attention class" — fits into a general multi-level approach. This begins with the basic inventory of infrastructure and leads, where applicable under the proposed methodology, to a full structural safety assessment. The results of this classification process and the subsequent evaluations serve as valuable input for any later assessment of the transport system's resilience. The guideline goes into detail on the necessary methodologies to apply this approach across the territory. These include the systematic collection of data on existing structures, the execution of initial and in-depth inspections aimed at producing defect reports, and the evaluation of the attention class based on relevant risks. These risks may be structural (including static and foundation-related aspects), seismic, or hydrogeological (such as hydraulic events or landslides). Initially, each type of risk is analyzed separately in terms of hazard, vul-

nerability, and exposure. They are then combined into a single general classification expressed by the attention class. Within this framework, the document provides the tools needed to understand the condition of bridges at the territorial scale and to define priorities for surveillance, monitoring, verification, or intervention. For structures with spans shorter than 6.0 meters, it is the responsibility of the infrastructure owner or operator to determine the appropriate methods and inspection intervals, based on the specific characteristics of the structures and the surrounding area. Finally, given the broad applicability of its principles and general rules, the methodology presented in this guideline can be applied to both road and railway bridges. The use of a multilevel approach for managing existing bridges is justified by the vast number of infrastructure assets across the Italian territory. The complexity and cost of inspections, investigations, controls, monitoring, and verifications are calibrated each time —approximately and qualitatively —based on the actual condition and urgency of each structure, leading to a consistent and uniform method for determining the attention class across various types of infrastructure. This multilevel approach combines broad, rapid territorial assessments, such as census activities, inspections, and classification, with more in-depth, site-specific evaluations focused on individual structures. Starting with a reasoned census based on the collection of as much information as possible and structured visual inspections, the attention class of each bridge is determined, guiding the type and depth of any subsequent assessments. The approach comprises six levels of increasing complexity and detail:

• Level 0 involves compiling an inventory of all structures and their main characteristics based on the available documentation.
• Level 1, applied to bridges identified in Level 0, includes direct visual inspections and rapid surveys of structural, geomorphological, and hydraulic characteristics, to assess degradation and potential risks such as landslides or hydrodynamic actions.
• Level 2 leads to the definition of the attention class based on the hazard, vulnerability, and exposure parameters derived from the previous levels. Depending on the outcome, the process continues with higher levels.
• Level 3 involves preliminary evaluations to determine whether more detailed assessments (level 4) are required, based on the type and extent of damage observed in level 1.
• Level 4 includes comprehensive evaluations that follow the current Technical Stan-

dards for Construction.

• Level 5, not explicitly addressed in these guidelines, applies to strategically significant bridges within the network and includes advanced analyses such as resilience assessments of the transportation network, considering socio-economic consequences of potential bridge outages, with reference to authoritative international sources.

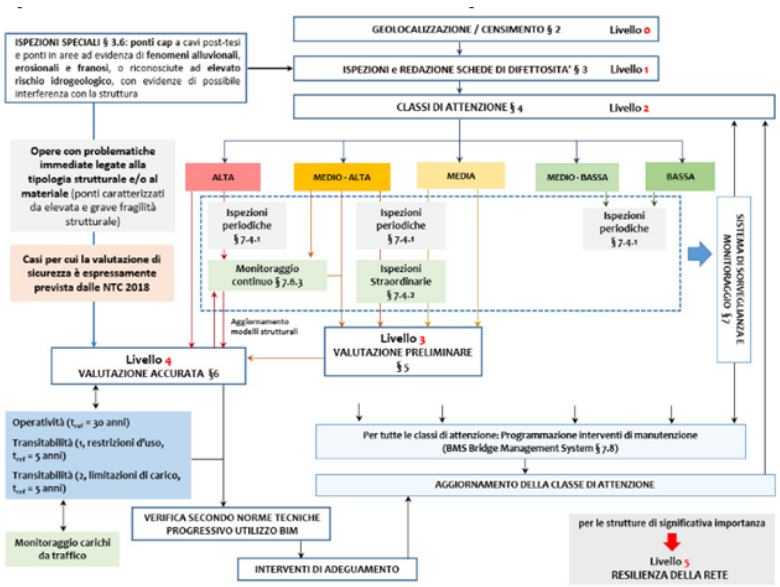

Figure 2.1: Multi-levels approach and relations between analysis levels

As the process moves from Level 0 to Level 5, the complexity, detail, and cost of investigations increase, while the number of structures assessed and the uncertainty of results decrease. The core of this approach is Level 2, the definition of the Attention Class (CdA), which is determined based on hazard, vulnerability, and exposure, and categorized as high, medium-high, medium, medium-low, or low. Each class corresponds to specific actions in terms of inspections, monitoring, and verifications. High-CdA bridges require immediate detailed evaluations, potentially including geotechnical and structural analyses (Level 4), periodic ordinary and, if necessary, extraordinary inspections, and the installation of continuous or periodic monitoring systems. For medium-high class bridges, preliminary evaluations (Level 3), ordinary inspections, and, if necessary, extraordinary inspections and monitoring are required, with the potential for Level 4 evaluations depending on observed damage. Medium class bridges follow a similar path, with additional inspections and

potential upgrades to medium-high or high class based on findings. Medium-low and low class bridges require only frequent or regular inspections, respectively, without further evaluations unless future inspections indicate otherwise. Regardless of the CdA, all bridges must undergo essential maintenance identified through inspections, in addition to scheduled maintenance. Moreover, the Attention Class must be re-evaluated following periodic inspections, monitoring results, or interventions, and at least every two years for bridges in the medium and medium-high categories. Bridges in the high class must always undergo Level 4 evaluations and any necessary resulting interventions. Knowledge of the structure represents a crucial step in understanding the actual behavior of the construction, considering its construction history, degradation phenomena, and any transformations undergone over the years. The primary objective of the cognitive process is to reduce uncertainties related to load assessment, material and structural behavior, thereby achieving appropriate knowledge levels commensurate with the required verifications. To this end, progressive levels of knowledge deepening, investigation, and verification are defined, as outlined in the Explanatory Circular. Information on construction details and material properties can be obtained through successive investigative campaigns, each characterized by increasing detail and planned based on indications derived from preliminary safety assessments that enable identification of critical issues and development of various investigation plans. The deepening of investigations based on results obtained from preliminary verifications allows for organic and critical enhancement of knowledge, focusing attention where necessary. This progressive investigation approach ensures the development of structural models characterized by increasing accuracy and consequently enables more reliable safety assessments that better represent the actual structural behavior of the structure, as well as the appropriately justified use of confidence factors and partial factors that are progressively reduced where possible. In this regard, reference is made to section 2.5.2 of NTC 2018:

"In the case of variable actions characterized by extreme value distributions dependent on time, the characteristic value is assumed to be that characterized by an assigned return period. For environmental actions (snow, wind, temperature) the return period is set equal to 50 years, corresponding to a 2% annual probability of exceedance; for traffic actions on road bridges the return period is conventionally assumed equal to 1000 years." Therefore, the characteristic value of traffic load, which

must be further amplified for Ultimate Limit State calculations, should have a 1000-year return period; this value, provided that traffic monitoring is implemented, may be subject to reduction, except for providing adequate verifications at the end of residual life and adopting consequent measures, including, as a last resort in extreme cases, decommissioning and replacement. For the purposes of these Guidelines, the following definitions are established:

1) ADEQUATE, an existing bridge for which verifications performed according to Technical Standards using the loads and partial factors specified therein are satisfied. The only permitted reduction is that of the partial factor relating to permanent loads, provided the hypotheses are verified as specified in § 8.5.5 of the Technical Standards.

2) OPERATIONAL, a bridge for which verifications performed using principles set forth in the Technical Standards are satisfied, but with reference to a reduced time horizon in evaluating partial factors relating to loads and materials. The reference time value, conventionally assumed at an indicative level in these Guidelines, is equal to 30 years. In calculating the partial factor relating to permanent loads, the reduction provided for in § 8.5.5 of the Technical Standards may obviously still be applied, provided the hypotheses are verified. The bridge and verification results must therefore be reported in regional and national institutional databases.

3) TRANSITIONAL, a bridge for which verifications performed over a reduced time horizon are satisfied, within which adaptation or operational works are designed and implemented, adopting measures: (a) "limitation of permitted loads" or (b) "restriction of bridge use." Detailed temporal programming of works must be known and transferred to regional and national institutional databases. In evaluating partial factors relating to loads and materials, a reduced reference time is adopted, which in these Guidelines is assumed not greater than 5 years. In calculating the partial factor relating to permanent loads, the reduction provided for in § 8.5.5 of the Technical Standards may obviously still be applied, provided the hypotheses are verified. Knowledge of the bridge's history represents an indispensable element, both for current safety assessment and for defining interventions and predicting their effectiveness. The cognitive pathway comprises diverse and strictly interconnected activities to be performed with successive levels of deepening to optimize, both quantitatively and in terms of costs and time, direct interaction with the struc-

ture. These activities include historical-critical analysis, original project analysis, surveying (geometric-structural, construction details, crack patterns and damage), geological-technical site characterization, and investigations aimed at characterizing construction details and materials. As previously stated, assessments are conducted at multiple levels, depending on the purpose for which they are required and to optimize the subsequent decision-making process regarding measures and interventions to be undertaken. The Table 2.2 provides, for clarity of presentation, a summary of analysis levels to be performed and fundamental parameters.

	Obiettivi	Carichi da traffico	t_{ref}
COMPLETA ADEGUATEZZA **Valutazione del livello di sicurezza secondo le norme attuali (NTC 2018)**	Valutazione del livello di sicurezza strutturale, sismico e idraulico (alluvioni e frane) come previsto dalle NTC 2018, con eventuale riduzione fattori parziali carichi permanenti	Schemi convenzionali previsti dalle NTC 2018	Vita nominale (V_N) come da NTC 2018
Se il livello di sicurezza strutturale (statica/geotecnica) è insufficiente rispetto alle NTC			
OPERATIVITA'	Valutazione del livello di sicurezza strutturale con t_{ref} ridotto e fattori parziali ridotti	Schemi da NTC 2018, con fattori parziali ridotti	30 anni
TRANSITABILITA' NTC 2018 (Immediata transitabilità 1)	Valutazione del livello di sicurezza strutturale con t_{ref} ulteriormente ridotto imponendo restrizioni all'uso del ponte e fattori parziali ridotti	Schemi da NTC 2018, con restrizioni di uso e fattori parziali ridotti	5 anni
TRANSITABILITA' CdS • **PESANTE** • **INTERMEDIA** • **LEGGERA** • **AUTOVEICOLI** **(Immediata transitabilità 2)**	Valutazione del livello di sicurezza strutturale con t_{ref} ulteriormente ridotto, imponendo limitazione dei carichi secondo CdS e con relativi fattori parziali ridotti	Schemi da CdS con relativi fattori parziali ridotti	5 anni

Figure 2.2: Analysis levels for different assessment goals

2.2 Historical Design Code: Italian Road Bridges in the 1960s

[11]The evolution of Italian standards for road bridge design from 1960 to the present represents a paradigmatic shift in design philosophy. The standards in force during the 1960s, based on the Circular of the Ministry of Public Works of February 14, 1962, and the subsequent Circular No. 6736 of July 19, 1967, were founded on the allowable stress method and a deterministic approach to load schemes. The design approach of that era provided for the classification of roads into two categories (1st category for civil and military loads, 2nd category for civil loads only) and the use of rigidly codified load schemes: indefinite columns of 12-ton trucks, 18-ton road rollers, military loads up to 74.5 tons, and distributed crowd loads of 400 kg/m^2. For what concerns the "global" effects, in order to evaluate the stress conditions of the beams, the analysis is usually carried out through two types of checks:

b1) global bending moment acting on the deck;

b2) global bending moment (and shear) acting on the most stressed beam, usually the edge one, obtained in the case of validity of the hypothesis of infinitely rigid crossbeams, with the classical Courbon's formula.

In fact, only recently have decks and beams begun to be designed and built, with increasing frequency, with only end crossbeams and without intermediate crossbeams (for which Courbon's distribution is no longer valid).

For the preliminary assessments' purposes, it is possible to rely on the tables of the considered Code, since the calculation approach prescribed by the standards over time has always remained essentially the same, namely:

- the convetional width of each "load lane" is specified (this term, adopted by the current code, is used here for immediate clarity);
- on the deck, starting from the curb or sidewalk, one or more "load lanes" are arranged, placing the most severe load with maximum eccentricity, compatibly with the width of the carriageway (although the various codes prescribe a minimum number of load lanes to be considered as a function of carriageway

width);

- in addition, when more severe load effects are required for the structural element under consideration, the effect of a compact crowd load is applied to one or both sidewalks.

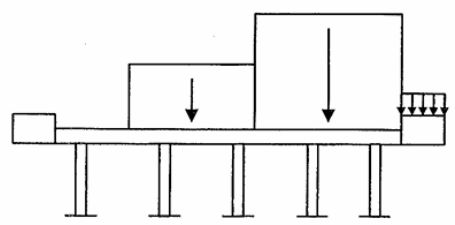

Figure 2.3: Load configurations in the transverse section

It is therefore always a matter, for the purpose of evaluating the stress level of the cross-section of the entire deck and of the individual beams, of assessing the effects of one or more load lanes on the significant sections. The simplest static scheme, which we will now examine, is that of the simply supported beam.

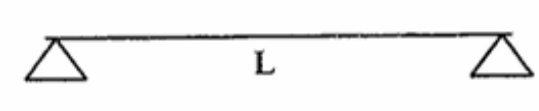

Figure 2.4: Simply supported scheme adopted

For a simply supported beam, it is well known that the following values must be investigated:

- $M_{\max}$ at midspan ($x = L/2$)
- $T_{\max}$ at the support ($x = 0$)

The tables reported in the code allow a rapid determination of these values (according to the various codes) and therefore a quick comparison.

First, the "global" values acting on the complete cross-section of the deck are derived, with a simple Courbon distribution (for the sake of the designer, although Courbon's formula is not repeated in this article). Then, the stresses relevant to each individual beam are evaluated.

Two tables have been compiled, for each standard that has appeared over time:

a) $M_{\max}$ $(x = L/2)$

b) $T_{\max}$ $(x = 0)$

Circolare N. 384 del 14-2-62 del Min. LLPP

Max Mf ad x=L/2 (mezzeria) in travi appoggiate - effetto di una singola colonna di carico (valori in ton x m)

	valori senza Φ					valori con Φ				
Lc =	Φ =	Schema I civ	Schema II civ	Schema V mil	Schema VI mil	Φ =	Schema I civ	Schema II civ	Schema V mil	Schema VI mil
10,0	1,000	28,0	36,5	–,–	90,1	1,338	37,5	48,8	–,–	120,6
12,0	1,000	38,0	45,4	–,–	117,4	1,325	50,4	60,1	–,–	155,5
14,0	1,000	52,0	54,3	–,–	145,4	1,313	68,3	71,3	–,–	190,9
16,0	1,000	68,0	–,–	–,–	176,7	1,302	88,5	–,–	–,–	229,9
18,0	1,000	84,5	–,–	–,–	210,4	1,290	109,0	–,–	–,–	271,4
20,0	1,000	104,0	–,–	–,–	244,3	1,278	132,9	–,–	–,–	312,3
22,0	1,000	124,0	–,–	–,–	278,3	1,267	157,1	–,–	–,–	352,5
24,0	1,000	146,0	–,–	–,–	314,1	1,256	183,3	–,–	–,–	394,4
26,0	1,000	172,0	–,–	355,7	–,–	1,244	214,0	–,–	442,7	–,–
28,0	1,000	200,0	–,–	405,7	–,–	1,234	246,7	–,–	500,4	–,–
30,0	1,000	228,5	–,–	463,9	–,–	1,223	279,4	–,–	567,2	–,–
32,0	1,000	260,0	–,–	524,6	–,–	1,212	315,1	–,–	635,9	–,–
34,0	1,000	292,0	–,–	594,8	–,–	1,202	350,9	–,–	714,7	–,–
36,0	1,000	326,0	–,–	671,8	–,–	1,191	388,4	–,–	800,3	–,–
38,0	1,000	364,0	–,–	751,5	–,–	1,181	430,0	–,–	887,8	–,–
40,0	1,000	404,0	–,–	821,3	–,–	1,171	473,3	–,–	962,1	–,–
42,0	1,000	444,0	–,–	903,7	–,–	1,162	515,8	–,–	1049,9	–,–
44,0	1,000	488,0	–,–	993,7	–,–	1,152	562,3	–,–	1144,9	–,–
46,0	1,000	532,0	–,–	1084,0	–,–	1,143	608,0	–,–	1238,9	–,–
48,0	1,000	578,0	–,–	1179,2	–,–	1,134	655,4	–,–	1337,1	–,–
50,0	1,000	628,0	–,–	1289,4	–,–	1,125	706,5	–,–	1450,5	–,–
52,0	1,000	680,0	–,–	1392,9	–,–	1,116	759,1	–,–	1554,9	–,–
54,0	1,000	732,5	–,–	1504,6	–,–	1,108	811,6	–,–	1667,0	–,–
56,0	1,000	788,0	–,–	1607,1	–,–	1,100	866,6	–,–	1767,5	–,–
58,0	1,000	844,0	–,–	1722,3	–,–	1,092	921,5	–,–	1880,5	–,–
60,0	1,000	902,0	–,–	1843,3	–,–	1,084	978,0	–,–	1998,5	–,–
		Largh. 3.00	Largh. 3.00	Largh. 3.50	Largh. 3.50		Largh. 3.00	Largh. 3.00	Largh. 3.50	Largh. 3.50

Figure 2.5: Maximum Bending Moment table from Circular of the Ministry of Public Works of February 14, 1962

Circolare N. 384 del 14-2-62 del Min. LLPP

Max T ad x=0 (appoggio) in travi appoggiate - effetto di una singola colonna di carico (valori in ton x m)

	valori senza Φ					valori con Φ				
Lc =	Φ =	Schema I civ	Schema II civ	Schema V mil	Schema VI mil	Φ =	Schema I civ	Schema II civ	Schema V mil	Schema VI mil
10,0	1,000	14,4	16,2	–,–	44,4	1,338	19,3	21,7	–,–	59,3
12,0	1,000	16,0	16,5	–,–	48,5	1,325	21,2	21,9	–,–	64,2
14,0	1,000	18,3	–,–	–,–	51,5	1,313	24,0	–,–	–,–	67,7
16,0	1,000	20,3	–,–	–,–	54,4	1,302	26,4	–,–	–,–	70,8
18,0	1,000	22,0	–,–	–,–	56,6	1,290	28,4	–,–	–,–	73,0
20,0	1,000	24,2	–,–	–,–	58,4	1,278	30,9	–,–	–,–	74,7
22,0	1,000	26,2	–,–	–,–	59,9	1,267	33,2	–,–	–,–	75,8
24,0	1,000	28,0	–,–	–,–	61,1	1,256	35,2	–,–	–,–	76,7
26,0	1,000	30,2	–,–	–,–	62,1	1,244	37,5	–,–	–,–	77,3
28,0	1,000	32,1	–,–	65,7	–,–	1,234	39,6	–,–	81,0	–,–
30,0	1,000	34,0	–,–	69,8	–,–	1,223	41,6	–,–	85,3	–,–
32,0	1,000	36,1	–,–	73,6	–,–	1,212	43,8	–,–	89,2	–,–
34,0	1,000	38,1	–,–	77,6	–,–	1,202	45,8	–,–	93,3	–,–
36,0	1,000	40,0	–,–	82,0	–,–	1,191	47,7	–,–	97,7	–,–
38,0	1,000	42,1	–,–	86,1	–,–	1,181	49,7	–,–	101,7	–,–
40,0	1,000	44,1	–,–	89,9	–,–	1,171	51,7	–,–	105,3	–,–
42,0	1,000	46,0	–,–	94,0	–,–	1,162	53,4	–,–	109,2	–,–
44,0	1,000	48,1	–,–	98,3	–,–	1,152	55,4	–,–	113,3	–,–
46,0	1,000	50,1	–,–	102,4	–,–	1,143	57,2	–,–	117,0	–,–
48,0	1,000	52,0	–,–	106,3	–,–	1,134	59,0	–,–	120,5	–,–
50,0	1,000	54,1	–,–	110,4	–,–	1,125	60,8	–,–	124,2	–,–
52,0	1,000	56,1	–,–	114,7	–,–	1,116	62,6	–,–	128,1	–,–
54,0	1,000	58,0	–,–	118,8	–,–	1,108	64,3	–,–	131,6	–,–
56,0	1,000	60,1	–,–	122,7	–,–	1,100	66,1	–,–	134,9	–,–
58,0	1,000	62,1	–,–	126,8	–,–	1,092	67,8	–,–	138,5	–,–
60,0	1,000	64,0	–,–	131,1	–,–	1,084	69,4	–,–	142,1	–,–
		Largh. 3.00	Largh. 3.00	Largh. 3.50	Largh. 3.50		Largh. 3.00	Largh. 3.00	Largh. 3.50	Largh. 3.50

Figure 2.6: Maximum Shear table from Circular of the Ministry of Public Works of February 14, 1962

Each table refers to the case of a simply supported beam of span L, and the values (maximum M and maximum T) are expressed in meters and tons, as a function of the load lane configuration considered by each standard.

To facilitate comparison of the data, the conventional width of the load lanes is also shown in the table headings.

To allow an immediate check, the values of $M_{\max}$ (or $T_{\max}$) are reported in two different ways:

- First, without the amplification due to the dynamic coefficient ϕ, i.e. with $\phi = 1.00$
- Second, including the dynamic coefficient ϕ prescribed by the relevant standard.

In fact, all the successive codes have specified the dynamic coefficient ϕ in function of the span length; only the 1980 standard (in force from 1980 to 1991) expressed ϕ as a function of the ratio G/Q between permanent and live loads of the structural element under examination. For practical use, in this case, a tabulation of $M_{\max}$

and $T_{\max}$ was prepared in the two limiting cases:

$$a)\ G/Q = 1$$
$$b)\ G/Q = 2$$

The dynamic coefficient was calculated using a deterministic formula:

$$\phi = \frac{100 - L}{100 - (250 - L)} \quad \text{for } L \leq 100 \text{ m} \tag{2.1}$$

$$\phi = 1.00 \quad \text{for } L > 100 \text{ m} \tag{2.2}$$

where L is the span length in meters.

2.3 Evolution of Italian Road Bridge Design Standards from 1960 to Present

The method proposed in the '60s was focused on the principle that the maximum service stresses in materials do not exceed predetermined values, defined as a fraction of the characteristic strength of the material itself, typically through the application of global safety factors. The epochal transition to contemporary standards, culminating with the NTC 2018 (Italian Technical Standards for Construction), introduced a complete methodological revision through the adoption of the Limit States Method (ULS - Ultimate Limit States and SLS - Serviceability Limit States). This transition, which found its definitive affirmation in the Technical Standards for Construction of 2008 and subsequent revisions, involved the complete elimination of any residual reference to the allowable stress method. The new design philosophy is based on a probabilistic approach that separately considers the variability of actions and material resistance through partial safety factors, allowing for a more refined and realistic evaluation of structural behavior. The NTC 2018, in Chapter 5 specifically dedicated to bridges, also introduced more stringent criteria for durability, seismic risk assessment, and infrastructure lifecycle management aspects that were marginally considered or completely absent in the 1960s standards. This regulatory evolution reflects not only progress in scientific and technological

knowledge but also greater awareness of the importance of infrastructure safety and the need for more sophisticated design criteria to meet contemporary challenges in transportation and sustainability. The shift from deterministic load schemes with fixed values to probabilistic traffic load models represents a fundamental advancement in engineering practice, moving from an empirical-deterministic approach to a scientific-probabilistic one. Furthermore, current standards also allow the use of strut-and-tie modeling for the verification of shear-critical elements, as highlighted in the following chapters.

2.4 Regulatory Framework for Nonlinear Finite Element Analysis

The use of advanced methodologies based on nonlinear finite element analysis for structural assessment is explicitly recognized and authorized by current Italian and European structural design codes. Both the Italian Technical Standards for Construction (NTC2018) and Eurocode 2 (EN 1992-1-1) recognize and permit the use of nonlinear analysis methods for structural verification, provided that fundamental mechanical principles and appropriate material characterization are properly implemented.

The Italian Technical Standards for Construction (NTC2018) provide explicit authorization for nonlinear analysis in Section 4.1.1.3, which states: *"L'analisi non lineare può essere usata per valutare gli effetti di azioni statiche e dinamiche, sia per gli stati limite di esercizio, sia per gli stati limite ultimi, a condizione che siano soddisfatti l'equilibrio e la congruenza. Al materiale si può attribuire un diagramma tensioni-deformazioni che ne rappresenti adeguatamente il comportamento reale, verificando che le sezioni dove si localizzano le plasticizzazioni siano in grado di sopportare allo stato limite ultimo tutte le deformazioni non elastiche derivanti dall'analisi, tenendo in appropriata considerazione le incertezze. Nell'analisi si trascurano gli effetti di precedenti applicazioni del carico e si assume un incremento monotono dell'intensità delle azioni e la costanza del rapporto tra le loro intensità. L'analisi può essere del primo o del secondo ordine."* This provision establishes that nonlinear analysis may be employed to evaluate the effects of static and dynamic actions for both serviceability and ultimate limit states, provided that equilibrium and compatibility are

satisfied. The code specifies that materials may be assigned stress-strain diagrams that adequately represent their actual behavior, and that sections where plasticization occurs must be capable of sustaining all inelastic deformations resulting from the analysis at the ultimate limit state, with appropriate consideration of uncertainties. The analysis should neglect the effects of previous load applications and assume a monotonic increase in action intensity with constant proportions between their intensities.

Eurocode 2 (EN 1992-1-1), which serves as the fundamental reference for reinforced and prestressed concrete design throughout Europe, provides comprehensive guidance for nonlinear analysis in Section 5.7. The standard explicitly states: *"Nonlinear methods of analysis may be used for both ULS and SLS, provided that equilibrium and compatibility are satisfied and an adequate non-linear behaviour for materials is assumed. The analysis may be first or second order."* Furthermore, Eurocode 2 specifies that *"at the ultimate limit state, the ability of local critical sections to withstand any inelastic deformations implied by the analysis should be checked, taking appropriate account of uncertainties."* The code also recognizes that *"for structures predominantly subjected to static loads, the effects of previous applications of loading may generally be ignored, and a monotonic increase of the intensity of the actions may be assumed,"* which corresponds to standard loading protocols for nonlinear analysis. Regarding material characterization, Section 3.1.5 of Eurocode 2 provides flexibility in the selection of stress-strain relationships, stating that *"other idealised stress-strain relations may be applied, if they adequately represent the behaviour of the concrete considered."* This provision supports the implementation of specialized constitutive models that incorporate material nonlinearities such as cracking and crushing capabilities, representing realistic approximations of actual material behavior under complex stress states.

Therefore, both regulatory frameworks provide a solid foundation and explicit authorization for the implementation of nonlinear finite element analysis as a code-compliant methodology for the structural assessment of critical elements in existing concrete structures.

Chapter 3

Literature Review: Modeling and Analysis of Gerber Beam Half-Joints

The structural analysis and design of Gerber beam half-joints have been the subject of extensive research and development over several decades, reflecting the complexity of these critical structural elements and their widespread use in bridge construction during the mid-20th century. The peculiar geometry of half-joints, characterized by abrupt cross-sectional variations and the concentration of support reactions in reduced beam sections, creates complex stress distributions that defy conventional beam theory assumptions and require specialized analytical approaches. Among the various modeling methodologies that have been developed and refined over the years, ranging from simplified empirical formulations to sophisticated finite element analyses, the strut-and-tie model has emerged as the predominant approach for both historical design practice and contemporary assessment procedures. This preference stems from the method's ability to provide a rational, mechanics-based representation of the internal load-carrying mechanisms within discontinuity regions, where traditional sectional analysis methods fail to capture the true structural behavior. The strut-and-tie approach has proven particularly effective for half-joint analysis

because it explicitly accounts for the three-dimensional stress fields that develop in these geometrically complex regions, providing engineers with both physical insight into structural behavior and practical design tools. This chapter presents a comprehensive review of the evolution of Gerber beam half-joint modeling approaches, tracing the development from early empirical methods through the establishment of strut-and-tie methodology as the standard practice, and examining current advances in computational modeling that continue to build upon this fundamental framework. The review encompasses both theoretical developments and experimental validation studies that have shaped our understanding of half-joint behavior and established the foundation for current design and assessment practices.

3.1 Strut and Tie Modeling

The field of structural concrete design has undergone remarkable theoretical and practical developments throughout the past century. The strut-and-tie model has emerged as a fundamental methodology for addressing complex structural challenges, with contemporary researchers and practitioners universally acknowledging the truss model as the rational and scientifically sound foundation for designing cracked reinforced concrete beams subjected to bending, shear, and torsion loads. This widespread acceptance stems from decades of theoretical development and practical validation that have demonstrated the model's effectiveness in capturing the essential load-carrying mechanisms of reinforced concrete structures [12]. Strut-and-tie models (S&T - Strut and Tie) are utilized for designing reinforced concrete members that cannot be schematized as solid beams or "beams" following Saint Venant's principle for foundation behavior. This applies not only to concentrated load zones but also to slender beam regions subject to concentrated loads or characterized by abrupt cross-sectional variations. The model consists of recognizing a reticular trajectory with ties and struts, namely tensioned and compressed members, representing the resistant structural mechanism. Figure 10.1 shows one of these reticular mechanisms with reference to a wall beam. This concept is already found at the end of the 19th century and early 20th century in Ritter-Mörsch's trajectory (3.1) for designing trusses in reinforced concrete and subsequently adopted by Schlaich's school, which extensively applied it to designing all "stocky" reinforced

concrete members.

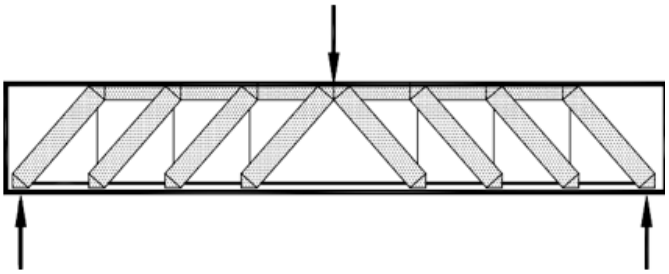

Figure 3.1: Ritter-Morsch truss

Compressed members (struts) are materialized by concrete, while tensioned members (ties) are constituted by reinforcement. According to EC2, strut-and-tie models can be utilized for designing structures with ultimate limit state or with "discontinuity" zones. Continuity regions are indicated as "B" regions (from "Bernoulli" or from the English "beam") and are constituted by those zones of beams and slabs where Bernoulli's hypothesis is satisfied. In the resistant stressed state, these are materialized by tensioned members (current reinforcement and wall reinforcement) and compressed members (current compression or inclined concrete struts). Discontinuity regions are instead characterized by the presence of static or geometric discontinuities ("D" regions, from the English "discontinuity"), where Bernoulli's hypothesis is not satisfied. Static discontinuities include the presence of concentrated loads, support zones, prestressing force introduction zones, etc., while geometric discontinuities include abrupt cross-sectional variations or axis direction changes, presence of openings, stocky elements (corbels, wall beams, Gerber half-joint beams, etc.). Once any distributed loads are replaced with equivalent concentrated loads, designing a reinforced concrete member using the S&T method consists of schematizing the stress field present in the structural element through a reticular truss of straight members in equilibrium with external loads. The curvatures of isostatic lines are concentrated at points called nodes, which represent the intersections of member axes with those of other members, with applied loads, or with support reactions. Once the truss geometry is defined, normal forces in the members are calculated, steel reinforcement is designed, and resistance verification of struts and nodes is performed. The S&T technique falls within plastic analysis methods for reinforced

concrete structures and can particularly be viewed as an application of the first theorem of limit analysis (lower bound theorem or static theorem). This theorem can be stated as follows: if the stress distribution within a structure satisfies all equilibrium conditions (internal and external) and does not violate the material resistance condition (plasticity condition), then the load associated with such distribution does not exceed the collapse load. Limit analysis can be applied to reinforced concrete structures only if they are sufficiently ductile. For example, in a frame structure, member sections must have sufficient rotation capacity to allow formation of all plastic hinges where the limit analysis model predicts them, therefore section collapse must occur through flexure with reinforcement in the plastic range. Conversely, limit analysis is not applicable to a frame whose sections collapse in shear or through flexure with concrete crushing and reinforcement in the elastic range or slightly above the elastic threshold. Similarly, the geometry of an S&T model must be chosen so that all truss members can reach their design resistance without premature failure of a member or node. "D" regions are located at static discontinuities (concentrated loads) and geometric discontinuities (such as abrupt axis line variations). Their extent can be determined by applying Saint Venant's postulate, according to which at sufficient distance from the area where external loads are applied, the stress state does not depend on the particular distribution of these loads, but only on the resultant and resulting moment. The distance at which this condition can be considered satisfied is approximately equal to the larger dimension of the loaded area.

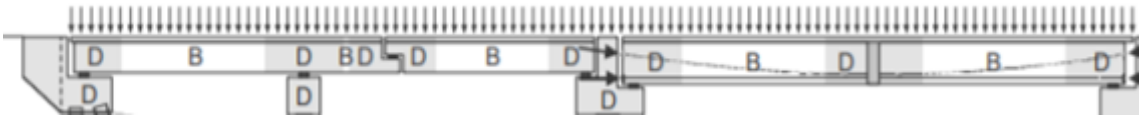

Figure 3.2: Polcevera Viaduct D and B regions

This rule is approximate; moreover, it serves only as a qualitative tool for identifying "D" regions and for subsequent development of the strut-and-tie model. If the element under examination is stocky (e.g., a wall beam with span not exceeding twice the height, fig. 10.4a), the discontinuity region coincides with the element itself.

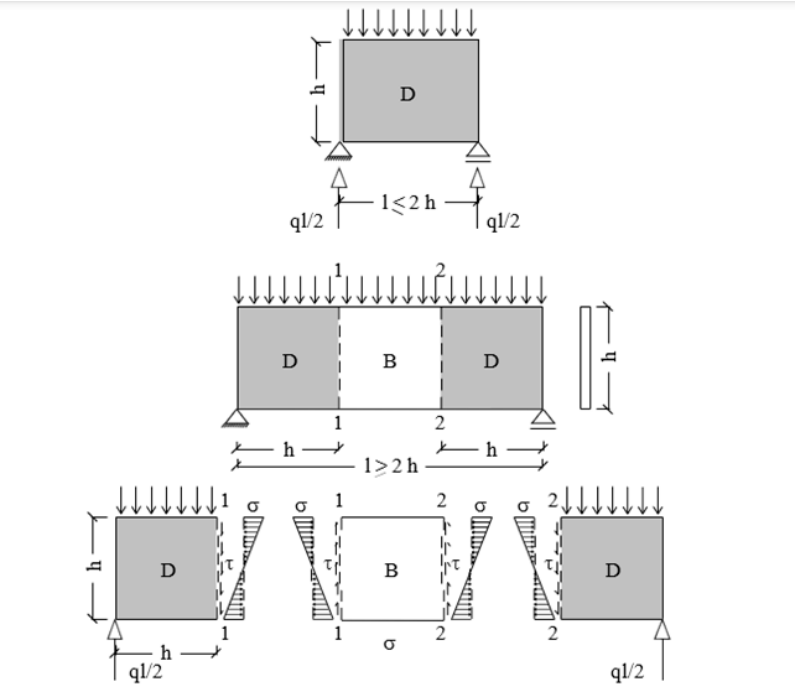

Figure 3.3: Determination of boundary forces for a D-region

In particular, for beams with high depth ($l \leq 2h$) the forces at the boundary coincide with the external loads and with the support reactions, while for low-rise beams ($l > 2h$) the forces at the edge of the "D" regions at the interface with the "B" region are given by the resultant moment and the resultant shear force in the extreme sections 1-1 and 2-2 of the "B" region [13].

3.1.1 Application to Half-Joint Design

The first step in modeling a half-joint is to clearly distinguish between the regions affected by the discontinuity and those where stress distribution follows classical beam theory. The disturbed region, known as the D-region, is directly influenced by the geometric discontinuity and extends vertically through the entire depth of the beam measured from the full cross-section beyond the nib. In contrast, the B-region is located sufficiently far from the source of disturbance and is characterized by regular stress distribution where the Bernoulli hypothesis remains valid [14].

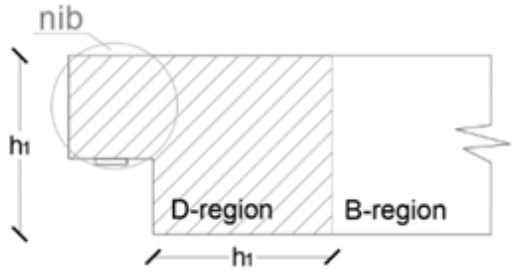

Figure 3.4: Example of D and B regions in an half-joint element

This subdivision is crucial for correctly applying the strut-and-tie model, as it allows the designer to treat the B-region using standard sectional analysis methods while applying a rational and mechanics-based approach in the D-region to capture complex stress flow and ensure structural safety. The two regions are typically defined based on the beam depth, following Saint-Venant's principle, with B-regions analyzed using conventional sectional properties and applied forces, while D-regions require the specialized strut-and-tie approach. For a strut-and-tie model to provide a valid lower bound solution, two key conditions must be satisfied. First, the model must maintain equilibrium with external loads, and second, internal forces in struts and ties must not exceed design strengths, assuming plastic behavior of materials. Any configuration satisfying these conditions, while allowing sufficient ductility to redistribute stresses from elastic to plastic states, represents a safe lower bound estimate of structural strength [6]. The areas of Gerber half-joints requiring focused attention during inspections must be identified based on failure mechanisms and their associated crack patterns.

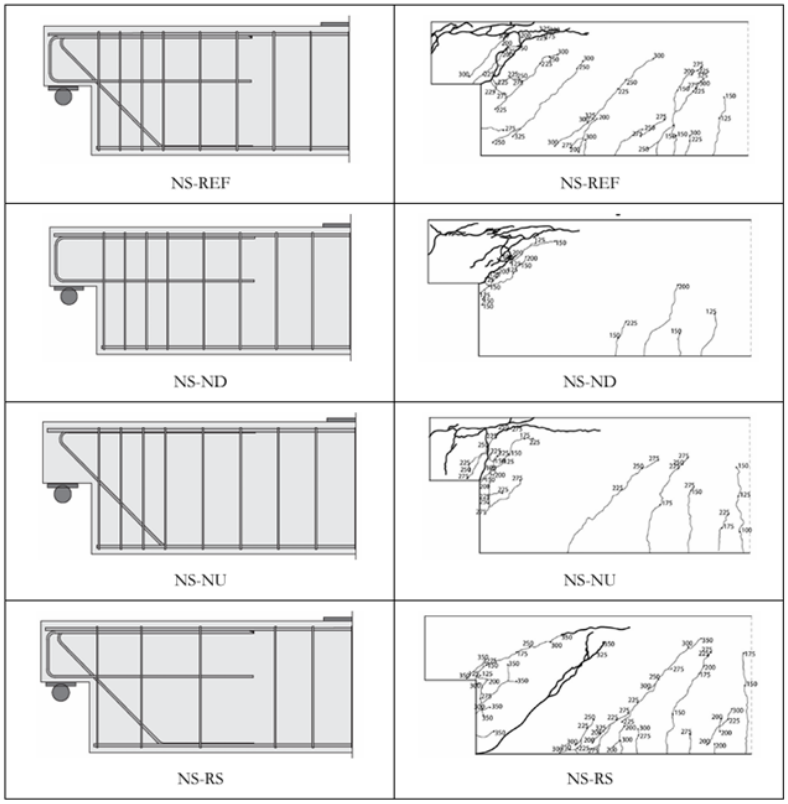

Figure 3.5: Common failure cracking patterns for half-joints elements

Figure 3.5 presents typical crack patterns at failure for non-prestressed Gerber half-joints, derived from experimental studies by Desnerck et al. (2016). The figure displays a comparative analysis where the left column shows the reinforcement configurations of tested half-joints, while the right column presents the corresponding crack patterns observed at failure during experimental testing. The baseline configuration, designated NS-REF, represents the reference design that would result from proper design practices consistent with the guidelines. The additional configurations were derived by systematically removing specific reinforcement elements from this reference case. The NS-ND configuration eliminates diagonal reinforcement, NS-NU removes the U-shaped bar at the support, and NS-RS reduces stirrups at the half-joint extremity. The experimental results reveal distinct failure modes characterized by critical cracks shown in bold that ultimately determine structural failure. For configurations NS-REF, NS-ND, and NS-NU, the critical crack patterns show remarkable similarity, developing horizontally along the upper edge of the half-joint and diagonally originating from the corner at the half-joint recess. A notable vari-

ation occurs in the NS-NU case, where the critical diagonal crack becomes nearly sub-vertical, accompanied by an additional vertical critical crack at the support location. Regarding non-critical secondary cracks, the NS-REF configuration exhibits more extensive and widespread diagonal cracking compared to the modified configurations, indicating better stress distribution through proper reinforcement detailing. The NS-RS configuration demonstrates a fundamentally different failure mechanism, exhibiting classic shear failure characteristics with diagonal cracks extending throughout the entire beam height, extensive and widespread diagonal cracking, and a critical diagonal crack initiating from the lower edge of the half-joint. However, it should be emphasized that the information presented in Figure3.5 and the accompanying analysis exclusively pertains to the load-bearing behavior of an originally intact Gerber half-joint. This represents a fundamental limitation in the applicability of these findings to real-world inspection scenarios. Consequently, various deterioration processes, such as reinforcement corrosion, can significantly modify the considerations presented here and therefore alter the crack patterns that may be encountered during actual inspections. Deterioration processes can fundamentally change the structural behavior by reducing effective cross-sectional area of reinforcing bars due to corrosion, altering bond characteristics between concrete and steel, creating new stress concentrations around corroded areas, and weakening concrete through expansive corrosion products. In deteriorated structures, crack patterns may deviate significantly from those observed in intact specimens because premature failure may occur in areas with severe reinforcement degradation, new crack initiation points may develop at locations of maximum deterioration, load redistribution changes due to reduced member capacity in affected zones, and secondary effects such as spalling and delamination may influence crack propagation. Understanding these failure patterns enables inspectors to focus their efforts on the zones most likely to exhibit distress, thereby improving the effectiveness of structural condition assessments. However, this limitation necessitates a comprehensive inspection approach that uses the intact structure crack patterns as a baseline reference rather than definitive guidance, incorporates deterioration assessment to identify areas of potential weakness, considers modified failure modes that may result from various deterioration mechanisms, and adapts inspection focus based on observed condition rather than solely on theoretical crack patterns. While the experimental crack pat-

terns provide valuable insight into fundamental structural behavior, inspectors must exercise professional judgment in applying this knowledge to aged or deteriorated structures, recognizing that actual crack development may differ substantially from the idealized cases presented [15]. The non-uniqueness of valid solutions is actually a strength of the method, as it allows designers to adapt models based on structural geometry, reinforcement detailing, and practical constraints while maintaining safety and consistency within a rigorous theoretical framework. This flexibility enables engineers to optimize designs for specific conditions and requirements. Often, the Gerber beam incorporates anchoring systems for precompression cables, whose forces constitute a component of the action and constraint system that must be considered when verifying the half-joint (Figure 3.1). Once the precompression action has been estimated in accordance with §4.1.2.5.3 of NTC2018, it must be incorporated into the Gerber half-joint verification scheme as it produces, for example, a vertical component that reduces the acting shear force. In the absence of precise evaluations regarding residual precompression, the contribution of precompression in the tie-strut mechanisms developed within the Gerber half-joint verification scheme may be conservatively neglected.

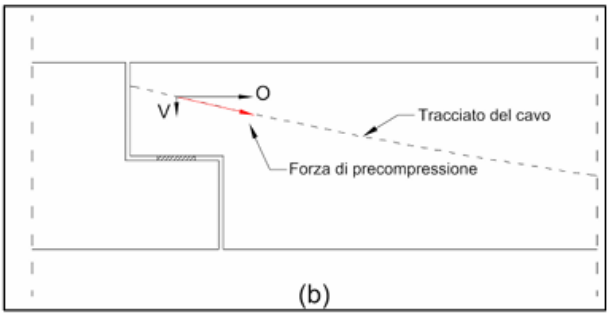

Figure 3.6: Decomposition of the prestressing action into vertical and horizontal components.

3.1.2 Structural Elements in Strut-and-Tie Models: Dual Model Approach

Resistance verifications for stocky Gerber half-joints can be conducted using the strut-and-tie method as suggested in section 10.9.4.6 of EC2-1-1 and in compliance with the indications provided in section 4.1.2.3.7 of NTC2018. The verification of the stocky half-joint can be performed using a simplified approach where the effect of precompression introduction and diffusion is treated separately from that of the bearing reaction introduction. When this approach is utilized, local verifications related to precompression introduction must be preliminarily performed, followed by those related to reaction introduction according to the models illustrated below. Obviously, the reinforcement necessary to satisfy verifications related to precompression introduction cannot be considered in models relating to reaction introduction. It should be noted that while in post-tensioning cases, precompression introduction can significantly increase the half-joint's capacity, in bonded cable precompression cases, due to the length of the section required to transfer precompression action from cables to the beam, the precompression effect may have little impact on half-joint capacity. When the precompression effect is neglected for verifying reaction introduction in the stocky half-joint, one can follow the suggestions of EC2-1-1 §10.9.4.6 and Schlaich & Schäfer (1991) using either of the two schemes shown in figures 3.7 and 3.8 or a combination of both. This approach can also be used in the absence of precompression.

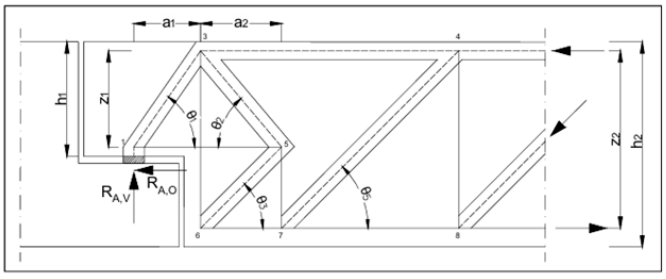

Figure 3.7: A scheme type

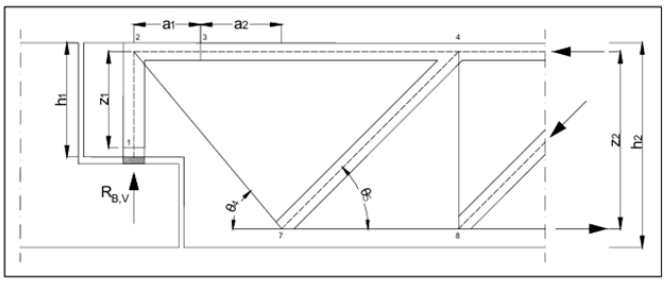

Figure 3.8: B scheme type

In the cited figures, struts are indicated with dashed lines while ties are shown with continuous lines. It should be noted that in some cases, depending on the direction of R and its magnitude relative to R, some struts in the figure 3.7 scheme might become ties. In these cases, this scheme must be appropriately adapted so that ties are consistent with the present reinforcement. The position of forces in the right section of the schemes in figures 3.7 and 3.8 is obtained from resolving the B region through classical beam theory. For correct utilization of strut-and-tie schemes in Gerber half-joint verification, knowledge of the reinforcement geometry present in the half-joint is fundamentally important. The overall vertical reaction $R_v = RA_v + RB_v$ to be divided between the two schemes in figures 3.7 and 3.8 depends on the present reinforcement. Generally, dividing the vertical reaction into parts such that $R_{B,v} \geq 0.5R_{A,v}$ ensures the best serviceability limit state behavior (i.e., limiting crack number and width) and guarantees satisfaction of strut-and-tie model compatibility conditions. Once the assumptions for using the two strut-and-tie schemes are defined and justified, it becomes possible to determine the forces acting in struts and ties. The value of angle θ_5 must equal that assumed for compressed members in shear verifications and therefore respect the limit values prescribed by NTC2018 for such verifications. Instead, the inclination angles of other compressed struts (i.e., θ_1, θ_2, θ_3) must be between 25° and 65° (cf. Muttoni et al. 1997, ACI 318-19). Different limits from those indicated here for other compressed strut angles (i.e., θ_1, θ_2, θ_3) may be assumed provided they are adequately justified by numerical analyses that consider both compliance with strut-and-tie model compatibility conditions and the relative reduction in strut resistance [15].

3.1.3 Assessment of half-joints elements in existing structures

Structural assessment is typically conducted when loads acting on a structure increase, deficiencies related to design or construction become apparent, deterioration occurs, or when current code provisions are more stringent than those used for the original structural design. However, retrofitting existing structures is expensive and complex, making it essential for assessment procedures to aim at avoiding or minimizing such interventions. This can typically be achieved through a levels-of-approximation approach, beginning with simple load-carrying models or combinations thereof and refining them whenever insufficient strength is obtained. It should be noted that during design, even when using rational approaches as previously presented, some elements are not considered within primary load-carrying models, such as the minimal reinforcement amount for crack control. This additional reinforcement should nevertheless be considered part of the load-carrying mechanism during assessment as it increases member strength in a potentially significant manner. Additionally, design based on lower-bound solutions according to limit analysis, such as stress fields or strut-and-tie models, implies that more efficient load-carrying models may develop within the member for the available geometry and reinforcement. When conventional analyses fail to ensure sufficient strength with respect to design actions, refined strength estimates become necessary. In this case, the best lower-bound solution that can be selected is the exact solution according to limit analysis, which provides the maximum strength among all possible lower-bounds. Different techniques can be used to obtain the exact solution, with two approaches examined herein: the former based on rigid-plastic stress fields and the latter on elastic-plastic stress fields. The use of rigid-plastic stress fields combined with mechanisms for searching exact solutions has been discussed extensively. This can be performed by first selecting a licit collapse mechanism (upper-bound solution) whose free bodies are separated by discrete cracks and concrete hinges (refer to Figure 3.9(a)). According to the upper-bound approach of rigid-plastic limit analysis, all reinforcement crossing the cracks reaches its yield strength so that tie forces at ultimate limit state can be calculated easily (Fig. 3.9, where concrete is assumed to carry no tensile stress). The contact zones between free bodies can be considered compression zones where struts or nodal regions develop (Fig. 3.9(c) through (e)).

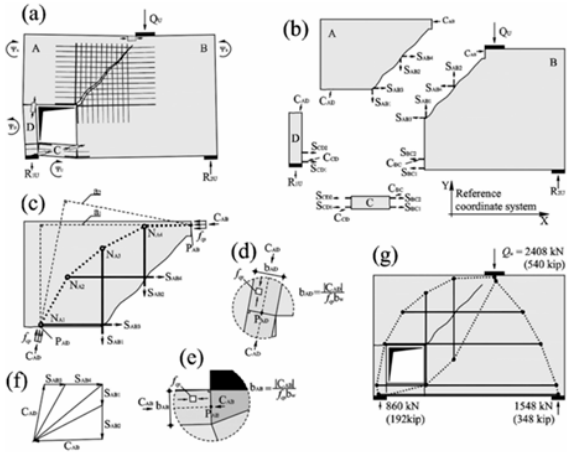

Figure 3.9: Assessment of strength using rigid-plastic mechanisms: (a) failure mechanism; (b) and (c) analysis of rigid bodies of mechanism; (d) and (e) analysis of critical struts; (f) Cremona diagram and thrust line inside rigid body; and (g) corresponding strut-and-tie model

Two methods exist for calculating load-carrying capacity related to a given mechanism. The first is based on the principle of virtual work, where external load work equals internal plastic dissipation. In the second method, equilibrium of every free body is treated separately. Solving equilibrium equations of every free body can be performed easily by following an iterative procedure, or contact forces between free bodies can be determined without iterations by solving a system of equations relating all implied variables. The load-carrying capacity of the selected mechanism (Fig. 3.9(a)), calculated by any of the previous procedures, is still not proven to correspond to that of the exact solution according to limit analysis, as other potential mechanisms can develop. Since this procedure is based on the upper-bound theorem of limit analysis, the exact load-carrying capacity could be lower than the calculated value. An interesting approach to verify if the selected mechanism corresponds to the exact solution can be performed by combining both theorems of limit analysis, as stated by Drucker that agreement of upper and lower bounds proves the load-carrying capacity is exactly determined. This procedure can be seen as an optimization where the criterion relates to load-carrying capacity. This can be accomplished by investigating internal equilibrium of all bodies as well as strengths of steel and concrete elements using strut-and-tie or stress field models. This is, for instance, shown in Fig.3.9(g). Despite the generality of the approach explained,

obtaining a solution following a rigid plastic approach might be time-consuming in some cases. A suitable alternative for overcoming this shortcoming is developing elastic-plastic stress fields that can be used to obtain exact solutions according to limit analysis in an automated and time-efficient manner. This type of stress field considers elastic behavior for concrete and steel following their elastic stiffness until the plastic plateau is reached, with no tensile stresses considered for concrete. The elastic-plastic stress field approach allows obtaining exact solutions in an automated manner [16].

Chapter 4

Canosilla Viaduct: a highway infrastructure case study

The following chapter presents a comprehensive analysis of a highway viaduct under concession to SINA S.p.A., a subsidiary of the ASTM Group, which generously provided the technical drawings and structural calculations that made this detailed case study possible. Through this real-world example, it was possible to analyse the structural behaviour of actual half-joint elements under real load cases and assess their performance according to shear verification procedures outlined in both current and former structural codes.

4.1 A15 Cisa Motorway

The A15 motorway, also known as the Cisa Motorway, is a major Italian highway that connects the Po Valley to the Tyrrhenian coast. It passes through the Taro Valley and the Lunigiana region, crossing the Tuscan-Emilian Apennines at the Cisa Pass. The route begins near Parma, where it links with the A1 motorway, and ends at Santo Stefano Magra, where it connects to the A12 motorway, close to La Spezia. The motorway is fully managed by SALT (Società Autostrada Ligure Toscana), which is part of the ASTM Group. Until November 1, 2017, the route was mostly managed by Autocamionale della Cisa S.p.A., which was later absorbed by SALT.

The A15 also forms part of the European route E33, making it a vital corridor for both national and international traffic. In 2025, the first section of the TIBRE corridor (Tirreno–Brennero) was opened. Also classified as A15, this new extension connects the A1 junction near Parma with the new toll station at Sissa Trecasali, providing improved north-south accessibility and expanding the motorway's reach. The original concept for the A15 dates back to the 1950s, when the goal was to create an alternative route between northern Italy and the Tyrrhenian coast. Due to the challenging mountainous terrain, its construction required numerous viaducts and tunnels, allowing the road to reach a maximum elevation of 745 meters above sea level near the entrance to the valico tunnel. The A15 is made up of two carriageways and features a particularly winding and complex layout, which makes driving demanding, especially for heavy vehicles. In fact, for several years, the motorway was used as a testing ground for trucks due to its technical difficulty. The road was officially opened to traffic on May 24, 1975. Today, the A15 consists of two continuous sections: the historic Parma–La Spezia route, and the TIBRE corridor, which is still under development beyond its initial segment. The main section climbs through the Taro Valley, with exits in Fornovo di Taro, Borgo Val di Taro, and Berceto in Emilia-Romagna, before crossing into Tuscany with exits at Pontremoli and Aulla, and finally entering Liguria at Santo Stefano Magra. Because of the complexity of its design and the high costs of maintenance required to manage its viaducts, tunnels, and the rugged Apennine landscape, frequent ordinary and extraordinary maintenance is necessary to ensure safety and functionality [17].

Figure 4.1: A15 Cisa Motorway

4.2 Canosilla Viaduct: Technical Description

Following the introduction of new regulations and requirements outlined in the Bridge Guidelines Text (DM 578 17/12/20), SINA s.p.a. engineering company, part of the ASTM Group, which operates in the major infrastructure sector and specializes in the design, construction, management, and upgrading of structures as a highway concessionaire with a network of approximately 5,900 kilometers, has initiated a comprehensive campaign to verify and upgrade its infrastructure assets. Through cutting-edge structural analyses, state-of-the-art monitoring systems, and continuous inspections, the company has prepared updated technical reports on its highway viaducts. Among these structures is the Canosilla Viaduct, which technical drawings and data were have been kindly provided.

The Canosilla Viaduct is located in the municipality of Villafranca in Lunigiana, in the province of Massa-Carrara, on the Cisa Highway A15 Parma – La Spezia. The viaduct, constructed between the late 1960s and early 1970s, consists of 2 spans for each carriageway with a total length of approximately 60 meters. Both carriageways develop along a curved planimetric layout with a radius of curvature of 600 meters.

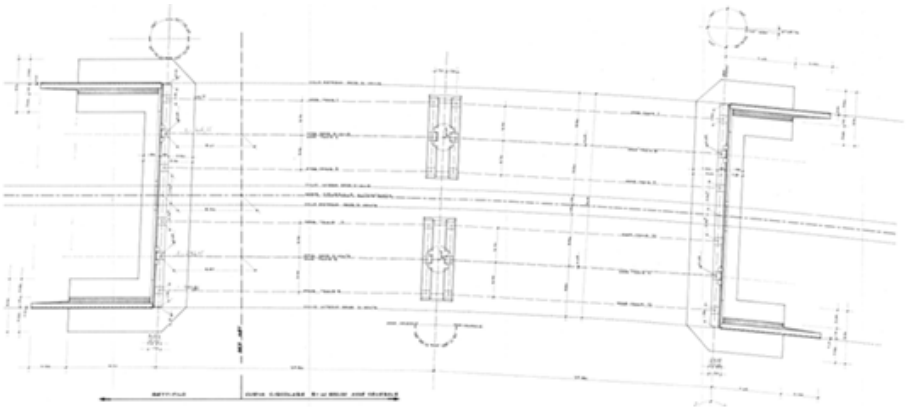

Figure 4.2: plan view of the viaduct

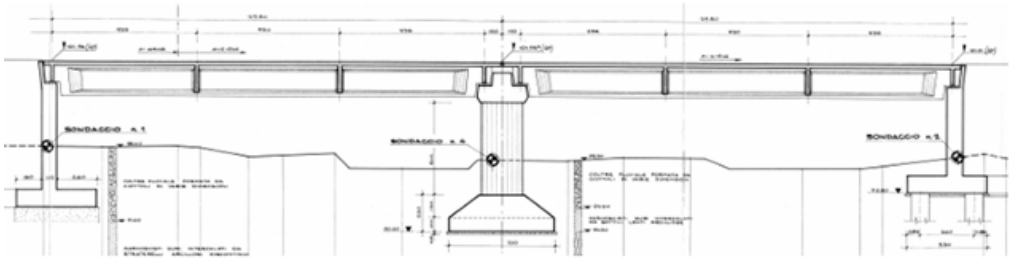

Figure 4.3: longitudinal profile of the viaduct

Both carriageways consist of 2 simply supported spans on piers and abutments, with all spans characterized by a center-to-center bearing distance of 28.6 meters. The decks are constructed using a grid system comprising 3 longitudinal prestressed reinforced concrete beams, 4 reinforced concrete cross-beams, and completed with a cast-in-place slab. The longitudinal beams have a total length of 29.6 meters (28.6 m clear span plus 0.5 m beam extension at each end), are positioned with constant spacing of 3.7 meters throughout their development, and are characterized by a height of 2.25 meters (including slab) and variable web thickness ranging from a minimum of 0.25 meters to a maximum of 0.75 meters.

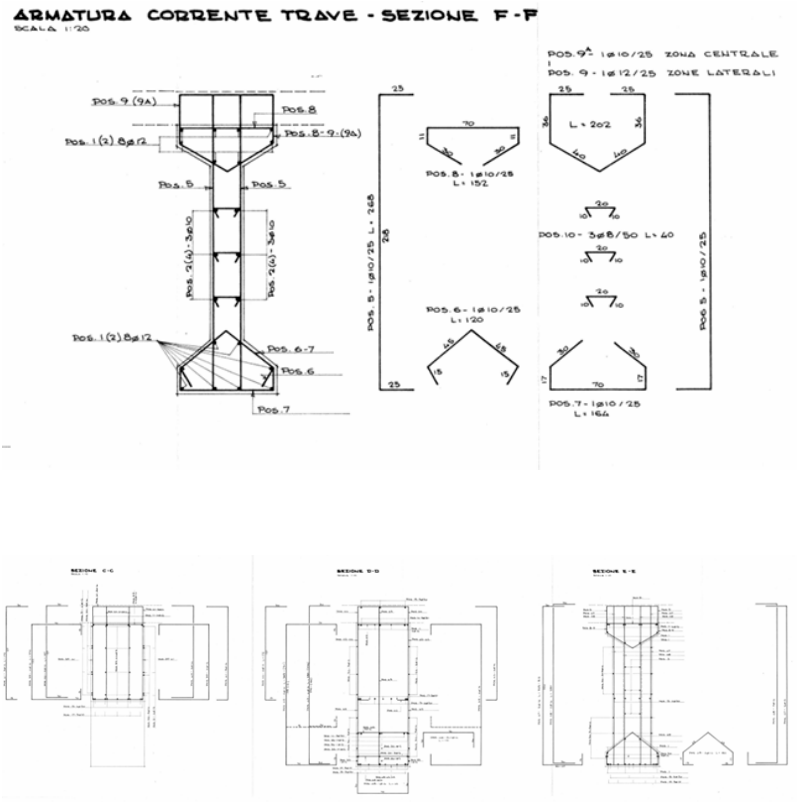

Figure 4.4: Variation of the cross-section of the viaduct beams with reinforcement configurations

At the bearings on abutments and pier caps, the beams feature the presence of a half-joint, where the height reduces from 2.25 to 1.35 meters. The transverse cross-beams (2 end beams and 2 span beams) are positioned with spacing of 9.50÷9.55 meters and are characterized by a thickness of 0.25 meters and height, including slab, of 1.35 meters for end cross-beams and 2.05 meters for span cross-beams. The grid system is completed with a reinforced concrete slab of 0.25 meters thickness and 11.0 meters width. The original section is completed with curbs of 50 cm width on which safety barriers are installed, resulting in a carriageway width of 10 meters. At the beam ends, there is still a longitudinal cantilever of the slab with a length of 1.20 meters (cantilever over pier).

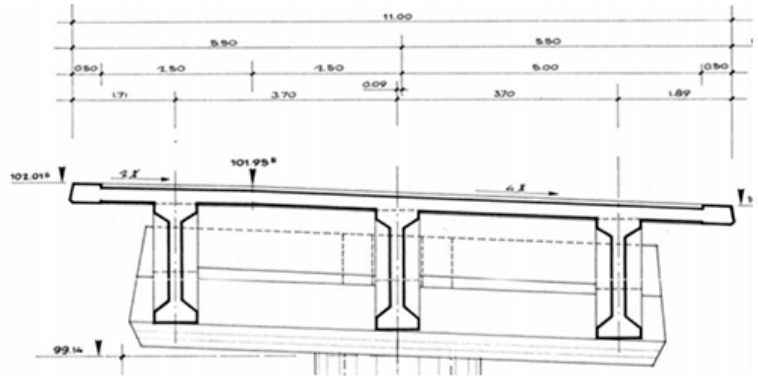

Figure 4.5: Cross-section at midspan

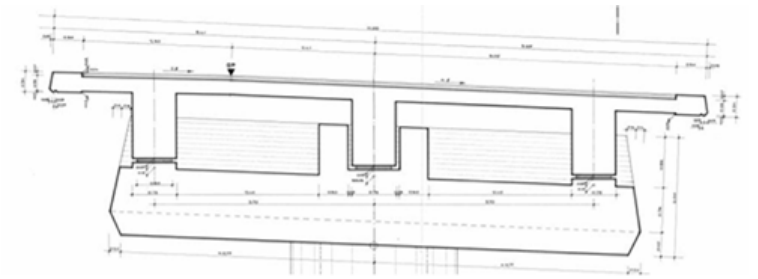

Figure 4.6: Cross-section at supports' axis

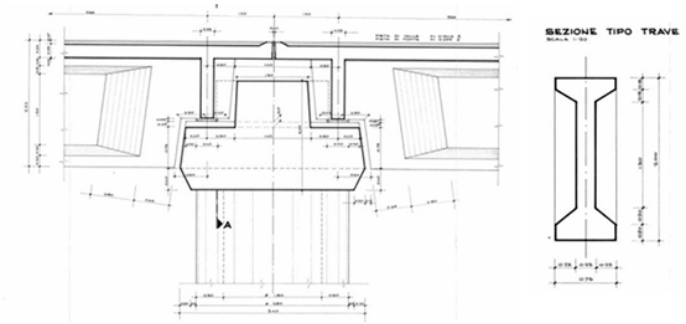

Figure 4.7: sx) Detail at pier; dx) Detail of beam dimensions – typical section

Examining the longitudinal section view of half the beam (shown by symmetry), the arrangement of both longitudinal and shear reinforcement becomes evident, particularly in the end elevation showing the beam's terminal section.

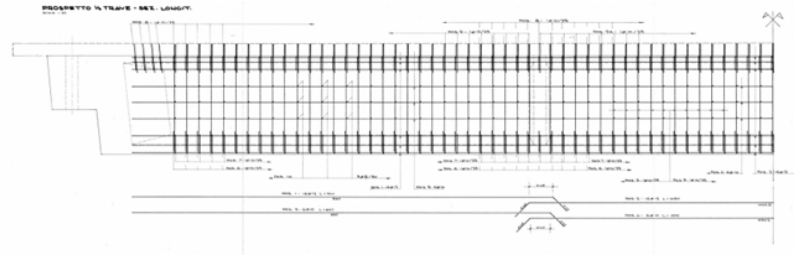

Figure 4.8: Elevation view of beam with reinforcement configurations

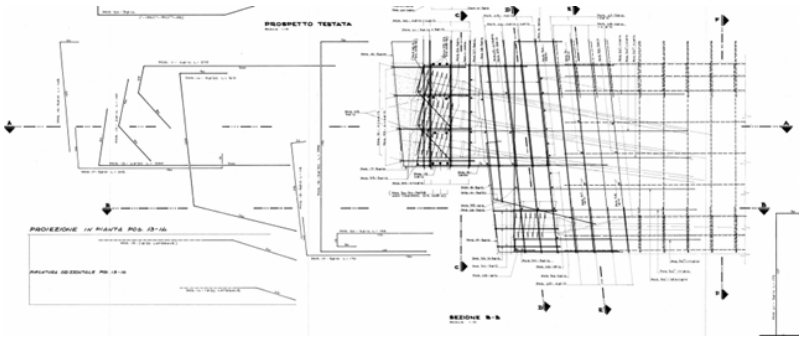

Figure 4.9: Elevation view of span with reinforcement configurations

The technical drawing reveals the reinforcement layout in the beam's end section, where the critical transition from full beam height to the reduced half-joint height occurs. The longitudinal reinforcement is clearly visible with multiple bars running along the beam length, showing proper continuity and anchorage details at the support region. However, what is particularly notable and concerning from a structural engineering perspective is the evident scarcity of shear reinforcement in this critical zone. The drawing shows minimal transverse reinforcement (stirrups) in the area where the beam geometry transitions from the constant section to the half-joint configuration. This lack of adequate shear reinforcement is especially problematic considering that the half-joint region experiences significant stress concentrations due to the abrupt change in cross-sectional geometry. The reduced beam height at the half-joint, combined with the concentration of support reactions, creates a zone of high shear stress that would typically require dense stirrup spacing and possibly additional shear reinforcement such as inclined bars or shear studs. The reinforcement detailing shown appears to follow older design practices from the 1960s-70s construction period, when shear design provisions were less stringent than current

standards. The sparse distribution of transverse reinforcement visible in the drawing suggests that the original design may not have adequately addressed the complex stress state that develops in Gerber half-joint connections, where the combination of vertical shear forces, horizontal forces from prestressing, and geometric discontinuities creates a challenging reinforcement requirement that appears to be insufficiently addressed in this structural detail. The prestressing of the beams is achieved through 5 post-tensioned cables, of which 4 consist of 32 wires $\phi 7$ while the remaining one consists of 42 wires $\phi 7$. All cables are arranged symmetrically with respect to the beam axis, following a first parabolic section and a second straight section.

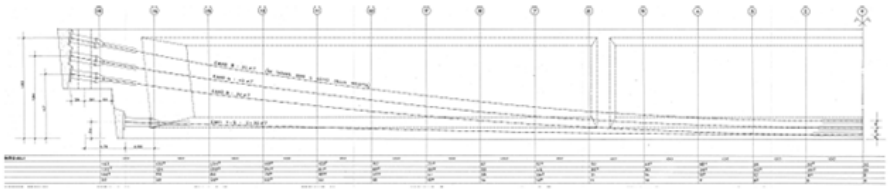

Figure 4.10: Longitudinal layout of prestressing cables

Regarding the substructures, the decks are simply supported at the piers and abutments (reinforced neoprene bearings). The piers consist of hollow circular shafts characterized by an external diameter of 2.80 meters and thickness of 0.50 meters. The shaft height varies from a minimum of 6.11 meters (upstream) to a maximum of 6.44 meters (downstream). The pier cap is characterized by an inverted T-section with maximum height of 2.00 meters and develops over a total width of 8.95 meters. At the bearings, reinforced concrete corbels with height of 10 cm and width of 0.75 meters are present.

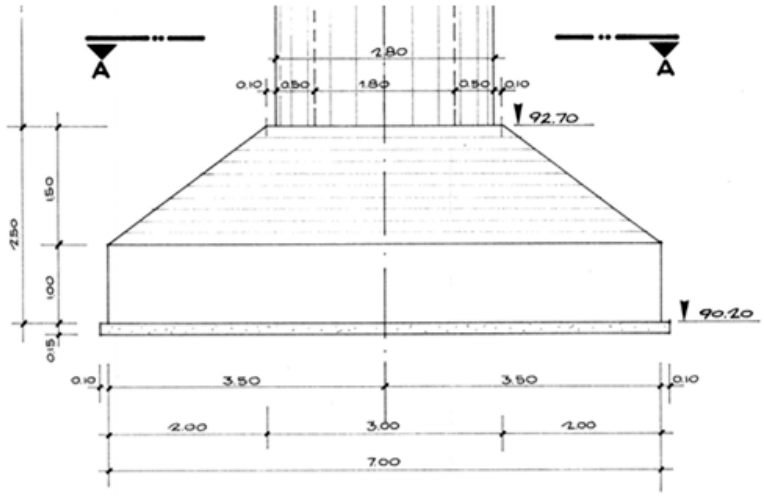

Figure 4.11: Front view of the foundation footing

The Parma-side abutment consists of a single body for both viaduct carriageways, constructed in reinforced concrete and comprising a debris wall of 1.50 meters height and 0.25 meters thickness, and a front wall with maximum width of 7.47 meters and thickness of 1.10 meters. The abutment is founded on a direct reinforced concrete raft of 1.20 meters thickness.

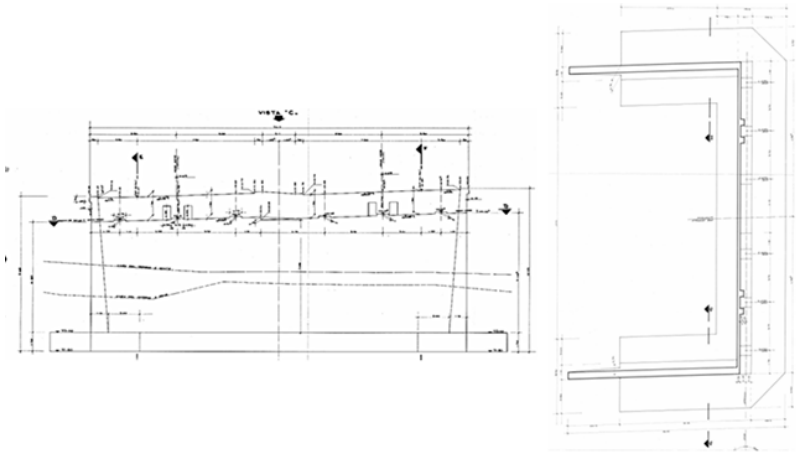

Figure 4.12: Front view of the foundation footing

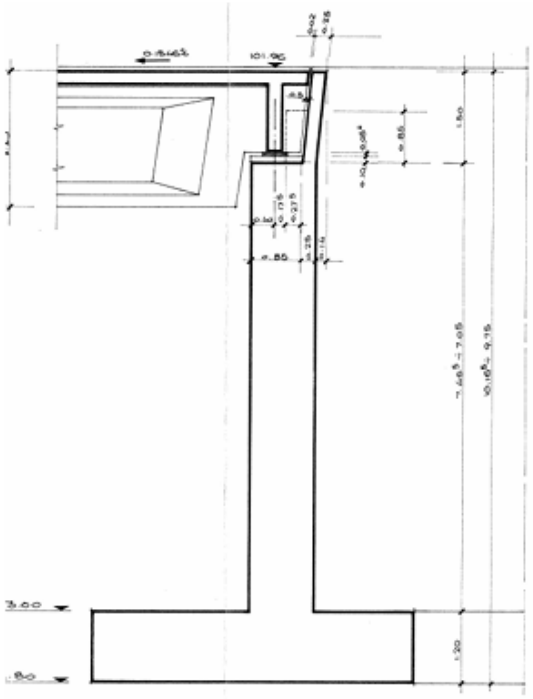

Figure 4.13: Front view of the foundation footing

The La Spezia-side abutment consists of a single body for the two viaduct carriageways, constructed in reinforced concrete and comprising a debris wall of 1.50 meters height and 25 cm thickness, and a front wall with maximum height of 6.42 meters and thickness of 1.10 meters. The abutment is founded on a reinforced concrete raft (1.20 meters thickness) resting on a pile foundation consisting of 16 piles ϕ1200.

4.2.1 Conservation State of the viaduct

Following an extraordinary inspection conducted by SINA S.p.A of the structure, the following conclusions have emerged, which have led to the identification of specific intervention requirements. The comprehensive assessment has revealed the current state of the structure and has informed the development of targeted enhancement measures. Following examination of inspection reports and photographic documentation, various conditions characterizing the current state of the structure have been identified. The structural elements generally present typical aging characteristics consistent with the structure's service life. Some areas show surface deterioration and minor concrete cover issues, while the overall structural integrity remains adequate for current loading conditions. Drainage system components show signs of normal wear and require routine maintenance to ensure proper water management. Joint systems present standard maintenance needs typical of infrastructure of this age and exposure conditions.

Figure 4.14: Detail of the span view of the viaduct

During close-range inspection, hammer testing of surfaces was performed to verify concrete conditions. Investigation was conducted focusing on areas where routine maintenance activities had been previously identified. The inspection confirmed the general structural soundness of the elements. Based on continuous monitoring

reports, the structure shows stable behavior with no significant evolution of existing conditions. Recent restoration and maintenance interventions have been effectively implemented.

Figure 4.15: Span view of the viaduct

4.3 Structural Analysis

4.3.1 Current Code: Shear Assessment

The definition of design actions for the viaduct has been calculated primarily according to the following standards:
- D.M. 17/01/2018 (NTC2018);
- Circular 21.01.2019, EN1991-2;
- Eurocode 1-part 2, Actions on bridges.
The actions are therefore divided into self-weight, permanent loads carried, wind action, thermal variations, variable traffic actions, braking action, centrifugal action, constraint resistances, and prestressing forces.

Self-weight

The self-weight of all structural elements has been evaluated assuming a specific weight of reinforced concrete equal to 25 kN/m^3

Carried Permanent loads

The structural analyses were conducted considering the following permanent loads:

- Pavement (Binder and wearing course): unit weight = 23 kN/m^3; thickness = 0.14 m; load per unit area = 3.22 kN/m^2.
- Reinforced concrete curb: unit weight = 25 kN/m^3; cross-sectional area = 0.043 m^2; load per unit length = 1.08 kN/m.
- Metallic safety barrier: load per unit length = 1.50 kN/m.

Variable Loads

Wind action

Wind action was evaluated in accordance with paragraphs §5.1.3.7 and §3.3 of NTC18 and §8.3.1 of EC1-1. Since the viaduct is located in zone III (Tuscany), at approximately 150 m above sea level, the reference basic wind velocity v_b equals:

$$v_b = v_{b,0} \cdot c_a = 27.0 m/s. \tag{4.1}$$

The reference velocity is obtained from the relationship: $v_r = v_b \cdot c_r$, where c_r represents the return coefficient, which is a function of the design return period T_r. Wind action is conventionally assimilated to a static horizontal and vertical load, calculated as a function of the pressure that the wind itself exerts on a well-defined incident surface. This pressure can be calculated with the following expression:

$$p = q_b \cdot c_a \cdot c_p \cdot c_d \tag{4.2}$$

Considering the shape coefficient for bridges according to UNI EN 1991-1-4:2005, the maximum horizontal wind pressure at a maximum height of 12 m from ground level (viaduct height near the highest overall height of the deck plus the conventional height of 3.0 m) results in approximately:
$p = 2.16 kN/\mathrm{m}^2$.

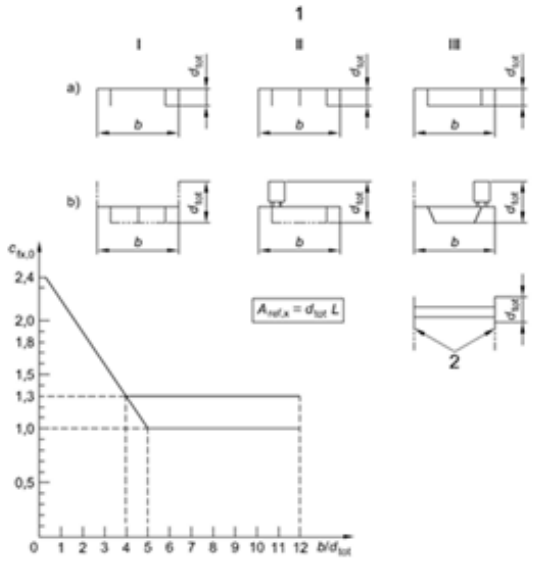

Figure 4.16: Shape coefficient for bridges - UNI EN 1991-1-4:2005 - Horizontal component

Temperature Variation

Temperature variation, both uniform and linear, does not contribute to the stress state of the structure since the decks are statically determinate with fixed and movable supports, and therefore was not considered for the purposes of the analyses.

Traffic Actions

Variable traffic actions were evaluated according to the provisions of paragraph §5.1.3.3 of the Technical Standards for Construction (NTC18). The number of traffic lanes that can be simultaneously arranged on the deck, each 3 m wide, depends on the total width of the carriageway. In this case, 3 traffic lanes can be arranged for both carriageways, to which the width of the remaining area (1.10 m) is added. For each verification, the arrangement and number of conventional lanes considered loaded were chosen to maximize the individual design stresses. The analyses were conducted taking into account load scheme 1 and 2 indicated in NTC18. In particular, load scheme 1 was employed for global and local verifications of the various structural elements of the work, while load scheme 2 was used exclusively for local verifications.

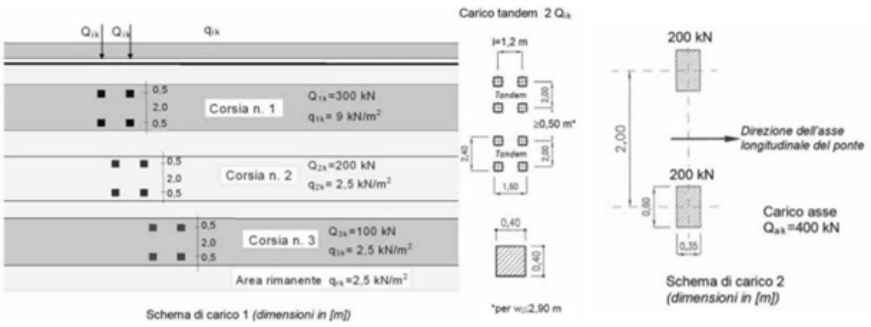

Figure 4.17: Traffic load patterns

Braking and Centrifugal Forces

The braking force was evaluated in accordance with point §5.1.3.5 of NTC18:

$$180 \leq q_3 = 0.6 \cdot 2 \cdot Q_{1k} + 0.1 \cdot q_{1k} \cdot w_1 \cdot L \leq 900\,\text{kN}, \tag{4.3}$$

where $Q_{1k} = 300kN$ is the axle load of the Tandem System for Lane 1, $q_{1k} = 9.00kN/m^2$ is the uniformly distributed load for Lane 1, $w_1 = 3.00m$ is the width of Lane 1, and L is the loaded length.

The loaded length considered corresponds to one deck span in order to evaluate the load pertaining to a single pier, equal to 31m (distance between pier axes). Therefore, the braking force acting on the single pier equals:

$$q_3 = 360 + 84 = 444kN. \tag{4.4}$$

This longitudinal force represents the horizontal action transmitted to the structure when vehicles decelerate on the bridge deck. The force is applied at the deck level and must be resisted by the pier and foundation system through their longitudinal stiffness and the constraint conditions at the supports.

Centrifugal action was taken into consideration for the verification of piers located in the curved section of the bridge. In this case, the minimum radius of curvature equals 600 m and, therefore, the action due to centrifugal force is evaluated as follows:

$$q_4 = 40 \cdot \frac{Q_v}{R} = 40 \cdot \frac{1200}{600} = 80kN. \tag{4.5}$$

This transverse horizontal force results from vehicles traveling along the curved alignment of the bridge and creates an outward force that must be resisted by the structural system. The centrifugal action is applied at the deck level and is transmitted to the piers through the bearing system, requiring adequate transverse stiffness and stability of the supporting elements.

Prestressing Forces

The data regarding deck prestressing were obtained from the design documents related to the historical executive project. In particular, all decks are characterized by the presence of 3 longitudinal prestressed beams using 5 post-tensioned tendons, of which 4 consist of 32 wires $\phi 7$ ($A = 1232\,\mathrm{mm}^2$: cables 1, 2, 3 and 5) and 1 consists of 42 wires $\phi 7$ ($A = 1616\,\mathrm{mm}^2$: cable 4). All tendons are characterized by a symmetrical layout, parabolic in the first section and straight near the mid-

span of the beams. The following figures show the tendons' layout for the generic longitudinal deck beam. The prestressing system provides the necessary internal forces to control deflections, limit crack formation, and enhance the overall structural performance of the concrete beams under service loads. The parabolic profile of the cables in the end regions allows for efficient transfer of prestressing forces while the straight central portion optimizes the moment resistance at mid-span where maximum positive moments occur.

Figure 4.18: Prestressing tendons longitudinal layout

	y [m] - distanza rispetto ad intradosso trave					y' [-] - inclinazione del cavo rispetto all'orizzontale				
x [m]	y_{cavo1}	y_{cavo2}	y_{cavo3}	y_{cavo4}	y_{cavo5}	y'_{cavo1}	y'_{cavo2}	y'_{cavo3}	y'_{cavo4}	y'_{cavo5}
0.50	-	-	1.11	1.43	1.75	-	-	-0.1223	-0.1445	-0.1695
1.00	-	-	1.05	1.36	1.66	-	-	-0.1223	-0.1445	-0.1695
1.73	0.28	0.28	0.96	1.25	1.54	-0.0266	-0.0266	-0.1216	-0.1437	-0.1685
2.51	0.26	0.26	0.87	1.14	1.41	-0.0259	-0.0259	-0.1168	-0.1383	-0.1620
3.36	0.24	0.24	0.77	1.03	1.27	-0.0250	-0.0250	-0.1104	-0.1309	-0.1530
4.50	0.21	0.21	0.65	0.88	1.11	-0.0239	-0.0239	-0.1016	-0.1209	-0.1408
5.65	0.19	0.19	0.54	0.75	0.95	-0.0228	-0.0228	-0.0929	-0.1109	-0.1287
7.94	0.14	0.14	0.34	0.52	0.68	-0.0194	-0.0194	-0.0755	-0.0909	-0.1045
9.65	0.11	0.11	0.23	0.38	0.53	-0.0137	-0.0137	-0.0576	-0.0695	-0.0797
11.37	0.09	0.09	0.15	0.28	0.41	-0.0081	-0.0081	-0.0384	-0.0463	-0.0531
13.08	0.08	0.08	0.10	0.22	0.34	-0.0024	-0.0024	-0.0192	-0.0232	-0.0266
14.80	0.08	0.08	0.08	0.20	0.32	0.0000	0.0000	0.0000	0.0000	0.0000

Figure 4.19: Position and inclination fo prestressing tendons

All cables are tensioned to a stress of 1100 MPa, derived from historical calculation reports. Furthermore, it should be noted that initially tendons 1, 2, 3 and 4 were tensioned (on the beam-only cross-section) while tendon 5 was tensioned only after casting of the reinforced concrete slab. In calculating the effects due to prestressing, both short-term stress losses (anchorage draw-in and friction) and long-term losses (rheological effects of concrete and steel relaxation) were taken into consideration. The Parameters are provided through which the stress in the tendons was evaluated, section by section, at infinite time (conventionally assumed equal to 70 years). The sequential tensioning procedure reflects the construction sequence where the initial cables provide support during the casting of the deck slab, while the final cable is applied to the composite section to optimize the prestressing distribution. The com-

prehensive analysis of prestress losses ensures accurate prediction of the long-term structural behavior and verifies that adequate prestressing forces are maintained throughout the design life of the structure.

Ultimate Limit State Combinations

Ultimate limit state verifications were performed in accordance with point §2.5.3 of NTC 2018, combining stresses as described below:
Fundamental combination

$$\gamma_{g1}G_1 + \gamma_{g2}G_2 + \gamma_p P + \gamma_{q1} \cdot Q_{k1} + \gamma_{q2} \cdot \Psi_{02} \cdot Q_{k2} + \gamma_{q3} \cdot \Psi_{03} \cdot Q_{k3} + \dots \quad (4.6)$$

This combination represents the basic design scenario for ultimate limit state verification and includes the simultaneous action of permanent loads, the leading variable action, and accompanying variable actions appropriately factored according to the specified partial safety factors and combination coefficients established in the technical standards. Regarding the partial safety factors and combination coefficients, reference was made to what is indicated, respectively, in the following Table 5.1.V and point §5.1.3.13 of NTC2018:

Tab. 5.1.VI - *Coefficienti ψ per le azioni variabili per ponti stradali e pedonali*

Azioni	Gruppo di azioni (Tab. 5.1.IV)	Coefficiente ψ_0 di combinazione	Coefficiente ψ_1 (valori frequenti)	Coefficiente ψ_2 (valori quasi permanenti)
Azioni da traffico (Tab. 5.1.IV)	Schema 1 (carichi tandem)	0,75	0,75	0,0
	Schemi 1, 5 e 6 (carichi distribuiti	0,40	0,40	0,0
	Schemi 3 e 4 (carichi concentrati)	0,40	0,40	0,0
	Schema 2	0,0	0,75	0,0
	2	0,0	0,0	0,0
	3	0,0	0,0	0,0
	4 (folla)	--	0,75	0,0
	5	0,0	0,0	0,0
Vento	a ponte scarico SLU e SLE	0,6	0,2	0,0
	in esecuzione	0,8	0,0	0,0
	a ponte carico SLU e SLE	0,6	0,0	0,0
Neve	SLU e SLE	0,0	0,0	0,0
	in esecuzione	0,8	0,6	0,5
Temperatura	SLU e SLE	0,6	0,6	0,5

Figure 4.20: Combination coefficients (for ULS and SLE)

Tab. 5.1.V – *Coefficienti parziali di sicurezza per le combinazioni di carico agli SLU*

		Coefficiente	EQU[1]	A1	A2
Azioni permanenti g_1 e g_3	favorevoli sfavorevoli	γ_{G1} e γ_{G3}	0,90 1,10	1,00 1,35	1,00 1,00
Azioni permanenti non strutturali [2] g_2	favorevoli sfavorevoli	γ_{G2}	0,00 1,50	0,00 1,50	0,00 1,30
Azioni variabili da traffico	favorevoli sfavorevoli	γ_Q	0,00 1,35	0,00 1,35	0,00 1,15
Azioni variabili	favorevoli sfavorevoli	γ_{Qi}	0,00 1,50	0,00 1,50	0,00 1,30
Distorsioni e presollecitazioni di progetto	favorevoli sfavorevoli	$\gamma_{\varepsilon 1}$	0,90 1,00[3]	1,00 1,00[4]	1,00 1,00
Ritiro e viscosità, Cedimenti vincolari	favorevoli sfavorevoli	$\gamma_{\varepsilon 2}$, $\gamma_{\varepsilon 3}$, $\gamma_{\varepsilon 4}$	0,00 1,20	0,00 1,20	0,00 1,00

Figure 4.21: Partial safety factors for ULS

Different values can be assumed for the partial safety factors of permanent actions (self-weight and permanent loads carried); these values refer to three different conditions:

CLASSE DI CONSEGUENZA	(1) CONDIZIONI STANDARD	(2) CON ACCURATO CONTROLLO STATISTICO DI MATERIALI E GEOMETRIA E COV<0,05	(3) COME (2) E CON ABBATTIMENTO INCERTEZZE DI MODELLO (§ 6.3.3.5)
CC3	1.35	1.25	1.20

Figure 4.22: Partial safety factors for permanent actions under adequacy conditions

CLASSE DI CONSEGUENZA	(1) CONDIZIONI STANDARD	(2) CON ACCURATO CONTROLLO STATISTICO DI MATERIALI E GEOMETRIA E COV<0,05	(3) COME (2) E CON ABBATTIMENTO INCERTEZZE DI MODELLO (§ 6.3.3.5)
CC3	1.26	1.16	1.10

Figure 4.23: Partial safety factors for permanent actions under serviceability/trafficability conditions

In this case, Condition 2 will be used ($\gamma_g = 1.25$ for adequacy; $\gamma_g = 1.16$ for operability/trafficability). Regarding verifications under operational conditions according to LG21, the partial safety factor for variable traffic actions can be assumed equal to 1.20.

Classe di conseguenza	Tempo di riferimento tref	Fattori parziali per le azioni variabili da traffico, γ_Q
CC3	5 anni (ponte TRANSITABILE, § 6.1.5.3)	1.20
	30 anni (ponte OPERATIVO, § 6.1.5.2)	1.20

Figure 4.24: Partial safety factors for permanent actions under adequacy conditions

The various elementary actions, are combined according to the coefficients shown in the following tables:

comb.	dead	permanenti	precompressione	vento	traffico	frenatura	centrifuga
STR1 - Traffico	1.25 (1.0)	1.25 (1.0)	1.0	0.9 (-0.9)	1.35 (0.0)	0.0	0.0
STR2a - Frenatura	1.25 (1.0)	1.25 (1.0)	1.0	0.9 (-0.9)	1.01 (0.0)	1.35 (-1.35)	0.0
STR2b - Centrifuga	1.25 (1.0)	1.25 (1.0)	1.0	0.9 (-0.9)	1.01 (0.0)	0.0	1.35 (0.0)
STR - Vento	1.25 (1.0)	1.25 (1.0)	1.0	1.5 (-1.5)	1.01 (0.0)	0.0	0.0

Figure 4.25: Combination factors for permanent actions under adequacy conditions

comb.	dead	permanenti	precompressione	vento	traffico	frenatura	centrifuga
STR1 - Traffico	1.25 (1.0)	1.25 (1.0)	1.0	0.9 (-0.9)	1.35 (0.0)	0.0	0.0
STR2a - Frenatura	1.25 (1.0)	1.25 (1.0)	1.0	0.9 (-0.9)	1.01 (0.0)	1.35 (-1.35)	0.0
STR2b - Centrifuga	1.25 (1.0)	1.25 (1.0)	1.0	0.9 (-0.9)	1.01 (0.0)	0.0	1.35 (0.0)
STR - Vento	1.25 (1.0)	1.25 (1.0)	1.0	1.5 (-1.5)	1.01 (0.0)	0.0	0.0

Figure 4.26: Combination factors for permanent actions under serviceability conditions

Shear Assessment

Tangential Stress Verification

The design shear resistance values are evaluated in accordance with NTC18 and UNI EN 1922 1-1 standards, making a distinction between the design resistance for elements reinforced against shear, which includes both $V_{Rd,s}$ and $V_{Rd,max}$ components, and the design resistance for elements without shear reinforcement, designated as $V_{Rd,c}$. This evaluation methodology ensures that structural elements are properly assessed based on their specific reinforcement configuration, with different calculation approaches applied depending on whether transverse reinforcement is present or absent in the concrete members being analyzed.

$$V_{Rd,c} = \max\{C_{Rd,c} \cdot k \cdot (100 \cdot \rho_1 \cdot f_{ck})^{\frac{1}{3}} + k_1 \cdot \sigma_{cp}; v_{min} + k_1 \cdot \sigma_{cp}\} \cdot b_w \cdot d; \quad (4.7)$$

$$V_{Rd,max} = \frac{\alpha_{cw} \cdot b_w \cdot z \cdot v_1 \cdot f_{cd}}{\cot\theta + \tan\theta}; \quad (4.8)$$

$$V_{Rd,s} = \frac{A_{sw}}{s} \cdot z \cdot f_{ywd} \cdot \cot\theta; \tag{4.9}$$

In the preceding expressions, the following terms appear:

- $C_{Rd,c} = 0.18/\gamma_c$;
- $k = 1 + \sqrt{200/d} \leq 2.0$ with d (effective depth) in mm;
- $\rho_1 = A_{sl}/b_w \cdot d \leq 0.02$;
- A_{sl} = area of tensile reinforcement;
- b_w = minimum width of the section in the tensile zone;
- $k_1 = 0.15$;
- $\sigma_{cp} = N_{ed}/A_c < 0.2 \cdot f_{cd}$;
- N_{ed} = axial force due to external actions;
- A_c = area of concrete cross-section;
- $v_{min} = 0.035 \cdot k^{\frac{3}{2}} \cdot f_{ck}^{\frac{1}{2}}$;
- $v_1 = v = 0.6 \cdot \left[1 - \frac{f_{ck}}{250}\right]$;
- $\cot\theta \in [1.0; 2.5]$;
- A_{sw}/s = mean area of shear reinforcement per unit length over distance $z \cdot \cot\theta$ starting from the section under investigation;
- f_{ywd} = design yield strength of shear reinforcement;
- $\alpha_{cw} = 1$.

Specifically, regarding the ultimate limit state shear verification of deck slabs, the shear resistance has been assumed, section by section, as the maximum value between the VRd,c evaluated as previously reported and the VRd,c calculated according to the Guidelines. This approach ensures that the most conservative and appropriate shear resistance value is adopted for each individual section of the deck slab, comparing the standard calculation method with the specific methodology

outlined in the referenced Guidelines. The selection of the maximum value between these two calculation approaches provides an enhanced level of safety and accuracy in the structural assessment of the deck elements.

$$V_{Rd,c,LG} = \frac{0.3 \cdot \sqrt{f_{ck}} \cdot b_w \cdot d}{\gamma_c \cdot (1 + 0.0022d)} \tag{4.10}$$

For the ultimate limit state shear verification of prestressed elements on simple supports, specifically the longitudinal deck beams, in zones not cracked by bending moment where the tensile stress in concrete does not exceed fctd, the design resistance can be evaluated through a simplified approach using the following formula. This simplified methodology is applicable specifically to prestressed concrete elements where the concrete remains uncracked due to the beneficial effects of prestressing forces. The approach recognizes that in these uncracked zones, the structural behavior differs significantly from cracked sections, allowing for a more favorable assessment of the shear resistance capacity. The verification process takes into account the prestressing effects and the concrete's ability to resist tensile stresses without developing cracks under the applied loading conditions.

$$V_{Rd} = 0.7 \cdot b_w \cdot d \cdot \left(f_{ctd}^2 + \sigma_{cp} \cdot f_{ctd}\right)^{\frac{1}{2}} \tag{4.11}$$

Resistance According to UNI EN1992-1-1:2023 Point 8.2.3

Shear resistance according to section 8.2.3 of UNI EN1992-1-1:2023 establishes the resistance criteria for elements that are reinforced against shear. For the verification to be considered satisfactory, it is necessary to fulfill specific conditions that ensure adequate structural performance. Section 8.2.3 of the UNI EN1992-1-1:2023 standard provides comprehensive guidance for calculating the shear resistance of reinforced concrete elements where transverse reinforcement is present. The verification process requires that multiple conditions be simultaneously met to guarantee that the structural element can safely resist the applied shear forces. This approach considers both the contribution of the concrete and the shear reinforcement in resisting the applied loads, ensuring that the design meets the required safety standards

and performance criteria established by the European structural codes.

$$\tau_{Ed} \leq \tau_{Rd,sy} \leq \frac{v \cdot f_{cd}}{2} \tag{4.12}$$

$$\sigma_{cd} \leq v \cdot f_{cd} \tag{4.13}$$

where:

- $\tau_{Ed} = V_{Ed}/(b_w \cdot z)$ = tangential stress;
- $\tau_{Rd,sy} = \rho_w \cdot f_{ywd} \cdot \cot\theta$ = steel side resistance;
- $\sigma_{cd} = \tau_{Ed} \cdot (\cot\theta + \tan\theta)$ = stress in compressed concrete strut;
- $\rho_w = \frac{A_{sw}}{s} \cdot \frac{1}{b_w}$ = geometric ratio of transverse reinforcement.

Regarding the definition of the inclination of the compression fields in the web (angle θ; truss model), this can be selected within the following range. The truss model approach allows for flexibility in determining the angle of the compression struts, recognizing that the actual stress distribution in reinforced concrete elements can vary depending on various factors including loading conditions, reinforcement configuration, and material properties. The selection of an appropriate angle within the permitted range enables engineers to optimize the design while maintaining structural integrity and compliance with safety requirements. This variable angle approach reflects the understanding that concrete elements under shear loading develop diagonal compression fields that can orient themselves at different inclinations based on the equilibrium requirements and the presence of transverse reinforcement.

$$1 \leq \cot\theta \leq \cot\theta_{min} \tag{4.14}$$

Where the cotangent of the minimum inclination of the compression fields ($\theta_m in$), can be assumed according to the following criteria. This provision establishes the lower bound for the compression field inclination, ensuring that the selected angle remains within physically reasonable limits that reflect the actual behavior of reinforced concrete elements under shear loading. The minimum inclination criteria serve as a safeguard against overly optimistic assumptions about the concrete's

capacity to develop steep compression fields, which could lead to unsafe design conditions. The specified criteria take into account various factors that influence the development of diagonal compression struts in the concrete web, including the interaction between longitudinal and transverse reinforcement, the concrete strength characteristics, and the overall structural geometry of the element being analyzed.

- $\cot\theta_{min} = 2.5$ - for elements with ordinary reinforcement not subjected to axial forces;
- $\cot\theta_{min} = 3.0$ - for elements subjected to a significant axial force ($|\sigma_m| \geq$ 3MPa) and characterized by a neutral axis depth x less than $0.25d$. For intermediate cases, values between 2.5 and 3.0 may be adopted through linear interpolation;
- $\cot\theta_{min} = 2.5 - 0.1 \cdot N_{ed}/|V_{ed}|$ - for elements subjected to tension.

Furthermore, section 8.2.3(12) specifies that in the case of concentrated forces applied at a distance $av = z \cdot \cot\beta_{incl} < z \cdot \cot\theta$ from the support, the shear resistance can be evaluated using the following method (equation 8.55).

$$\tau_{Rd} = v \cdot f_{cd} \cdot \frac{\cot\theta - \cot\beta_{incl}}{1 + \cot^2\theta} + \rho_w \cdot f_{ywd} \cdot \cot\beta_{incl} \leq v \cdot f_{cd} \cdot \frac{\cot\theta}{1 + \cot^2\theta} \qquad (4.15)$$

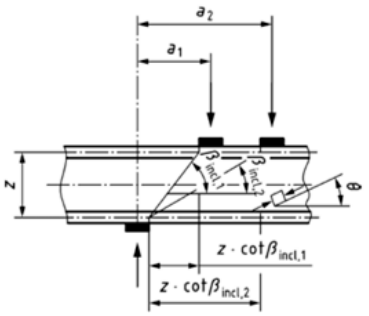

Figure 4.27: Shear evaluation scheme for concentrated forces

It is further specified that if distributed loads q_d are present in addition to the concentrated forces, the term $\rho_w \cdot f_{ywd}$ in the previous relationship can be replaced

by $(\rho_w \cdot f_{ywd} + q_d/b_w)$. In the case under examination, for simplicity, the contribution related to the distributed load is carried to the second term.

$$\tau_{Rd} = v \cdot f_{cd} \cdot \frac{\cot\theta - \cot\beta_{incl}}{1 + \cot^2\theta} + \rho_w \cdot f_{ywd} \cdot \cot\beta_{incl} \leq v \cdot f_{cd} \cdot \frac{\cot\theta}{1 + \cot^2\theta} - \frac{q_d}{b_w} \cdot \cot\beta_{incl} \tag{4.16}$$

Verification Results

Regarding the ultimate limit state shear verification of the deck's longitudinal beams, given the presence of a bearing seat near the supports, the conventional sectional verification was performed exclusively outside the discontinuity zone. Specifically, the discontinuity zone was limited to approximately 2.0 meters from the support axis, corresponding to one effective depth distance.

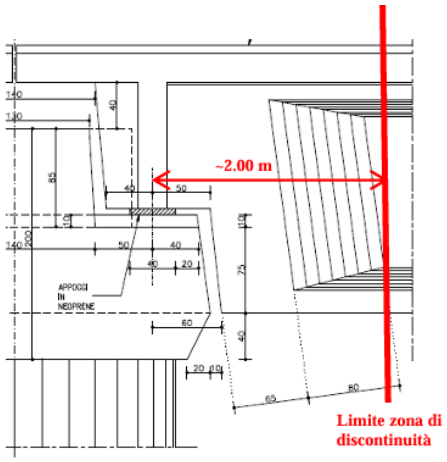

Figure 4.28: Discontinuity zone at beam ends

The ultimate limit state shear verifications for the longitudinal deck beams are NOT satisfied for both edge beams and internal beams, with safety factors below unity ($FS = \frac{V_{Rd}}{V_{Ed}} < 1$). The lowest safety factors occur at sections located 2.86 meters from the support axis. The verification fails throughout the entire span from 2.86 meters to 7.30 meters from the support for edge beams, and from 2.86 meters to 5.15 meters for internal beams. For sections characterized by the lowest safety factors, the analysis presents elementary stresses, combined ultimate limit

state stresses, and their comparison with resistant stresses. Based on these findings, the longitudinal deck beams, both edge and internal, are NOT classified as adequate regarding ultimate limit state shear verifications.

Table 4.1: Elementary stresses - Sez.T1.6

Load	**T1.6_2**	
	N [kN]	**V [kN]**
dead	-5.3	-481.6
permanent	-1.9	-179.1
wind	-0.2	-17.3
traffic-Vmin	-5.4	-869.3
remaining area	0.1	6.8
precompression	-4756.7	430.5

Table 4.2: ULS shear verification Sez.T1.6

sez.	$\mathbf{N_{Ed}}$ **[kN]**	$\mathbf{V_{Ed}}$ **[kN]**	$\mathbf{A_{sw}/s}$ **[cm^2/m]**	**d [m]**	$\mathbf{b_w}$ **[m]**	$\cot\theta$ **[-]**	$\mathbf{V_{Rd,s}}$ **[kN]**	**FS [-]**
T1.6_2	-4773.1	-1584.4	6.28	2.01	0.215	2.50	1030.7	0.65

When verification through standard code provisions is not satisfied, this does not necessarily indicate that the structure lacks load-bearing capacity, but rather suggests that alternative verification approaches must be considered. These advanced methodologies should incorporate the nonlinear aspects of the problem, including material aging effects, deterioration processes, and potential variations in structural schemes within the system due to the inherent characteristics of construction materials such as concrete and steel. Therefore, it is deemed necessary to model these elements using Strut and Tie models or through nonlinear finite element analyses, an approach that will be explored in depth in this research work. For completeness, a possible Strut and Tie modeling scheme for the half joint at piers and abutments is included.

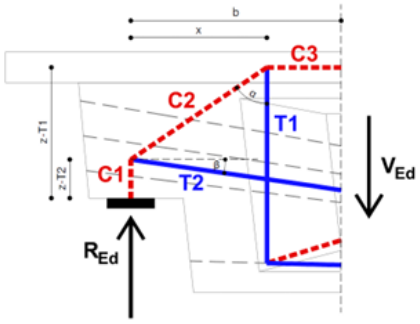

Figure 4.29: Strut and Tie scheme for half-joint element of Gerber beam

4.3.2 Design Code: Shear Assessment

The definition of design actions for the viaduct was calculated primarily according to the following standards:
- Italian Ministry of Public Works Circular n. 384 dated February 14, 1962;
- Italian Ministry of Public Works Decree dated June 16, 1976.
These regulatory frameworks were employed for the design of the analyzed viaduct and prescribed verifications based on allowable stress methods. The actions acting on the section considered critical for shear verification (about 3 meters from the bearing), according to currently applicable standards, are summarized in the following table.

Table 4.3: Load cases and shear forces for T1.6_2

T1.6_2	
load	**V (kN)**
dead	-481.6
permanent	-179.1
precompression	430.5
wind	-17.3
traffic	29

Specifically, dead loads, permanent loads, and prestressing loads remain unaltered, while traffic loads are based on civil load scheme 1.

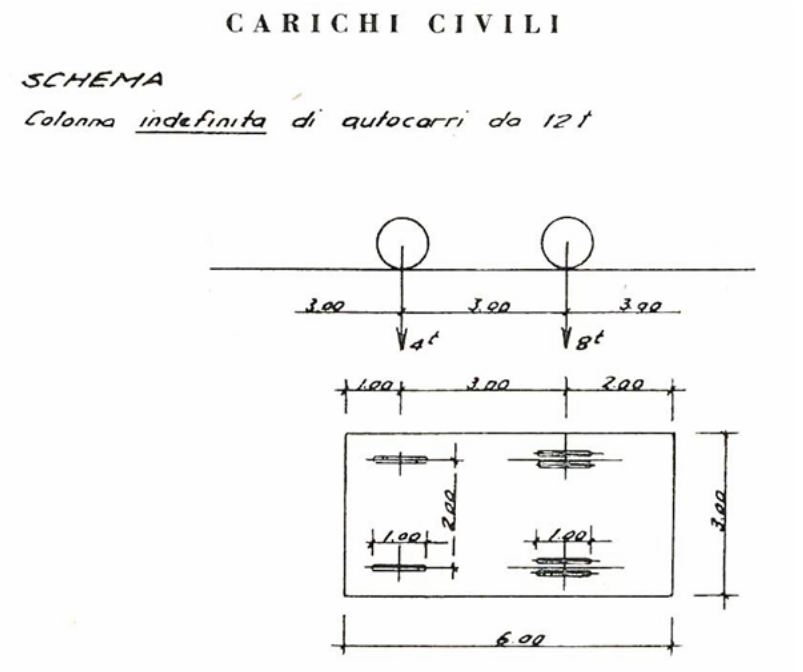

Figure 4.30: Load scheme 1 from Italian Ministry of Public Works Circular n. 384 dated February 14, 1962

In particular, the variable load values in tons/m can be determined as a function of the span length of the considered viaduct by the table offered by the code:

Segue CARICHI RIPARTITI EQUIVALENTI

Luce m	Carichi flettenti p_1 in t/ml					Luce m	Carichi taglianti p_2 in t/ml				
	Carichi civili		Carichi militari				Carichi civili		Carichi militari		
	Schema 1	Schema 2	Schema 4	Schema 5	Schema 6		Schema 1	Schema 2	Schema 4	Schema 5	Schema 6
23	2,028	1,432	4,000	4,304	4,475	23	2,359	1,497	4,829	4,827	5,261
24	2,028	1,378	3,936	4,286	4,363	24	2,333	1,438	4,795	4,778	5,091
25	2,022	1,327	3,870	4,257	4,255	25	2,330	1,382	4,750	4,742	4,930
26	2,036	1,280	3,818	4,220	4,151	26	2,320	1,331	4,702	4,720	4,778
27	2,041	1,236	3,790	4,177	4,051	27	2,305	1,284	4,664	4,709	4,635
28	2,041	1,196	3,766	4,145	3,954	28	2,296	1,240	4,634	4,702	4,500
29	2,036	1,157	3,737	4,118	3,860	29	2,283	1,199	4,600	4,688	4,372
30	2,031	1,121	3,703	4,106	3,771	30	2,267	1,160	4,559	4,665	4,251
31	2,031	1,088	3,666	4,104	3,685	31	2,264	1,124	4,515	4,635	4,137
32	2,031	1,056	3,626	4,105	3,602	32	2,258	1,090	4,477	4,608	4,028
33	2,028	1,026	3,584	4,110	3,522	33	2,248	1,058	4,436	4,591	3,924
34	2,021	0,997	3,567	4,125	3,446	34	2,242	1,028	4,391	4,578	3,825
35	2,012	0,971	3,567	4,137	3,327	35	2,233	0,999	4,357	4,571	3,732
36	2.012	0,945	3,583	4,157	3,302	36	2,222	0,972	4,340	4,568	3,642
37	2.010	0,921	3,612	4,169	3,233	37	2,221	0,947	4,330	4,558	3,557
38	2,017	0,898	3,634	4,174	3,168	38	2,216	0,922	4,314	4,543	3,475
39	2,020	0,876	3,648	4,173	3,105	39	2,209	0,899	4,294	4,523	3,397
40	2,020	0,856	3,657	4,167	3,044	40	2,205	0,878	4,276	4,508	3,323
45	2,015	0,765	3,673	4,107	2,771	45	2,181	0,782	4,212	4,475	2,993
50	2,010	0,691	3,658	4,116	2,541	50	2,163	0,706	4,135	4,429	2,722
55	2,010	0,631	3,646	4,138	2,345	55	2,147	0,643	4,079	4,400	2,496
60	2,004	0,580	3,621	4,107	2,177	60	2,133	0,590	4,041	4,380	2,304
70	2,005	0,500	3,570	4,124	1,903	70	2,116	0,507	3,962	4,337	1,997
80	2 005	0,439	3,602	4,104	1,689	80	2,101	0,444	3,923	4,306	1,762
90	2,003	0,391	3,597	4,107	1,518	90	2,089	0,396	3,878	4,286	1,576
100	2,003	0,353	3,577	4,112	1,379	100	2,079	0,356	3,849	4,268	1,426
120	2,001	0,295	3,583	4,107	1,164	120	2,061	0,289	3,799	4,239	1,197
140	2,002	0,253	3,570	4,103	1,007	140	2,051	0,255	3,765	4,220	1,031
160	2,001	0,222	3,577	4,104	0,887	160	2,043	0,224	3,741	4,205	0,906
180	2,000	0,198	3,572	4,106	0,793	180	2,037	0,199	3,722	4,190	0,808
200	2,001	0,178	3,571	4,086	0,717	200	2,033	0,179	3,707	4,179	0,729

Figure 4.31: Equivalent distributed loads from Italian Ministry of Public Works Circular n. 384 dated February 14, 1962

The action combinations according to the standards are interpreted as a simple summation of contributions with combination factors equal to 1. Therefore, the total shear acting on the critical section becomes:

$$V = 264,2 \text{ kN} \tag{4.17}$$

Shear Assessment

For shear verification according to allowable stresses for prestressed reinforced concrete structures in accordance with the law of November 5, 1971 (Part 2 of the Italian

Ministry of Public Works Decree dated June 16, 1976), if the principal tensile stress value is less than or equal to $0.02R'_{ck}$, it is not necessary to undertake the calculation of shear reinforcement, but it is nonetheless required to provide at least 3 stirrups per linear meter of the considered beam. Considering the beam cross-section net of the prestressing cable ducts, the acting shear stress is computed according to the Jourawski's formulation as follows:

$$\tau = \frac{V \cdot S_x}{I_x \cdot b} = 7.00 \text{ MPa} \tag{4.18}$$

where:

- V (kN) is the acting shear force from the action combination according to Italian Ministry of Public Works Circular n. 384 dated February 14, 1962
- S_x (mm^3) is the first moment of area of the cross-section net of prestressing cable ducts about the strong centroidal axis
- I_x (mm^4) is the second moment of area of the cross-section net of prestressing cable ducts about the strong centroidal axis
- b (mm) is the width of the cross-section at the centroidal axis

Considering the material properties of the cross-section components with a concrete having a characteristic cylindrical compressive strength of 450 kg/cm^2, the allowable limit stress value is:

$$\tau = 0.02 \cdot R'_{ck} = 9 \text{ MPa} \tag{4.19}$$

Verification Results

From the shear verification according to allowable stresses performed on the cross-section that appears critical under current applicable standards, it is evident that the section satisfies the verification requirements as per the original design. This finding underscores an important consideration: the cross-section is not inherently deficient in terms of structural shear capacity, but rather the transition from historical design

standards to contemporary regulatory frameworks, combined with the substantial increase in design loads—particularly variable and traffic loads—has resulted in this section being flagged as critical.

This analysis highlights the evolutionary nature of structural design codes and loading requirements. The original design, which was adequate under the standards and loading conditions of its time (Italian Ministry of Public Works regulations from 1962 and 1976), demonstrates satisfactory performance when evaluated using the allowable stress methodology for which it was conceived. However, the implementation of modern safety factors, updated load combinations, and increased traffic loading scenarios in current standards has effectively reclassified this previously adequate section as requiring attention.

The implications of this finding extend beyond the immediate structural assessment, revealing the broader challenge faced when evaluating existing infrastructure against contemporary design criteria. While the structure maintains its original design integrity, the evolving demands of modern usage patterns and enhanced safety requirements necessitate careful consideration of potential strengthening measures or operational limitations to ensure compliance with current standards.

Therefore, further verification using more sophisticated analytical methods, such as strut-and-tie modeling or nonlinear finite element analysis, may be considered to more accurately represent the true shear capacity of the cross-section. Such advanced computational approaches can capture complex material behaviors, stress redistribution mechanisms, and three-dimensional effects that simplified hand-calculation methods inherently cannot account for. This refined analysis could potentially demonstrate that the actual structural capacity exceeds the values predicted by conventional verification procedures, thereby providing a more realistic assessment of the section's performance under current loading scenarios.

4.3.3 Strut and Tie model verification

Strut-and-Tie model verification (Struts&Ties) for the ultimate limit state verification of Struts&Ties models, reference has been made to the criteria and provisions specified in UNI EN1992-1-1 at section §6.5. Particular attention is paid to the ver-

ification of ties (steel side) and the verification of nodes (concrete side). Regarding the ties, the verification is conducted according to the following criterion.

$$FS = \frac{T_{Rd}}{T_{Ed}} \geq 1; \quad T_{Rd} = A_s \cdot f_{yd} \tag{4.20}$$

where As represents the tie area while fyd represents the design yield stress of the steel, whether prestressing or ordinary reinforcement. If the Safety Factor (FS) is greater than unity, the verification is considered satisfied. Regarding nodes, the design values of compressive stresses can be determined as follows for different node types: CCC nodes representing compressed nodes where no ties are anchored within the node, CCT nodes representing compressed-tensile nodes with ties anchored in the node in a single direction, and CTT nodes representing compressed-tensile nodes with ties anchored in two directions.

$$\sigma_{Rd,max-CCC} = k_1 \cdot \nu' \cdot f_{cd} \tag{4.21}$$

$$\sigma_{Rd,max-CCT} = k_2 \cdot \nu' \cdot f_{cd} \tag{4.22}$$

$$\sigma_{Rd,max-CCT} = k_3 \cdot \nu' \cdot f_{cd} \tag{4.23}$$

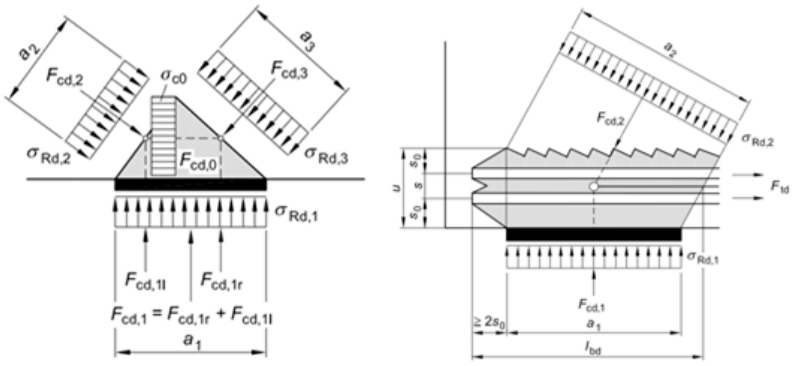

Figure 4.32: sx) CCC node; dx) CCT node

where f_{cd} represents the design compressive strength of concrete, k1, k2 and k3 are coefficients that account for the stress state of the node and equal 1.0, 0.85 and 0.75 respectively, while ν', in accordance with the national annex, is assumed equal to 0.83. The verification is considered satisfied if the stress transferred from the struts

to the nodes is lower than that evaluated according to the previous relationships.

4.3.4 Proposed Retrofitting Technique

Technical analysis has identified that while the structure maintains adequate performance for current service conditions, enhancement interventions are recommended to ensure optimal long-term operability, particularly regarding shear capacity optimization at critical sections. The longitudinal deck beams require shear reinforcement enhancement at the extremities near the supports, where stress concentrations are most significant. This intervention represents a proactive measure to enhance structural performance rather than addressing immediate deficiencies. Based on the assessment findings, interventions are proposed for achieving optimal operational conditions which, in accordance with LG21, must be designed and implemented within a 5-year timeframe. The primary intervention focuses on optimizing the shear resistance of longitudinal deck beams through targeted reinforcement at critical sections. The shear reinforcement enhancement at beam extremities involves the application of advanced composite reinforcement systems specifically designed for shear capacity enhancement. Carbon fiber reinforced polymer systems will be strategically applied to the longitudinal edge beams, extending up to a distance of 6.0 meters from the support axis. This enhancement measure addresses the critical shear zones where maximum stress transfer occurs between the deck structure and the supporting elements. The intervention methodology utilizes externally bonded carbon fiber strips configured to optimize shear resistance while maintaining structural continuity and aesthetic integrity.

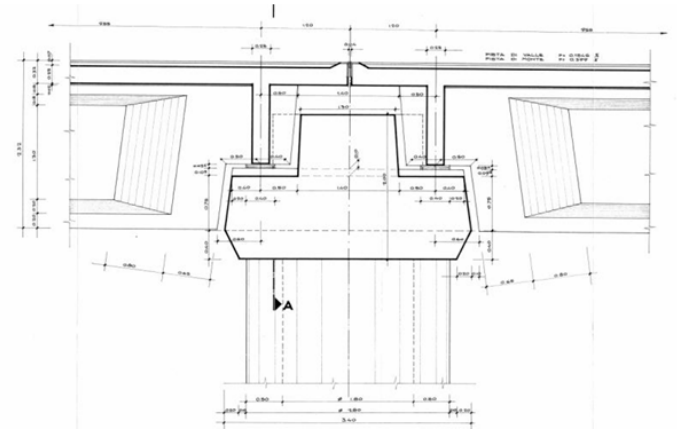

Figure 4.33: Frontal view of the elements potentially subjected to retrofitting

The reinforcement system is designed to enhance shear capacity at critical support regions, provide long-term durability under service conditions, integrate seamlessly with existing structural elements, and allow for future inspection and maintenance activities. Implementation will follow established industry standards for composite reinforcement applications, ensuring proper surface preparation, adhesive systems, and quality control procedures throughout the installation process. This comprehensive approach ensures that the structure will continue to provide reliable service while meeting contemporary performance standards and regulatory requirements.

Chapter 5

Non linear FEM Analysis-Ansys

5.1 Introduction

Following the global structural verification performed in the previous chapter, it was observed that cross-section T1.6_2, located at 2.86 m from the support of the edge beam, exhibited an unsatisfactory shear resistance safety factor, with a deficit of approximately 35%. To address this critical issue, a localized modeling approach was adopted, focusing on the beam segment extending from 2.36 m to 3.36 m along the same beam. The objective of this refined analysis is to simulate the actual structural behavior under ultimate limit state conditions, incorporating material non-linearities and the effective load distribution experienced by the segment.

Finite Element Method (FEM) provides an ideal framework for this investigation, as it enables the detailed representation of complex stress states, progressive material degradation, and failure mechanisms that cannot be adequately captured by simplified analytical methods. Through FEM, the interaction between bending and shear stresses, concrete cracking patterns, and steel reinforcement yielding can be explicitly modeled, offering valuable insights into the actual load-carrying capacity and potential redistribution effects within the critical region. This numerical ap-

proach allows for a more realistic assessment of the structural safety, particularly in cases where conventional design methods may prove overly conservative or fail to capture localized phenomena.

The analysis was conducted using Ansys Mechanical APDL® (ANSYS Parametric Design Language), a powerful finite element analysis software widely recognized for its capabilities in handling non-linear structural problems. Ansys APDL offers advanced material models suitable for reinforced concrete structures, including concrete crushing, cracking, and reinforcement plasticity. The software's robust solver algorithms and extensive element library make it particularly well-suited for simulating the complex behavior of concrete members subjected to combined stress states at ultimate limit conditions. Furthermore, its parametric programming environment facilitates the implementation of iterative analyses and sensitivity studies necessary for comprehensive structural assessment.

5.2 Materials and Non-linearities

Concrete

The concrete matrix was modeled using mechanical properties derived from recent structural inspections, ensuring that the analysis reflects the actual condition of the existing structure. The elastic modulus was set to:
$E = 31.4$ GPa ;
with a Poisson's ratio:
$\nu = 0.2$;
and an average density:
$\rho = 2{,}200$ kg/m^3.
These parameters characterize the linear elastic behavior of the concrete under low stress levels.

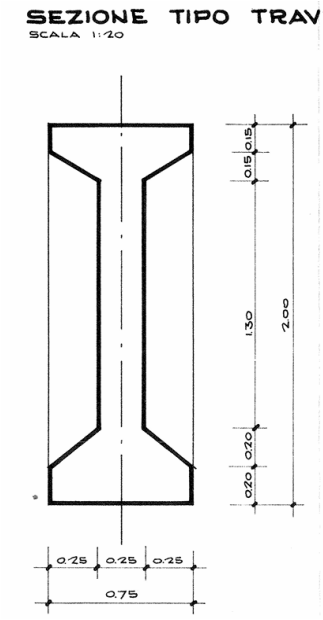

Figure 5.1: Beam transverse section

To capture the non-linear response of concrete under ultimate load conditions, a non-linear concrete cracking and crushing model was employed with the following properties taken from the past literature[9]:

- Open shear transfer coefficient: 0.24
- Closed shear transfer coefficient: 0.48
- Uniaxial cracking stress: 2,400 kN/m^2
- Uniaxial crushing stress: 24,000 kN/m^2

This constitutive model accounts for the progressive degradation of stiffness as the material approaches its compressive strength, as well as the brittle tensile behavior leading to cracking. The model incorporates both material non-linearity, through the stress-strain relationship beyond the elastic range, and captures the essential failure mechanisms of concrete. Crack formation and propagation were simulated using appropriate failure criteria, allowing the analysis to predict concrete crushing in compression zones and tensile cracking patterns that develop as the ultimate limit state is approached.

To model the concrete elements, the SOLID65 element type was selected, which

features an 8-node solid element with three degrees of freedom per node (translations in x, y, and z directions). This element is specifically designed for the analysis of reinforced concrete structures and is capable of simulating cracking in tension and crushing in compression.The detailed characteristics of this element are specified in Appendix A.

Steel Reinforcement

The reinforcement steel was modeled with the following mechanical properties:
elastic modulus:
$E = 206$ GPa;
Poisson's ratio:
$\nu = 0.3$;
and density:
$\rho = 7{,}850$ kg/m^3.

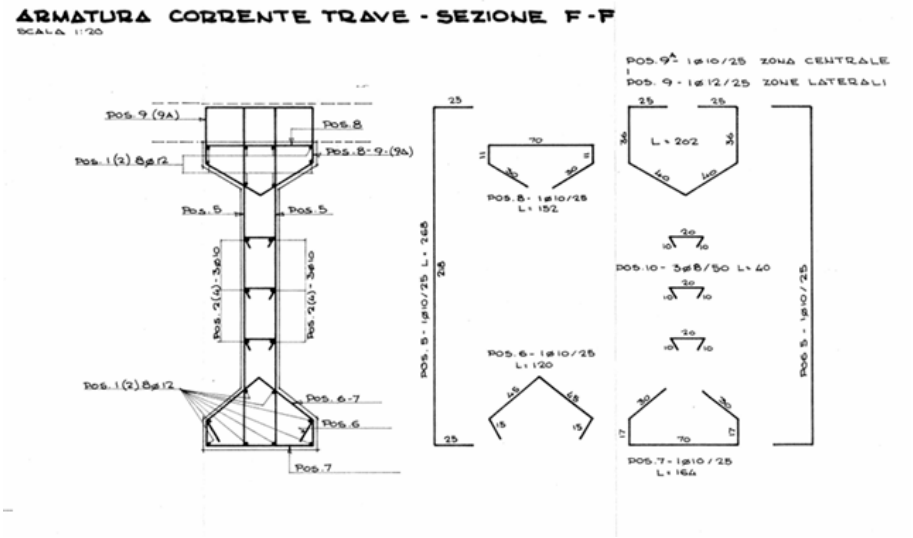

Figure 5.2: Beam Reinforcements' layouts

For the nonlinear response of the material, a bilinear kinematic hardening constitutive model was used with the following properties:

- Yield stress: 235 MPa

- Tangent modulus: 0 MPa (perfectly plastic behavior after yielding)
- Stress-strain rule: kinematic hardening rule (Rice model)

The element type used for modeling the reinforcement bars is LINK180, which is a 1D truss element with no flexural resistance.The detailed characteristics of this element are specified in Appendix B.

Prestressing Tendons

The prestressing tendons were modeled with a linear isotropic constitutive model with elastic modulus $E = 206$ GPa, Poisson's ratio $\nu = 0.3$, and density $\rho = 7{,}850$ kg/m^3, since the focus is not on the plastic capacity of the tendon under external loads but only on the stress state it induces in the concrete matrix.

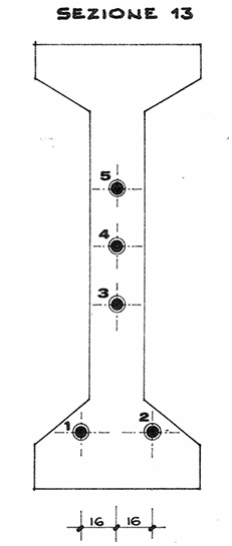

Figure 5.3: Section Prestressing Tendons' layout

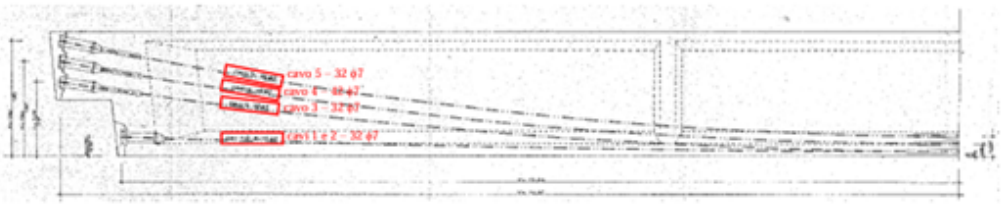

Figure 5.4: Beam Prestressing Tendons' layout

5.3 Boundary Conditions, Constraints and Load Application

To accurately simulate the structural behavior of the beam segment, it is essential to properly represent the boundary conditions and load distributions experienced by the extracted portion. As discussed in the previous chapter, the global beam model was analyzed as a simply supported structure. The local beam segment was therefore constrained to ensure structural continuity at its initial and final cross-sections, while respecting the overall support conditions.

Specifically, roller-type constraints were positioned on both faces oriented perpendicular to the beam longitudinal axis to restrain translations along the beam axis, thereby allowing the stresses activated by prestressing to develop and act within the segment while ensuring continuity with adjacent portions. At the base of the segment, hinge constraints were implemented to restrain the remaining degrees of freedom. This constraint configuration was necessary due to the highly nonlinear nature of the analysis and to prevent unrealistic deformations inconsistent with the actual structural behavior, while simultaneously maintaining the appropriate degrees of freedom to simulate the real boundary conditions of the segment within the continuous beam system.

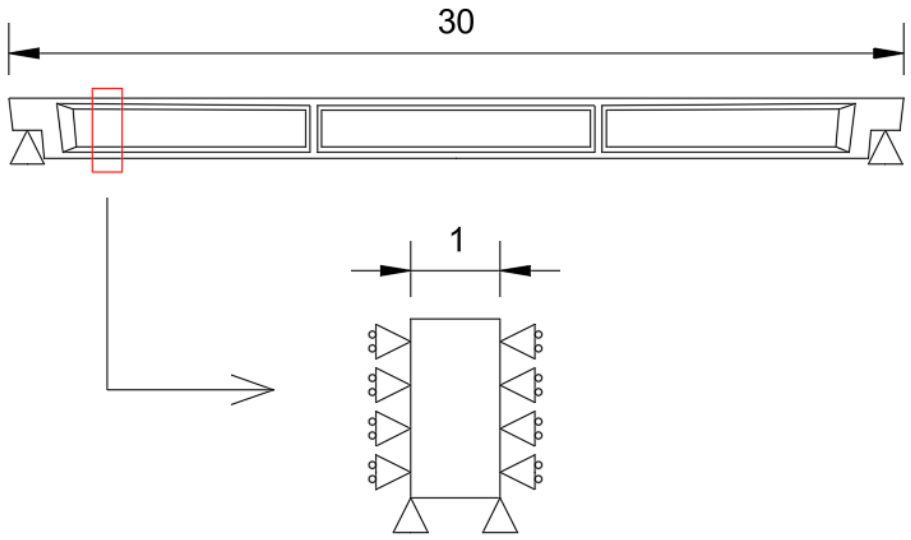

Figure 5.5: Local model scheme with respect to the global one

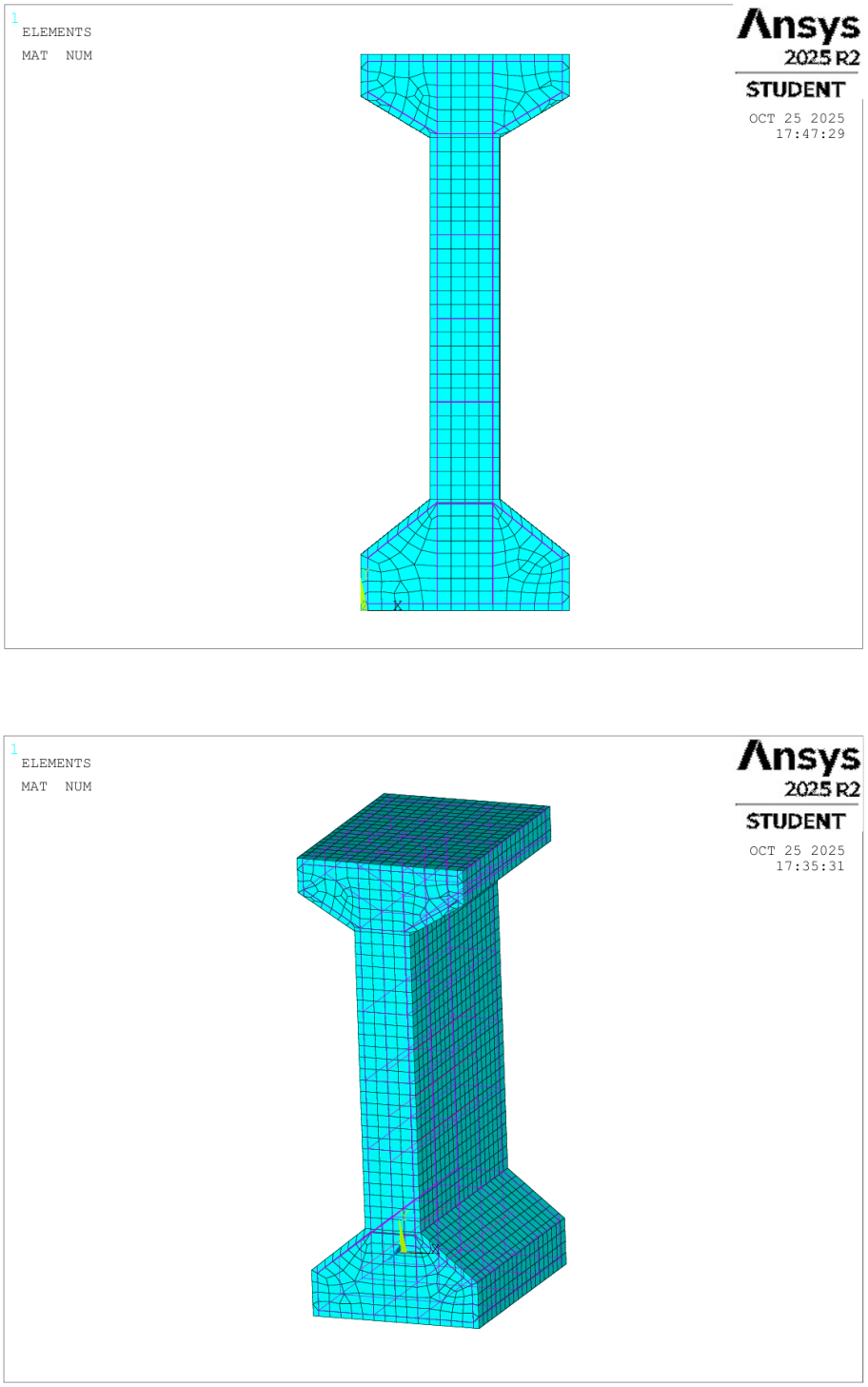

Figure 5.6: Local model scheme with reinforcements' layout

On one face, it was necessary to reproduce the internal forces acting on the segment due to beam continuity. Consequently, the shear force and bending moment at

2.36 m from the support were applied according to the ultimate limit state load configuration for shear verification of the analyzed section:

$$V_{Ed} = -1{,}600 \text{ kN}$$

$$M_{Ed} = 1{,}000 \text{ kNm}$$

The applied shear force and bending moment were distributed over the cross-section according to the stress resultants, ensuring consistency with the internal force distribution obtained from the global analysis. This approach allows the local model to capture the actual stress state and failure mechanisms that develop in the critical region under ultimate loading conditions, while maintaining compatibility with the boundary conditions imposed by the adjacent beam portions. Specifically, the bending moment was modeled as a linear distribution of normal stresses to induce compression and tension states relative to the neutral axis of the cross-section, while the shear force was applied as a distribution of tangential stresses.

Prestressing forces are induced in the structure through five tendons of varying cross-sections, which are inclined along the beam segment. To represent the forces transmitted to the structure, the tendons were modeled as straight elements, accounting for the equivalent shear and moment forces arising from the absence of inclination in the model. Specifically, these stresses are superimposed on those previously derived from the global analysis actions, being concordant in direction due to the proximity of the considered section to the support. This results in a total tangential shear force of:

$$V_{Ed} = -2{,}095 \text{ kN}$$

Furthermore, the axial prestressing force in the tendons was modeled through the application of a uniform thermal load. By assigning a coefficient of thermal expansion exclusively to the tendons ($\alpha = 1 \times 10^{-5}$ °C^{-1}), and applying a constant thermal load of $\Delta T = -350$ °C, the same stress state as the actual cable is achieved. This approach induces a compression state in the surrounding concrete matrix, which, having no assigned thermal expansion coefficient, does not respond in terms of strain but only experiences the resulting stress state transferred from the prestressing ten-

dons through bond interaction.

Therefore, the loads acting on the beam segment were considered as the combination of the following load components:

- **Global analysis forces:**
  - Shear force: $V_{Ed} = -2{,}095$ kN
  - Bending moment: $M_{Ed} = 1{,}000$ kNm
- **Permanent non-structural loads:**
  - Pavement: 9.6 kN/m
  - Reinforced concrete curb: 1.08 kN/m
  - Metallic safety barrier: 1.50 kN/m
- **Traffic loads:**
  - Uniformly distributed load (UDL): $q_{i,k} = 27$ kN/m
  - Tandem system: $Q_{i,k} = 300$ kN
- **Prestressing tendons:**
  - Temperature variation: $\Delta T = -350$ °C

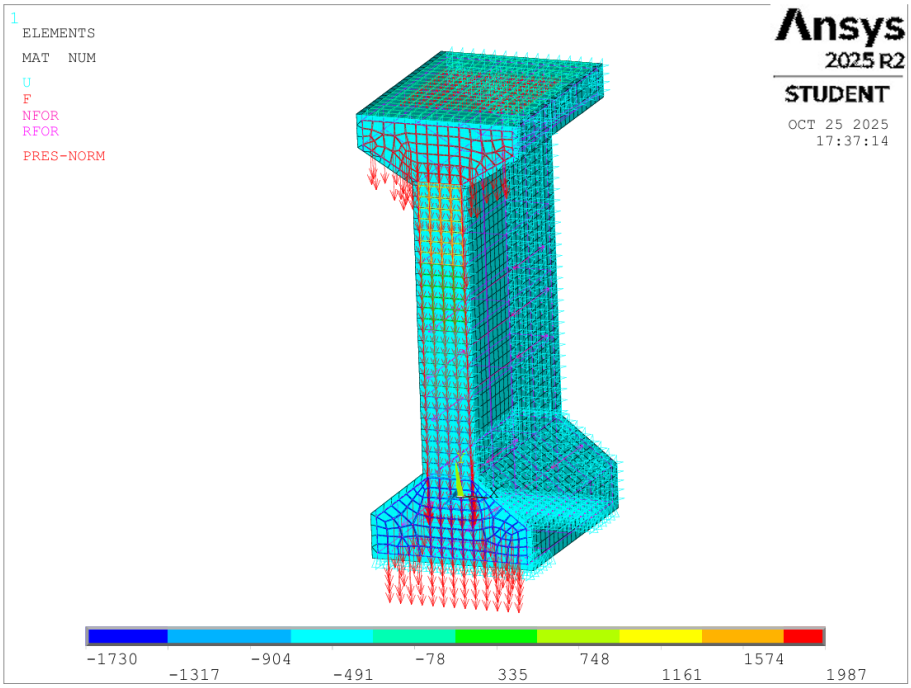

Figure 5.7: Local model with applied loads in kN

5.4 Convergence Procedure and Analysis Results

Given the highly nonlinear nature of the model, it was necessary to configure the analysis for convergence to ensure the absence of stress peaks at particular nodes and to prevent unrealistic deformations in specific portions of the model. To guarantee these conditions, following the modeling of the concrete matrix, reinforcement bars, and prestressing tendons, a solid mesh was generated for concrete elements and a linear mesh for steel elements, maintaining the most regular and simple element size distribution possible.

For the convergence analysis, loads were applied gradually to ensure a constant stress increment and avoid disproportionate peaks. Specifically, for the load case, the following settings were implemented:

```
                    S O L U T I O N   O P T I O N S

PROBLEM DIMENSIONALITY. . . . . . . . . . . . .3-D
DEGREES OF FREEDOM. . . . . . UX  UY  UZ
ANALYSIS TYPE . . . . . . . . . . . . . . . . .STATIC (STEADY-STATE)
OFFSET TEMPERATURE FROM ABSOLUTE ZERO . . . . .  273.00
NONLINEAR GEOMETRIC EFFECTS . . . . . . . . . .ON
PLASTIC MATERIAL PROPERTIES INCLUDED. . . . . .YES
NEWTON-RAPHSON OPTION . . . . . . . . . . . . .PROGRAM CHOSEN
GLOBALLY ASSEMBLED MATRIX . . . . . . . . . . .SYMMETRIC

                    L O A D   S T E P   O P T I O N S

LOAD STEP NUMBER. . . . . . . . . . . . . . . .    1
TIME AT END OF THE LOAD STEP. . . . . . . . . . 0.10000
TIME STEP SIZE. . . . . . . . . . . . . . . . . 0.20000E-03
MAXIMUM NUMBER OF EQUILIBRIUM ITERATIONS. . . .  200
STEP CHANGE BOUNDARY CONDITIONS . . . . . . . .DEFAULT
LINE SEARCH . . . . . . . . . . . . . . . . . .   ON
TERMINATE ANALYSIS IF NOT CONVERGED . . . . . .YES (EXIT)
CONVERGENCE CONTROLS. . . . . . . . . . . . . .USE DEFAULTS
COPY INTEGRATION POINT VALUES TO NODE . . . . .YES, FOR ELEMENTS WITH
                                               ACTIVE MAT. NONLINEARITIES
PRINT OUTPUT CONTROLS . . . . . . . . . . . . .NO PRINTOUT
DATABASE OUTPUT CONTROLS
   ITEM     FREQUENCY   COMPONENT
    ALL        ALL
```

Figure 5.8: Analysis Parameters

Multiple calculation sub-steps were implemented with gradual load incrementation, ensuring model convergence. In particular, a fictitious time step of 0.0002 s was adopted to cycle through the different load increments, within a total analysis time interval of 0.1 s, considering a maximum number of iterations for the calculation of force and displacement equilibrium of 200 iterations.

Upon applying the described loads to the model and performing a nonlinear finite element analysis accounting for material nonlinearities, convergence was achieved. The following plots illustrate the resulting shear stresses distribution on the overall model and specifically on the analyzed section.
The resulting shear stresses are expressed in kN/m^2, consistent with the units adopted during the modeling phase.

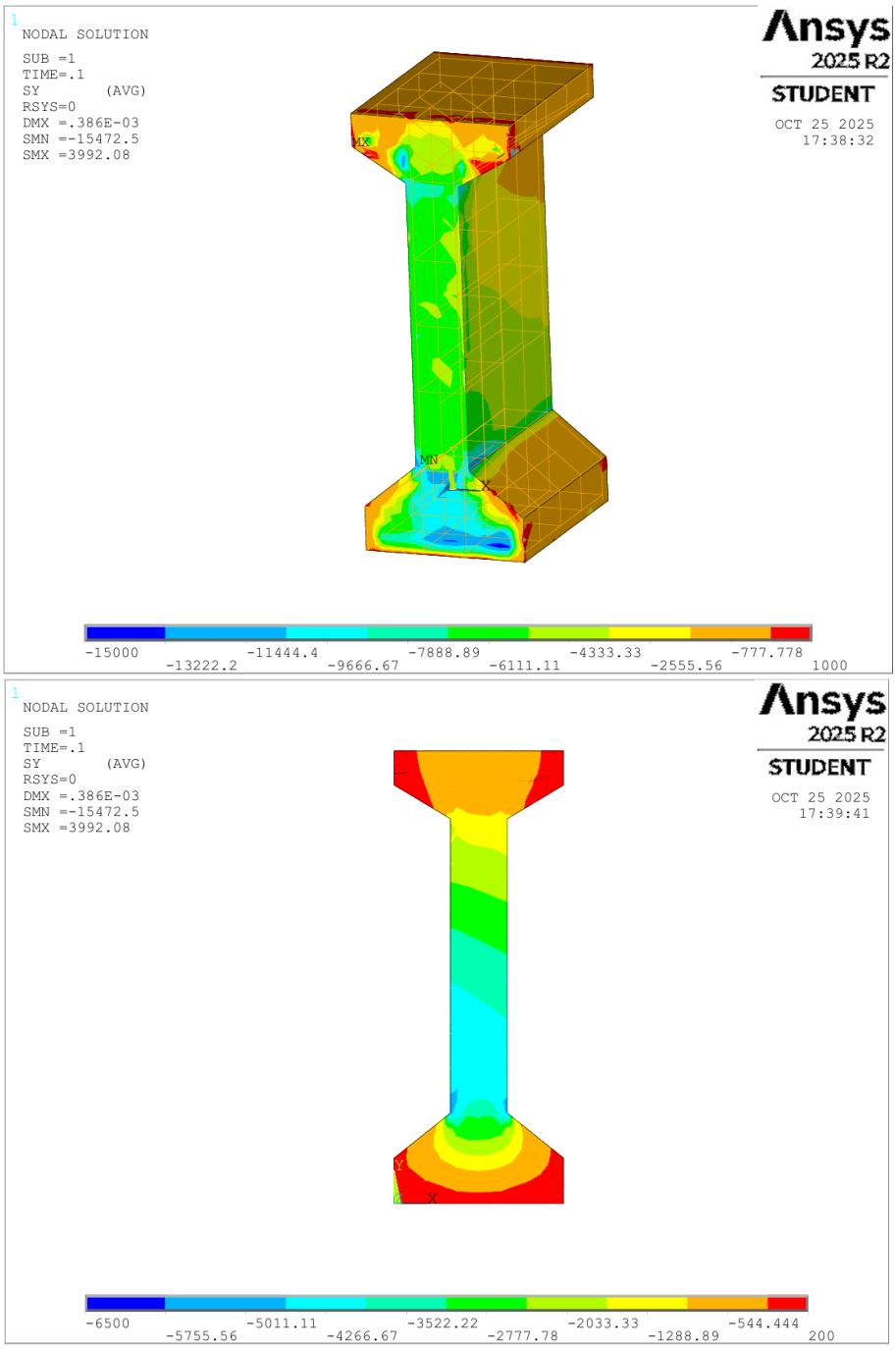

Figure 5.9: Tangential stresses in kN/m^2 on the overall model and on the analyzed section under the described loading condition

The nonlinear finite element model demonstrated improved shear capacity and overall structural performance under applied loads. Notably, when subjected to the same loads for which current code provisions (NTC2018) predicted a safety factor of 0.65, indicating a severe structural capacity deficiency, the nonlinear model showed no collapse mechanisms. Specifically, by exploiting the plastic reserve capacity of materials and utilizing the adopted modeling assumptions, the section resists the loads deemed critical by current standards. This result, acknowledging the modeling approximations that must inevitably be considered, suggests a potential reduction in the extent of structural strengthening interventions. To assess the actual shear resistance capacity of the section, an incremental load analysis was performed, progressively increasing the applied loads beyond the critical values identified by code provisions. The analysis was continued until model failure, and results were extracted from the last converged substep immediately preceding collapse. The resulting shear stress distributions, expressed in kN/m^2 consistent with the modeling units, revealed the ultimate load-carrying capacity of the section.

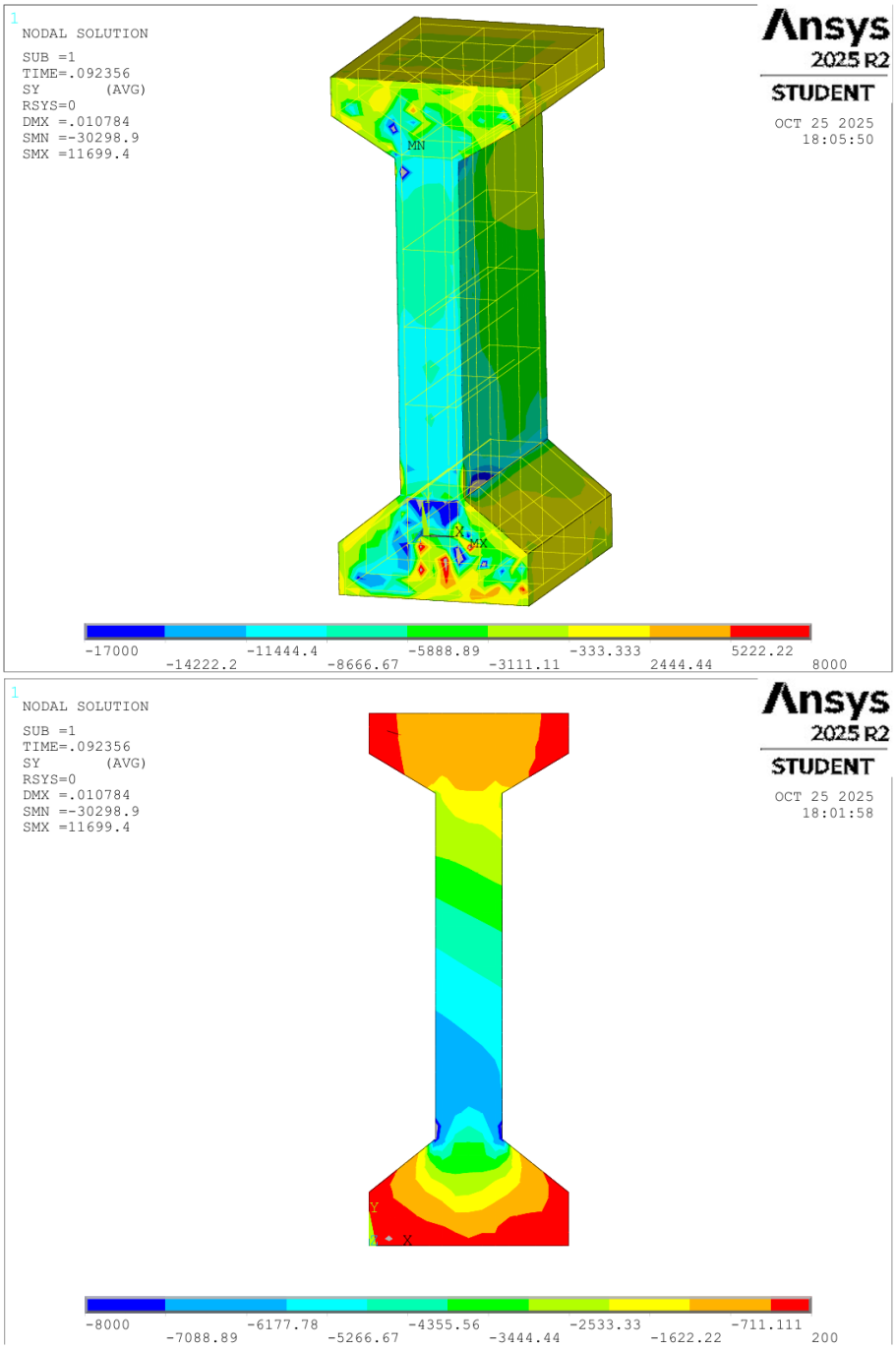

Figure 5.10: Tangential stresses in kN/m^2 on the overall model and on the analyzed section under the ultimate loading condition

In particular, the shear resistance obtained through the nonlinear model was calculated by integrating the corresponding shear stresses over the studied section:

$$V_{Rd} = 1810 \text{ kN}$$

Therefore, a safety factor for the section can be calculated through the nonlinear model:

$$FS = \frac{V_{Rd}}{V_{Ed}} = \frac{1810kN}{1584kN} = 1.14 \tag{5.1}$$

Table 5.1: Safety factor comparison and capacity increase

Method	**Safety Factor [-]**	**Capacity Increase [%]**
NTC2018	0.65	-
Nonlinear FEM Model	1.14	+76.0

Results indicate that the safety factor increased from 0.65 to 1.14, demonstrating that the section can sustain loads significantly higher than those considered critical by current standards. This represents a substantial enhancement in the structural capacity of the section of about 76% and provides additional confidence in its performance under extreme loading.

Moreover, the following two images represent respectively the cracking configuration at failure and the distribution of principal stresses in the prestressed beam.

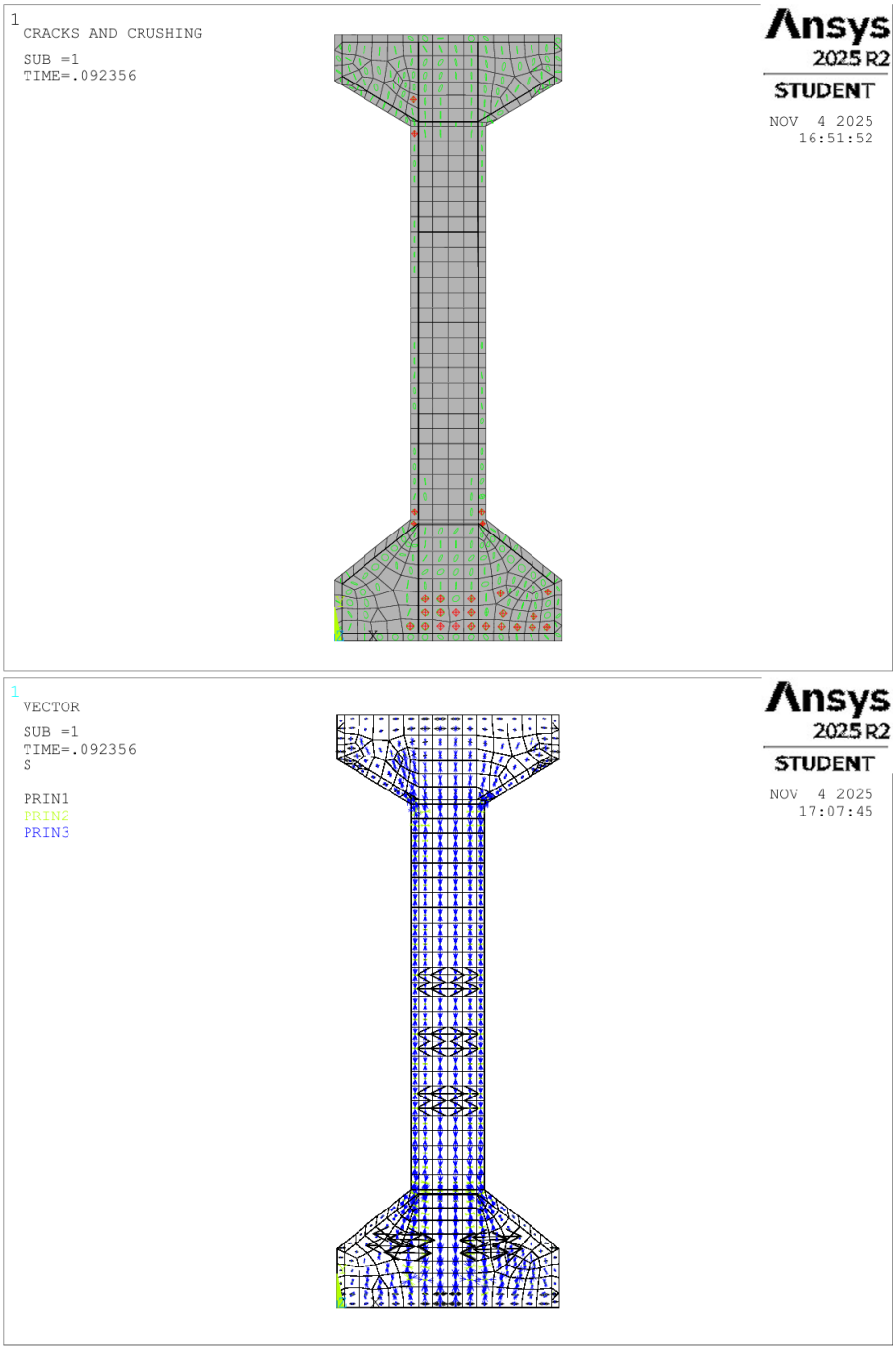

Figure 5.11: Cracking pattern (top) and principal stress vectors' distribution (bottom) in the section at ultimate load configuration.

The upper image displays the concrete cracking and crushing pattern, where red indicates crushed concrete elements and green represents intact concrete regions. The lower image shows the principal stress vectors (displayed as blue lines) oriented

perpendicular to the crack trajectories, consistent with classical reinforced concrete theory. The vector density and orientation indicate that the highest stress concentrations occur at the specimen extremities where prestressing forces are transferred to the concrete, and at the transition zones between the narrow web and the wider end blocks.

An important consideration must be made for the proper interpretation of the model results, as a model with such reduced dimensions may inherently exhibit behavior similar to that of a deep beam, whose structural response differs from conventional beam theory. The development of a probable strut-and-tie mechanism within the segment contributes to an enhancement of the shear capacity of the section. Similarly, the exploitation of the plastic reserve capacity of the materials and the consequent nonlinear behavior of the beam further increases the shear resistance capacity. The results obtained from the model are therefore significantly influenced by both the deep beam effect and the material nonlinearities, as well as by potential scale effects and the imposed boundary conditions in terms of constraints and applied forces, in addition to the plasticity parameters of the concrete matrix.

5.5 Model Validation Procedure

Due to the various factors listed in the previous paragraph that may influence the validity of the model, a validation procedure was necessary to confirm the shear resistance capacity obtained from the local beam segment model. To this end, both an analytical analysis of a global model and a finite element modeling of a more extended beam portion were performed.

The analytical approach consisted of a simplified global model developed using average cross-sectional characteristics and material properties of the beam of interest, implementing the same loading conditions applied to the local model. The following shows the shear diagram in the beam analyzed using the global analytical model and its comparison with the shear values experienced by the local nonlinear model.

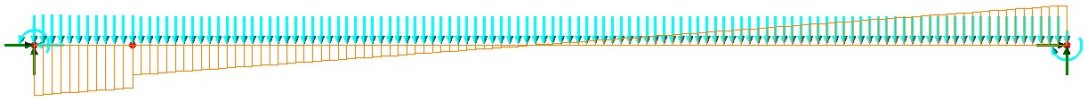

Figure 5.12: Shear diagram and load application on the validation global model; the analyzed section is marked in red

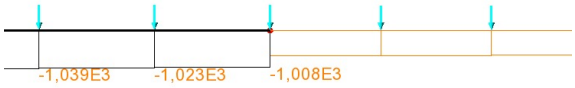

Figure 5.13: Shear Force values in kN around the analyzed section (marked in red)

Table 5.2: Comparison of shear force results between local and global models

FEM Model	**Shear Force [kN]**	**Difference [%]**
Non-linear Local Model	1015	-
Validation Global Model	1008	-0.69

These results confirm that the local model can be considered reliable according to the modeling assumptions adopted and described in the previous sections.

In parallel, a nonlinear finite element analysis developed with ANSYS using the same modeling approach as the local model was performed to verify that the reduced dimensions of the model and the boundary conditions to which it was subjected did not influence the shear resistance of the section. Specifically, a 7-meter-long beam portion was modeled with boundary conditions applied to represent the beam extending from 1 meter after the support up to 8 meters in length.

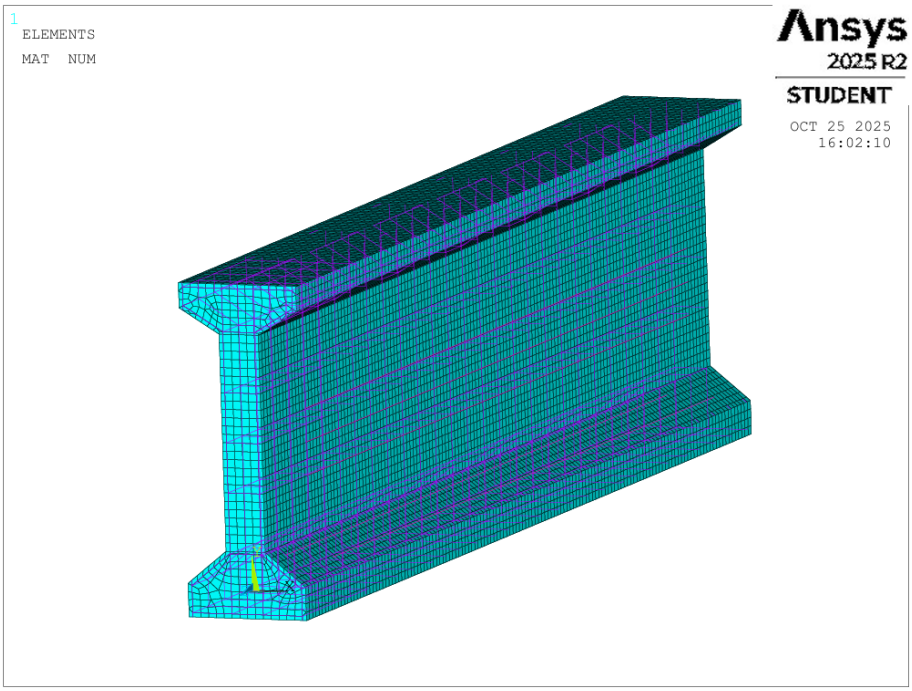

Figure 5.14: Analyzed extended model

To achieve this, the same ultimate loads applied to the local model were imposed, thereby investigating the reliability of the local model.

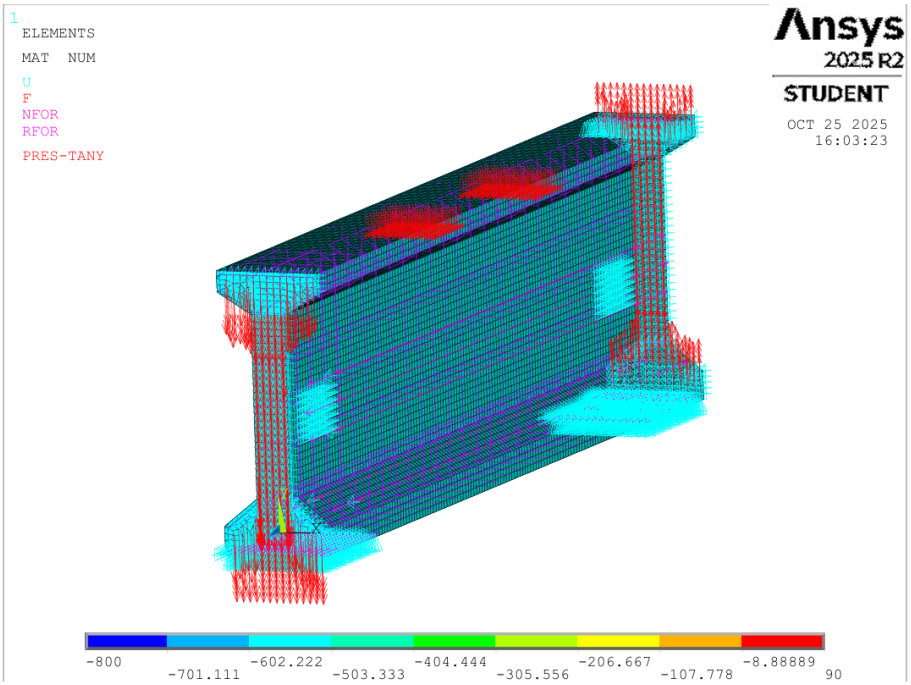

Figure 5.15: Loaded analyzed extended model, with loads in kN

Incrementing the variable loads up to failure, as done in the local model, the analysis revealed that the shear resistance of the section was slightly modified and reduced by approximately 6% with respect to the local model analysis.

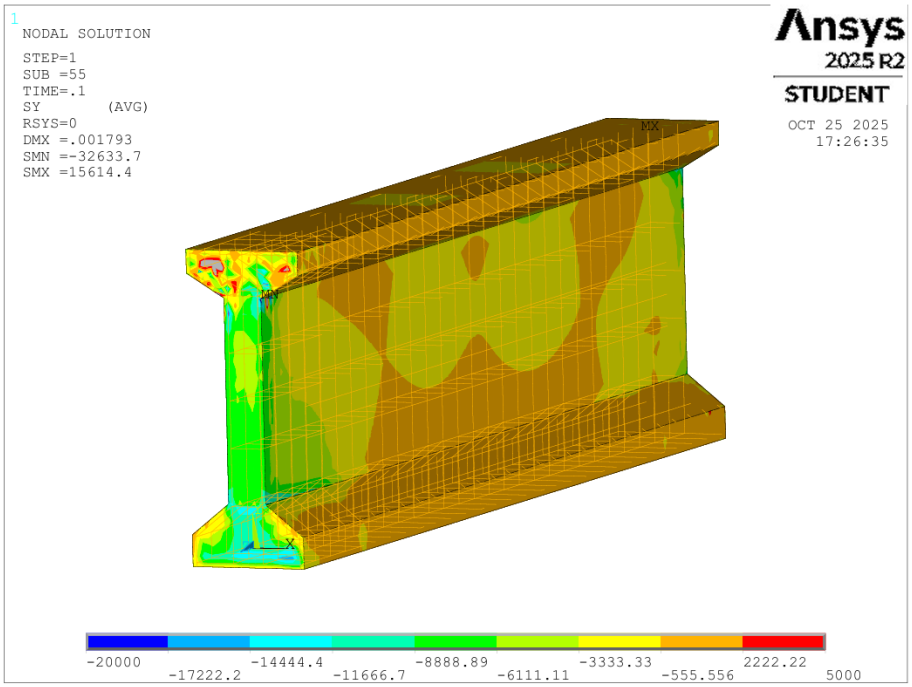

Figure 5.16: Tangential stresses in kN/m^2 on the extended validation model under the ultimate loading condition

This percentage effectively represents the resistance that the local model overestimated; thus, by modeling a more extended beam portion, the more developed beam can resist loads that are lower by the same percentage. This leads to a new developed resistance of the model that can be expressed as:

$$V_{Rd} = 1701 \text{ kN}$$

The shear resistance obtained from the extended model, although reduced compared to that of the local model, still represents a satisfied verification for the section and especially, it validates the reliability of the local model approach developed. This result is confirmed by both types of validation procedures performed: the analytical verification through the simplified global LUSAS model and the nonlinear finite element analysis of the extended beam portion in ANSYS. It can therefore be concluded that the actual shear load-bearing capacity of the section remains in all cases significantly greater than that predicted by current code provisions, ultimately leading to a successful structural verification for the critical half-joint connection.

An additional model was developed to provide a clearer understanding of the crack pattern and support reactions in the simplified configuration under different boundary conditions. This 3-meter model features roller supports constraining the beam bearing and a free face permitted to experience vertical deflections. Equivalent forces representing the internal forces acting on the section within the complete beam were applied to this free surface.

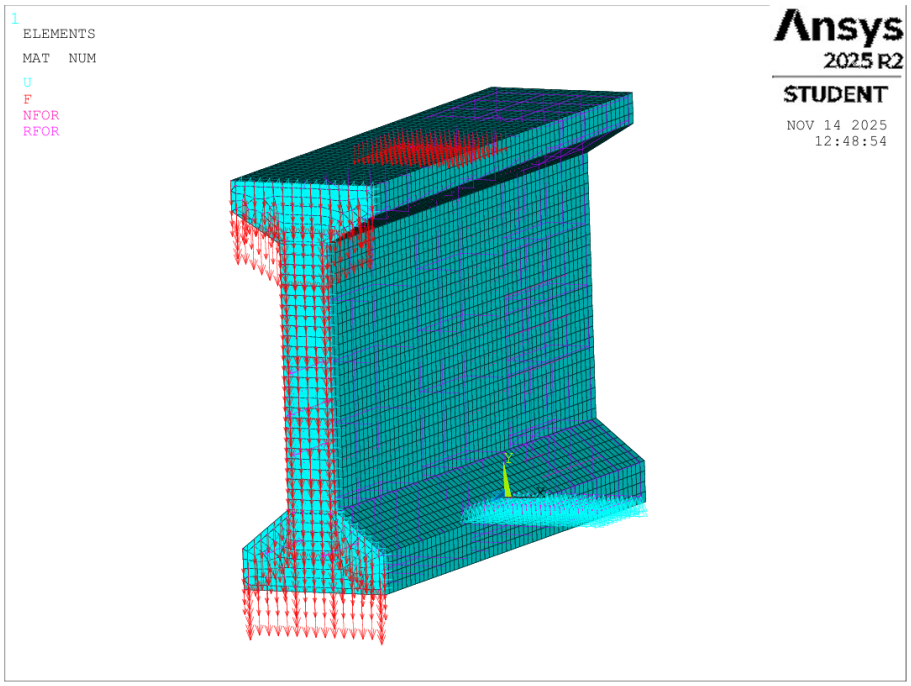

Figure 5.17: Loaded Model of 3m with the different boundary conditions

The most interesting results from the analysis concentrate on the plastic behavior of concrete and its cracking pattern, and on the values of support reactions which are to be compared with those obtained from the model employed in the main analysis.

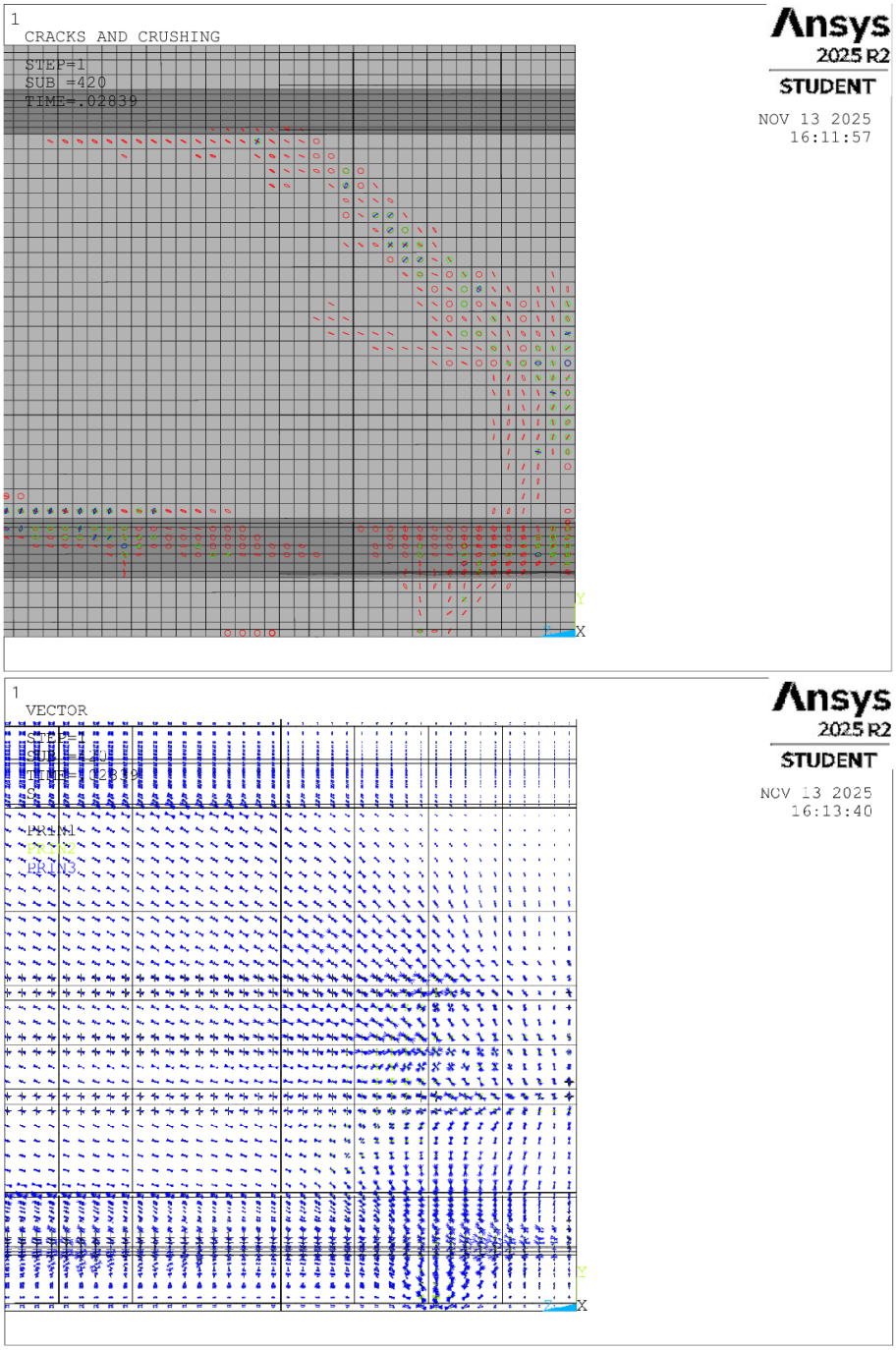

Figure 5.18: Cracking pattern (top) and principal stress vectors' distribution (bottom) in the validation model

In particular, the obtained cracking configuration proves to be compatible with that induced by shear failure in similar beam typologies tested in laboratory conditions as documented in the literature.[18]

Figure 5.19: Shear testing of a 54-inch deep, LWHPC prestressed girder in the Structural Testing Laboratory at the Turner-Fairbank Highway Research Center.

It can be observed that the cracks align in the initial portion of the beam according to an oblique orientation of approximately 45°, denoting shear stress as the governing cause of structural failure. Additionally, the principal stress distributions, which are congruent with the observed crack pattern, are presented.
Concerning the support reactions developed by the model, these were compared with those obtained from the model employed in the strength analysis. The differences result in approximately 2.2%, demonstrating a high level of accuracy in the numerical prediction.

***** POST1 TOTAL REACTION SOLUTION LISTING *****

LOAD STEP= 1 SUBSTEP= 19
TIME= 0.28356E-01 LOAD CASE= 0

THE FOLLOWING X,Y,Z SOLUTIONS ARE IN THE GLOBAL COORDINATE SYSTEM

NODE	FY
13739	1.6872
13740	3.9098
13876	4.9147
13877	4.4952
13878	4.0358
13879	3.7016
13880	0.82555
13881	0.83812
13882	1.0604
13883	1.4686
13884	0.99167
13885	1.0051
13886	1.2414
13887	1.6709
13888	1.2720
13889	1.2922
13890	1.5368
13891	1.9850
13892	1.5433
13893	1.5621
13894	1.8062
13895	2.2561
13896	1.0504
13897	1.1281
13898	1.3314
13899	1.7623
13900	4.0173
14211	0.22762
14212	0.31973
14213	0.46160
14214	0.60168
14218	0.49727

TOTAL VALUES
VALUE 579.36

***** POST1 TOTAL REACTION SOLUTION LISTING *****

LOAD STEP= 1 SUBSTEP= 420
TIME= 0.28390E-01 LOAD CASE= 0

THE FOLLOWING X,Y,Z SOLUTIONS ARE IN THE GLOBAL COORDINATE SYSTEM

NODE	FY
13889	-1.1377
13890	-1.3594
13891	-1.4309
13892	-1.1564
13893	-0.99662
13894	-1.3228
13895	-1.6831
13896	-0.22199
13897	0.15331
13898	0.51135
13899	0.79508
13900	1.1885
14211	-0.37010
14212	-0.48425
14213	-0.46464
14214	-0.16819
14218	-0.39520
16336	-0.26392E-001
16343	-0.22458E-001
16625	-0.74433E-001
16626	-0.29799
16627	0.15682
16628	0.34647
16629	0.23300
16630	0.12949
16631	-0.39078
16632	0.26722
16633	0.21341
16634	0.22447
16635	0.12724
16636	-0.14583
16637	-0.17652E-001

TOTAL VALUES
VALUE 592.49

Figure 5.20: Support reactions at selected bearing nodes and total value in the analyzed model (left) and support reactions at selected bearing nodes and total value in the validation model (right), expressed in kN.

Moreover, Figure 5.21 illustrates the evolution of support reactions during the incremental load application for both models.

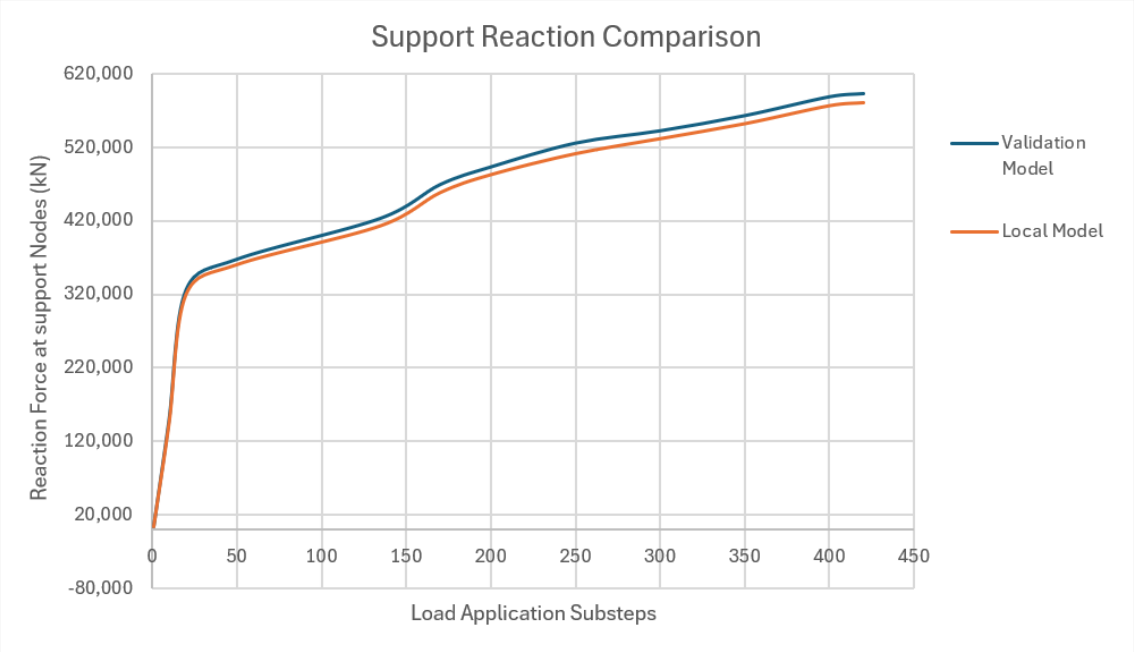

Figure 5.21: Evolution of support reactions vs load application substeps: comparison between validation and local models.

The curves demonstrate excellent agreement throughout the entire loading history. Initially, both models exhibit a linear elastic response up to approximately substep 25, after which a distinct nonlinear behavior develops, as hypothesized. This nonlinearity corresponds to the onset of plasticity in the structure, evidenced by the progressively decreasing slope of the reaction curves. The validation model and the local model converge to final reaction values of approximately 590 kN and 577 kN respectively, confirming the 2.2% difference mentioned above. The close correlation in both the elastic and plastic regimes validates not only the geometric representation but also the material constitutive modeling employed in the local analysis.

5.5.1 Validation Conclusions

In conclusion, the comprehensive validation process conducted in this chapter has demonstrated the robustness and accuracy of the numerical methodology adopted through a systematic progression of verification steps.

The validation strategy began with an analytical approach, verifying the global load distribution behavior and ensuring that fundamental equilibrium conditions were satisfied. This preliminary step established confidence in the basic modeling assumptions and confirmed that the numerical framework correctly captures the overall structural response in terms of internal force distributions and support reactions.

Subsequently, a more detailed 7-meter model was developed to investigate the contribution of size effect and to assess the transition between deep beam and slender beam behavior. This intermediate-scale analysis provided valuable insights into how geometric configurations influence the structural response and confirmed that the modeling assumptions remain valid across different scales, bridging the gap between simplified representations and more detailed local models. Incrementing the variable loads up to failure, as performed in the local model, the analysis revealed that the shear resistance of the section was slightly modified and reduced by approximately 6% with respect to the local model analysis. This difference can be attributed to the size effect and the different boundary conditions inherent to the extended geometric configuration, confirming the importance of local refinement in critical regions for accurate ultimate capacity prediction.

The local 3-meter model, refined from the global analysis through the submodeling technique, demonstrated excellent agreement with the validation model employed in the strength analysis. The support reactions showed a difference of only 2.2%, and the evolution of these reactions throughout the loading history was consistently captured by both models. Particularly noteworthy is the accurate prediction of the transition from linear elastic to nonlinear plastic behavior at approximately substep 25, validating both the geometric representation and the material constitutive modeling. Furthermore, the detailed cracking patterns obtained from the local model show good correlation with experimental evidence documented in the literature,

particularly regarding the characteristic diagonal crack formation associated with shear-dominated failure mechanisms.

Regarding regulatory compliance, the nonlinear finite element model developed in this research for the shear capacity assessment of prestressed Gerber beam half-joints fully complies with the provisions established by both NTC2018 and Eurocode 2 for nonlinear structural analysis. The analysis satisfies equilibrium conditions through proper constraint implementation and load application, while ensuring compatibility through appropriate element formulations and mesh configurations. The model employs realistic stress-strain relationships for both concrete and steel materials that adequately represent their actual behavior, as required by Section 4.1.1.3 of NTC2018 and Section 5.7 of Eurocode 2. The material constitutive models implemented in the ANSYS finite element environment, including the concrete cracking and crushing model for the concrete matrix and the bilinear kinematic hardening model for reinforcement steel, represent the nonlinear behavior of materials in accordance with code requirements. The analysis explicitly accounts for material nonlinearities through progressive stiffness degradation in concrete and plastic yielding in steel reinforcement, capturing the actual load-carrying mechanisms and stress redistribution phenomena that occur as the structure approaches ultimate limit conditions. Furthermore, the model verifies that critical sections can sustain the inelastic deformations resulting from the analysis at ultimate limit state, with appropriate consideration of uncertainties, as prescribed by both regulatory frameworks. The monotonic incremental loading procedure implemented ensures consistent stress development and enables accurate identification of the ultimate load-carrying capacity without introducing artificial load history effects, in full accordance with the provisions that require neglecting previous load applications and assuming a monotonic increase in action intensity with constant proportions between their intensities.

Collectively, these validation analyses demonstrate the overall reliability and accuracy of the modeling strategy employed. The consistency observed across different model scales, boundary conditions, and verification approaches provides confidence in the predictive capabilities of the numerical framework and establishes a solid foundation for the detailed analysis and performance assessment of the structure. Nevertheless, opportunities for further validation remain, particularly through com-

parison with full-scale experimental testing or more refined three-dimensional simulations, which could be pursued in future research to enhance the robustness of the conclusions drawn from this study.

Chapter 6

Results and Discussion

6.1 Conclusions

This thesis, developed in collaboration with SINA S.p.A. of the ASTM Group, investigated the structural adequacy of prestressed Gerber beam bridges constructed during Italy's 1970s highway infrastructure expansion, with particular focus on the critical shear assessment of girder beam end half-joints. These structural elements exhibit insufficient transverse reinforcement according to contemporary design standards, raising concerns about their long-term serviceability and safety. To accurately evaluate the actual load-bearing capacity of these critical structural elements, an advanced nonlinear finite element model was implemented using ANSYS software. The model incorporates material plasticity, prestressing effects, concrete cracking behavior, and realistic loading conditions to simulate the complex stress distribution patterns and failure mechanisms within the half-joint connection. Particular attention was devoted to the modeling of disturbed regions (D-regions) where geometric discontinuities create stress concentrations, employing constitutive models capable of capturing both the nonlinear behavior of concrete and the yielding of reinforcement. The analysis was conducted through incremental loading until failure, allowing for the identification of the ultimate shear resistance capacity accounting for stress redistribution and the exploitation of plastic reserve capacity.

The nonlinear finite element model developed in this research fully complies with the

regulatory provisions of NTC2018 (Section 4.1.1.3) and Eurocode 2 (Section 5.7) for nonlinear structural analysis. The analysis satisfies equilibrium and compatibility requirements through proper constraint implementation, appropriate element formulations, and realistic stress-strain relationships for both concrete and steel materials. The constitutive models implemented in ANSYS—including concrete cracking and crushing, and bilinear kinematic hardening for reinforcement—adequately represent material nonlinear behavior through progressive stiffness degradation and plastic yielding. The monotonic incremental loading procedure ensures consistent stress development and accurate identification of ultimate capacity, in accordance with code provisions that prescribe monotonic loading with constant action proportions.

A summary schematization of the obtained results is presented below, compared with reference standards including the currently enforced NTC2018 and the Circular of the Italian Ministry of Public Works Decree dated June 16, 1976, which represent the original design codes:

Table 6.1: Comparison of shear resistance: code provisions vs. nonlinear FEM model

Method/Standard	**Parameter**	**Value**
Italian Decree 16/06/1976	τ_{amm} (V_{Rd})	9 MPa (4500 kN)
NTC2018	V_{Rd}	1030.7 kN
Nonlinear FEM Model	V_{Rd}	1810 kN

where V_{Rd} in the Nonlinear FEM Model represents the shear resistance capacity obtained by integrating the shear stress distribution (τ) over the cross-sectional area of the analyzed section.

It can be noted that the shear resistance on the same section is notably different when considering different codes. This is due to the fundamental evolution of structural design philosophies: the method proposed in the 1960s and 1970s was based on allowable stress design with global safety factors, while contemporary standards (NTC 2018) adopt the Limit States Method with a probabilistic approach that separately considers the variability of actions and material resistance through partial safety factors. This transition represents a shift from an empirical-deterministic approach

to a scientific-probabilistic one, including more stringent criteria for durability and the possibility of using strut-and-tie models for shear verification.

The nonlinear FEM analysis performed with ANSYS, demonstrates that the actual shear resistance capacity significantly exceeds the value predicted by current code provisions. The resistance obtained from the local model ($V_{Rd} = 1810$ kN) is approximately 76% higher than the NTC2018 code-based verification ($V_{Rd} = 1030.7$ kN), effectively bridging the gap between historical design approaches and contemporary conservative assessments. This enhanced capacity is attributable to the exploitation of material plastic reserve capacity, the development of beneficial strut-and-tie mechanisms within the half-joint geometry, and more accurate representation of stress redistribution phenomena that cannot be captured by linear elastic code-based approaches.

To ensure conservative results and account for potential effects related to the reduced dimensions of the local model and imposed boundary conditions, the shear resistance was validated through a three-stage verification procedure: an analytical global model, an extended beam model analysis, and an alternative boundary condition model. In particular, a nonlinear finite element verification was performed using ANSYS on a 7-meter beam portion, modeling a more realistic structural configuration to investigate size effects and deep beam behavior. Additionally, a model with different boundary conditions was developed to examine support reaction compatibility and crack pattern development, with support reactions differing by only 2.2% between models. The extended 7-meter analysis revealed that the local model slightly overestimated the resistance by approximately 6%. Conservatively accounting for this reduction factor, the validated shear resistance capacity can be expressed as:

$$V_{Rd,validated} = 1701 \text{ kN} \tag{6.1}$$

Considering the design shear demand $V_{Ed} = 1584$ kN, the final safety factor can be calculated as:

$$SF = \frac{V_{Rd,validated}}{V_{Ed}} = \frac{1701}{1584} = 1.07 \tag{6.2}$$

which demonstrates adequate structural performance and confirms the reliability of the assessment methodology developed. The safety factor of approximately 1.05 satisfies the structural adequacy requirement under design loads, confirming that the half-joint connection possesses sufficient shear capacity. This verification substantiates the conclusion that the structure, despite exhibiting insufficient transverse reinforcement according to contemporary code-based assessments, maintains adequate safety margins when evaluated through advanced nonlinear analysis.

The comprehensive validation procedure, incorporating analytical verification through a simplified global LUSAS model, numerical analysis of an extended 7-meter beam portion in ANSYS, and verification through an alternative boundary condition model, substantiates the robustness of the nonlinear FEM approach and its capability to accurately predict the actual structural behavior of these critical elements. The convergence of results from these multiple modeling approaches reinforces confidence in the predicted shear capacity.

The results of this research have significant implications for infrastructure management and assessment strategies. The demonstrated adequacy of existing half-joint connections under design loads suggests that many bridges currently flagged for strengthening interventions based on conventional linear elastic code assessments may actually possess sufficient structural capacity. The initial prediction of structural deficiencies up to 35% indicated by code-based procedures is contradicted by the refined nonlinear analysis, which accounts for the actual material behavior and stress redistribution mechanisms. This finding could enable more cost-effective maintenance strategies, allowing prioritization of interventions based on actual structural deficiencies rather than overly conservative code-based predictions.

The advanced nonlinear modeling methodology developed in this thesis provides bridge owners and managers with a validated tool for refined structural assessment of existing infrastructure. The integration of strut-and-tie modeling principles within a sophisticated computational framework, with particular attention to disturbed regions (D-regions) where geometric discontinuities create stress concentrations, represents a significant advancement in the assessment of complex structural details. This approach can be extended to similar structural typologies characteristic of 1970s bridge construction, supporting evidence-based decision-making in the evaluation

and management of aging bridge networks. The nonlinear finite element methodology developed in this thesis satisfies all fundamental requirements established by both NTC2018 and Eurocode 2 for the application of nonlinear analysis to structural assessment. The implementation ensures equilibrium through proper formulation of boundary conditions representing the actual support configuration and load distribution experienced by the half-joint connection within the continuous beam system, guarantees compatibility through appropriate finite element discretization that captures the geometric discontinuities and stress concentrations characteristic of half-joint regions, employs constitutive models that adequately represent the nonlinear behavior of concrete and steel materials, including cracking, crushing, and plastic yielding phenomena, and verifies the capacity of critical sections to withstand the inelastic deformations resulting from ultimate limit state loading conditions.

In conclusion, this thesis demonstrates that advanced nonlinear finite element analysis, properly calibrated and validated through multiple verification approaches, represents a powerful tool for the realistic assessment of existing bridge structures. The methodology developed bridges the gap between conservative code-based approaches and actual structural behavior, enabling more informed and cost-effective infrastructure management decisions while maintaining appropriate safety levels for these critical transportation assets. The findings support the optimization of assessment procedures and the reduction of potentially unnecessary strengthening interventions, contributing to more sustainable and economically efficient management of Italy's aging highway bridge infrastructure.

6.2 Future Research

The findings of this research demonstrate the potential of advanced nonlinear finite element analysis for the assessment of existing prestressed Gerber beam bridges. However, several aspects warrant further investigation to enhance the methodology's applicability and reliability for practical engineering applications.

While the current study successfully validated the nonlinear modeling approach for a single critical half-joint connection from the Canosilla Viaduct, future research should extend this methodology to multiple case studies encompassing diverse geometric configurations, reinforcement layouts, and material properties characteristic of 1970s Italian highway infrastructure. By systematically analyzing a representative sample of existing structures, it would be possible to develop a parametric framework that identifies key variables governing the shear behavior of half-joint connections, including nib geometry, reinforcement configuration, prestressing cable layout, and concrete strength characteristics.

A full-scale modeling approach of the entire beam would be theoretically desirable to capture the complete structural response and interaction effects along the 30-meter span. However, this presents significant practical challenges in terms of computational feasibility. To adequately represent critical details such as the concrete cover of reinforcement bars, a mesh size of only a few centimeters would be required. Applying such a refined mesh to the entire beam length would result in an excessively large finite element model with prohibitive computational demands. An alternative approach that could mitigate this issue involves the use of embedded reinforcement elements, where steel bars are incorporated directly into concrete solid elements without requiring mesh refinement at the reinforcement locations. This technique would allow for a more appropriate mesh size while maintaining adequate representation of reinforcement effects, potentially enabling full-scale analyses with manageable computational resources.

Furthermore, the accuracy and reliability of future analyses would benefit significantly from enhanced material constitutive models calibrated against experimental data obtained from laboratory testing of actual bridge specimens. Dedicated experimental programs involving extraction and testing of concrete cores and reinforce-

ment bars from existing structures would provide accurate stress-strain relationships including post-peak softening behavior for concrete and actual yield strength and strain-hardening characteristics for aged steel materials.

Finally, the current modeling approach assumes perfect bond between concrete and reinforcement steel, which, while commonly adopted and adequate for preliminary assessments, neglects important phenomena that can significantly influence actual structural behavior. Future research should incorporate nonlinear bond-slip constitutive relationships through interface elements or cohesive zone models at the reinforcement-concrete interface, enabling simulation of progressive bond degradation and potential slip between materials under increasing load levels.The implementation of such refined models, validated through comparison with experimental test results on full-scale or large-scale specimens, would provide a more comprehensive understanding of actual load-carrying mechanisms and failure modes, supporting more informed decisions regarding the necessity and extent of strengthening interventions for existing bridge infrastructure.

Bibliography

[1] F. Bencardino and A. Cascardi. Revitalizing an existing reinforced concrete bridge: Deficiencies, repair techniques and the role of frps. *Procedia Structural Integrity*, 62:972–982, 2024.

[2] E. Menduni. *L'Autostrada Del Sole: Identità italiana*. Il Mulino, 1999.

[3] M. di Prisco. Critical infrastructures in italy: State of the art, case studies, rational approaches to select the intervention priorities.

[4] G. Santarsiero, A. Masi, V. Picciano, and A. Musano. Preliminary assessment of pre-1980 girder bridges in the framework of the italian guidelines. *Procedia Structural Integrity*, 62:121–128, 2021.

[5] R. Asso, M. Domaneschi, G. C. Marano, F. Palmisano, and G. Palombella. Behavior of half-joints: Design and simulation of laboratory tests. *Infrastructures*, 7(12):160, 2022.

[6] P. Desnerck. Strut-and-tie models for deteriorated reinforced concrete half-joints, 2018.

[7] J. Mathivat. *The Cantilever Construction of Prestressed Concrete Bridges*. J. Wiley, 1983.

[8] Z. Šauman. Carbonization of porous concrete and its main binding components. *Cement and Concrete Research*, 1(6):645–662, 1971.

[9] M. Domaneschi, C. Pellecchia, E. De Iuliis, G. P. Cimellaro, M. Morgese, A. A. Khalil, and F. Ansari. Collapse analysis of the polcevera viaduct by the applied element method. *Engineering Structures*, 214:110659, 2020.

[10] Ministero delle Infrastrutture e dei Trasporti, Consiglio Superiore dei Lavori Pubblici. Linee guida per la classificazione e gestione del rischio, la valutazione della sicurezza ed il monitoraggio dei ponti esistenti, aprile 2020. Allegate al parere del Consiglio Superiore dei Lavori Pubblici n.88/2019, espresso in modalità "agile" a distanza dall'Assemblea Generale in data 17.04.2020.

[11] Associazione Mondiale della Strada - AIPCR, Comitato Nazionale Italiano. Linee guida per la revisione ed integrazione delle normative sulla manutenzione e gestione dei "ponti stradali", 2024. XXIV Convegno Nazionale Stradale, Comitato C 11 "Ponti Stradali". Proposta legislativa di revisione della Circolare Min. LL.PP. N. 6736 del 19.07.1967. Presidente: Ing. Carlo Strassi; Vice Presidente: Ing. Mariano Romagnolo.

[12] J. Schlaich, K. Schafer, and M. Jennewein. Toward a consistent design of structural concrete. *PCI Journal*, 32(3):74–150, 1987.

[13] Franco Angotti and Maurizio Orlando. *Progetto delle strutture in calcestruzzo armato: Con l'Eurocodice 2 e le Norme Tecniche per le Costruzioni 2018*. HOEPLI EDITORE, 2018.

[14] M. de Saint-Venant. L'académie.

[15] Consorzio FABRE. Ispezioni speciali su selle gerber di ponti esistenti in c.a. e c.a.p. ai sensi delle linee guida: la conoscenza e la verifica locale, marzo 2022. Presidente del Consorzio: Walter Salvatore; Direttore Tecnico: Andrea Dall'Asta.

[16] A. Muttoni, M. Fernández Ruiz, and F. Niketić. Design versus assessment of concrete structures using stress fields and strut-and-tie models. *ACI Structural Journal*, 112(5), 2015.

[17] Wikipedia contributors. Autostrada a15 (italia), 2025. Accesso: 22 agosto 2025.

[18] Federal Highway Administration. Lightweight concrete. `https://www.fhwa.dot.gov/publications/research/articles/lightweight_concrete.cfm`. Accessed: November 18, 2025.

Appendix A

ANSYS Mechanical APDL Element Reference: SOLID65

Source: ANSYS Mechanical APDL Element Reference, pages 283-292,
Release 14.0,
November 2011.

SOLID65

3-D Reinforced Concrete Solid

MP ME ST <> <> <> <> <> <> <> <> PP <> EME MFS
Product Restrictions

SOLID65 Element Description

SOLID65 is used for the 3-D modeling of solids with or without reinforcing bars (rebar). The solid is capable of cracking in tension and crushing in compression. In concrete applications, for example, the solid capability of the element may be used to model the concrete while the rebar capability is available for modeling reinforcement behavior. Other cases for which the element is also applicable would be reinforced composites (such as fiberglass), and geological materials (such as rock). The element is defined by eight nodes having three degrees of freedom at each node: translations in the nodal x, y, and z directions. Up to three different rebar specifications may be defined.

The concrete element is similar to a 3-D structural solid but with the addition of special cracking and crushing capabilities. The most important aspect of this element is the treatment of nonlinear material properties. The concrete is capable of cracking (in three orthogonal directions), crushing, plastic deformation, and creep. The rebar are capable of tension and compression, but not shear. They are also capable of plastic deformation and creep. See SOLID65 in the *Mechanical APDL Theory Reference* for more details about this element.

Figure 1 SOLID65 Geometry

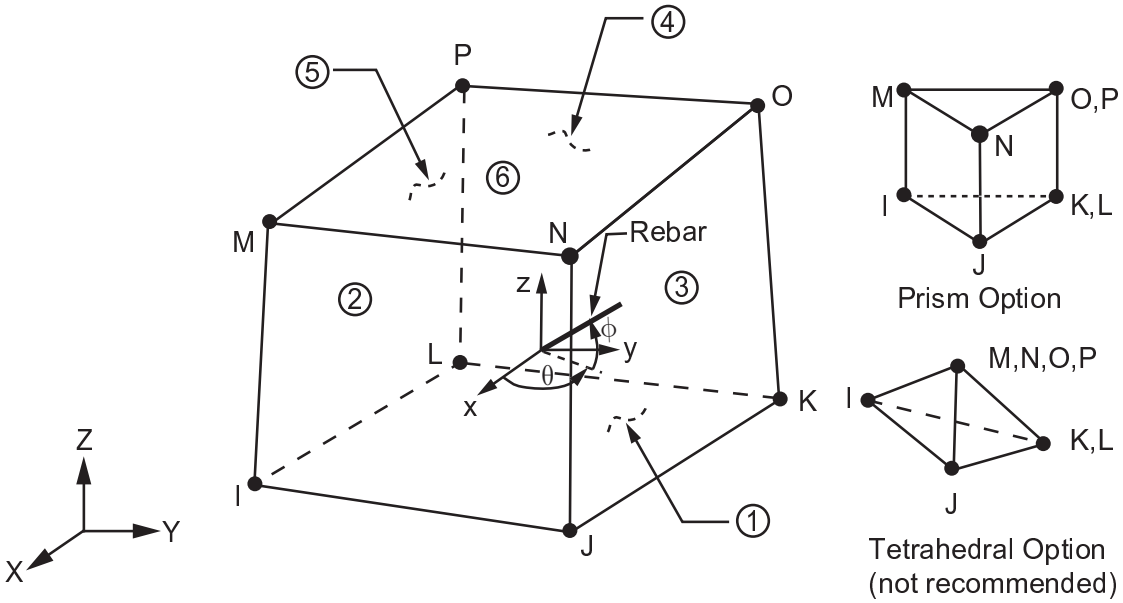

SOLID65 Input Data

The geometry, node locations, and the coordinate system for this element are shown in *Figure 1* (p. 283). The element is defined by eight nodes and the isotropic material properties. The element has one solid material and up to three rebar materials. Use the **MAT** command to input the concrete material properties. Rebar specifications, which are input as real constants, include the material number (MAT), the

volume ratio (VR), and the orientation angles (THETA, PHI). The rebar orientations can be graphically verified with the **/ESHAPE** command.

The volume ratio is defined as the rebar volume divided by the total element volume. The orientation is defined by two angles (in degrees) from the element coordinate system. The element coordinate system orientation is as described in *Coordinate Systems* (p. 56). A rebar material number of zero or equal to the element material number removes that rebar capability.

Additional concrete material data, such as the shear transfer coefficients, tensile stresses, and compressive stresses are input in the data table, for convenience, as described in *Table 1: SOLID65 Concrete Material Data* (p. 287). Typical shear transfer coefficients range from 0.0 to 1.0, with 0.0 representing a smooth crack (complete loss of shear transfer) and 1.0 representing a rough crack (no loss of shear transfer). This specification may be made for both the closed and open crack. When the element is cracked or crushed, a small amount of stiffness is added to the element for numerical stability. The stiffness multiplier CSTIF is used across a cracked face or for a crushed element, and defaults to 1.0E-6.

Element loads are described in *Nodal Loading* (p. 49). Pressures may be input as surface loads on the element faces as shown by the circled numbers on *Figure 1* (p. 283). Positive pressures act into the element. Temperatures and fluences may be input as element body loads at the nodes. The node I temperature T(I) defaults to TUNIF. If all other temperatures are unspecified, they default to T(I). For any other input pattern, unspecified temperatures default to TUNIF. Similar defaults occurs for fluence except that zero is used instead of TUNIF.

Use the **BETAD** command to specify the global value of damping. If **MP**,BETD is defined for the material number of the element (assigned with the **MAT** command), it is summed with the value from the **BETAD** command. Similarly, use the **TREF** command to supply the global value of reference temperature. If **MP**,REFT is defined for the material number of the element, it is used for the element instead of the value from the **TREF** command. But if **MP**,REFT is defined for the material number of the rebar, it is used instead of either the global or element value.

KEYOPT(1) is used to include or suppress the extra displacement shapes. KEYOPT(5) and KEYOPT(6) provide various element printout options (see *Element Solution* (p. 51)).

The stress relaxation associated with KEYOPT(7) = 1 is used only to help accelerate convergence of the calculations when cracking is imminent. (A multiplier for the amount of tensile stress relaxation can be input as constant C9 in the data table; see *Table 1: SOLID65 Concrete Material Data* (p. 287)) The relaxation does not represent a revised stress-strain relationship for post-cracking behavior. After the solution converges to the cracked state, the modulus normal to the crack face is set to zero. Thus, the stiffness is zero normal to the crack face. See the *Mechanical APDL Theory Reference* for details.

The program warns when each unreinforced element crushes at all integration points. If this warning is unwanted, it can be suppressed with KEYOPT(8) = 1.

If solution convergence is a problem, it is recommended to set KEYOPT(3) = 2 and apply the load in very small load increments.

You can include the effects of pressure load stiffness in a geometric nonlinear analysis using **SOLCONTROL**,,,INCP. Pressure load stiffness effects are included in linear eigenvalue buckling automatically. If an unsymmetric matrix is needed for pressure load stiffness effects, use **NROPT**,UNSYM.

A summary of the element input is given in *"SOLID65 Input Summary"* (p. 285). A general description of element input is given in *Element Input* (p. 43).

SOLID65 Input Summary

Nodes

I, J, K, L, M, N, O, P

Degrees of Freedom

UX, UY, UZ

Real Constants

MAT1, VR1, THETA1, PHI1, MAT2, VR2,
THETA2, PHI2, MAT3, VR3, THETA3, PHI3, CSTIF

(where MAT*n* is material number, VR*n* is volume ratio, and THETA*n* and PHI*n* are orientation angles for up to 3 rebar materials)

Material Properties

EX, ALPX (or CTEX *or* THSX), PRXY or NUXY, DENS (for concrete)
EX, ALPX (or CTEX *or* THSX), DENS (for each rebar), ALPD
Specify BETD only once for the element (use **MAT** command to assign material property set). REFT may be supplied once for the element, or may be assigned on a per rebar basis. See the discussion in *"SOLID65 Input Data"* (p. 283) for more details.

Surface Loads

Pressures --

face 1 (J-I-L-K), face 2 (I-J-N-M), face 3 (J-K-O-N),
face 4 (K-L-P-O), face 5 (L-I-M-P), face 6 (M-N-O-P)

Body Loads

Temperatures --

T(I), T(J), T(K), T(L), T(M), T(N), T(O), T(P)

Fluences --

FL(I), FL(J), FL(K), FL(L), FL(M), FL(N), FL(O), FL(P)

Special Features

Adaptive descent
Birth and death
Concrete
Cracking
Creep
Crushing
Elasticity
Large deflection
Large strain
Plasticity
Stress stiffening
Swelling
User-defined material

KEYOPT(1)

Extra displacement shapes:

0 --
Include extra displacement shapes

1 --
Suppress extra displacement shapes

KEYOPT(3)
Behavior of totally crushed unreinforced elements:

0 --
Base

1 --
Suppress mass and applied loads, and warning message (see KEYOPT(8))

2 --
Features of 1 and apply consistent Newton-Raphson load vector.

KEYOPT(5)
Concrete linear solution output:

0 --
Print concrete linear solution only at centroid

1 --
Repeat solution at each integration point

2 --
Nodal stress printout

KEYOPT(6)
Concrete nonlinear solution output:

0 --
Print concrete nonlinear solution only at centroid

3 --
Print solution also at each integration point

KEYOPT(7)
Stress relaxation after cracking:

0 --
No tensile stress relaxation after cracking

1 --
Include tensile stress relaxation after cracking to help convergence

KEYOPT(8)
Warning message for totally crushed unreinforced element:

0 --
Print the warning

1 --
Suppress the warning

SOLID65 Concrete Information

The data listed in *Table 1: SOLID65 Concrete Material Data* (p. 287) is entered in the data table with the **TB** commands. Data not input are assumed to be zero, except for defaults described below. The constant table is started by using the **TB**command (with *Lab* = CONCR). Up to eight constants may be defined

with the **TBDATA** commands following a temperature definition on the **TBTEMP** command. Up to six temperatures (*NTEMP* = 6 maximum on the **TB** command) may be defined with the **TBTEMP** commands. The constants (C1-C9) entered on the **TBDATA** commands (6 per command), after each **TBTEMP** command, are:

Table 1 SOLID65 Concrete Material Data

Constant	Meaning
1	Shear transfer coefficients for an open crack.
2	Shear transfer coefficients for a closed crack.
3	Uniaxial tensile cracking stress.
4	Uniaxial crushing stress (positive).
5	Biaxial crushing stress (positive).
6	Ambient hydrostatic stress state for use with constants 7 and 8.
7	Biaxial crushing stress (positive) under the ambient hydrostatic stress state (constant 6).
8	Uniaxial crushing stress (positive) under the ambient hydrostatic stress state (constant 6).
9	Stiffness multiplier for cracked tensile condition, used if KEYOPT(7) = 1 (defaults to 0.6).

Absence of the data table removes the cracking and crushing capability. A value of -1 for constant 3 or 4 also removes the cracking or crushing capability, respectively. If constants 1-4 are input and constants 5-8 are omitted, the latter constants default as discussed in the *Mechanical APDL Theory Reference*. If any one of Constants 5-8 are input, there are no defaults and all 8 constants must be input.

SOLID65 Output Data

The solution output associated with the element is in two forms:

- Nodal displacements included in the overall nodal solution
- Additional element output as shown in *Table 2: SOLID65 Element Output Definitions* (p. 288)

Several items are illustrated in *Figure 2* (p. 288). The element stress directions are parallel to the element coordinate system. Nonlinear material printout appears only if nonlinear properties are specified. Rebar printout appears only for the rebar defined. If cracking or crushing is possible, printout for the concrete is also at the integration points, since cracking or crushing may occur at any integration point. The **PLCRACK** command can be used in POST1 to display the status of the integration points. A general description of solution output is given in *Solution Output* (p. 50). See the *Basic Analysis Guide* for ways to view results.

Figure 2 SOLID65 Stress Output

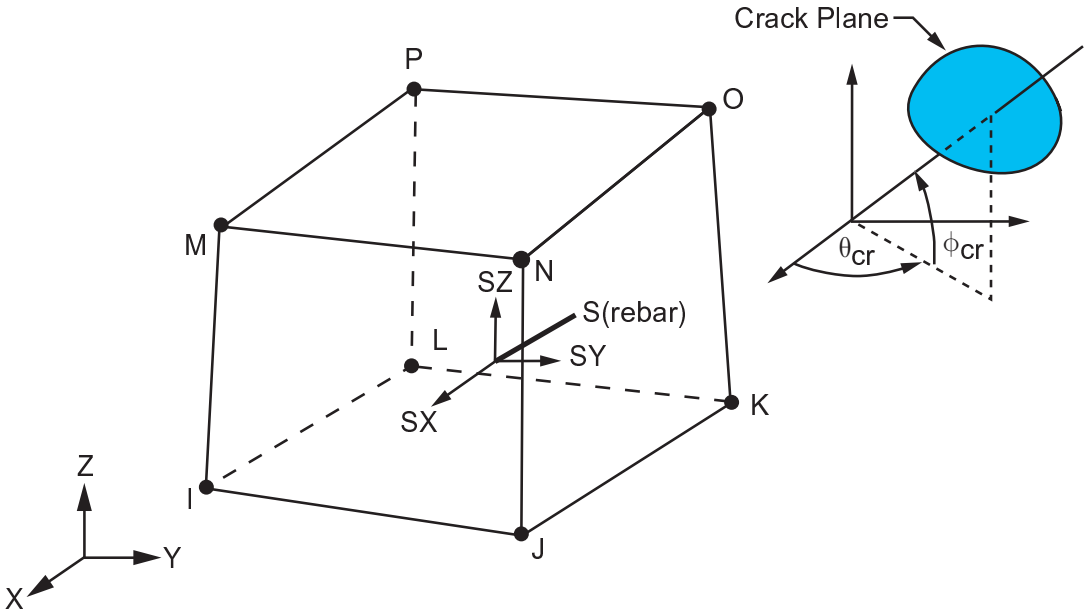

The Element Output Definitions table uses the following notation:

A colon (:) in the Name column indicates that the item can be accessed by the Component Name method (**ETABLE**, **ESOL**). The O column indicates the availability of the items in the file `Jobname.OUT`. The R column indicates the availability of the items in the results file.

In either the O or R columns, "Y" indicates that the item is *always* available, a number refers to a table footnote that describes when the item is *conditionally* available, and "-" indicates that the item is *not* available.

Table 2 SOLID65 Element Output Definitions

Name	Definition	O	R
EL	Element number	Y	Y
NODES	Nodes - I, J, K, L, M, N, O, P	Y	Y
MAT	Material number	Y	Y
NREINF	Number of rebar	Y	-
VOLU:	Volume	Y	Y
PRES	Pressures P1 at nodes J, I, L, K; P2 at I, J, N, M; P3 at J, K, O, N; P4 at K, L, P, O; P5 at L, I, M, P; P6 at M, N, O, P	Y	Y
TEMP	Temperatures T(I), T(J), T(K), T(L), T(M), T(N), T(O), T(P)	Y	Y
FLUEN	Fluences FL(I), FL(J), FL(K), FL(L), FL(M), FL(N), FL(O), FL(P)	Y	Y
XC, YC, ZC	Location where results are reported	Y	*6*
S:X, Y, Z, XY, YZ, XZ	Stresses	*1*	*1*
S:1, 2, 3	Principal stresses	*1*	*1*

Name	Definition	O	R
S:INT	Stress intensity	1	1
S:EQV	Equivalent stress	1	1
EPEL:X, Y, Z, XY, YZ, XZ	Elastic strains	1	1
EPEL:1, 2, 3	Principal elastic strains	1	-
EPEL:EQV	Equivalent elastic strains [7]	1	1
EPTH:X, Y, Z, XY, YZ, XZ	Average thermal strains	1	1
EPTH:EQV	Equivalent thermal strains [7]	1	1
EPPL:X, Y, Z, XY, YZ, XZ	Average plastic strains	4	4
EPPL:EQV	Equivalent plastic strains [7]	4	4
EPCR:X, Y, Z, XY, YZ, XZ	Average creep strains	4	4
EPCR:EQV	Equivalent creep strains [7]	4	4
NL:EPEQ	Average equivalent plastic strain	4	4
NL:SRAT	Ratio of trial stress to stress on yield surface	4	4
NL:SEPL	Average equivalent stress from stress-strain curve	4	4
NL:HPRES	Hydrostatic pressure	-	4
THETCR, PHICR	THETA and PHI angle orientations of the normal to the crack plane	1	1
STATUS	Element status	2	2
IRF	Rebar number	3	-
MAT	Material number	3	-
VR	Volume ratio	3	-
THETA	Angle of orientation in X-Y plane	3	-
PHI	Angle of orientation out of X-Y plane	3	-
EPEL	Uniaxial elastic strain	3	-
S	Uniaxial stress	3	-
EPEL	Average uniaxial elastic strain	5	5
EPPL	Average uniaxial plastic strain	5	5
SEPL	Average equivalent stress from stress-strain curve	5	5
EPCR	Average uniaxial creep strain	5	5

1. Concrete solution item (output for each integration point (if KEYOPT(5) = 1) and the centroid)
2. The element status table (*Table 4: SOLID65 Element Status Table* (p. 290)) uses the following terms:
   - Crushed - solid is crushed.
   - Open - solid is cracked and the crack is open.
   - Closed - solid is cracked but the crack is closed.

- Neither - solid is neither crushed nor cracked.

3. Rebar solution item repeats for each rebar
4. Concrete nonlinear integration point solution (if KEYOPT(6) = 3 and the element has a nonlinear material)
5. Rebar nonlinear integration point solution (if KEYOPT(6) = 3 and the rebar has a nonlinear material)
6. Available only at centroid as a ***GET** item.
7. The equivalent strains use an effective Poisson's ratio: for elastic and thermal this value is set by the user (**MP**,PRXY); for plastic and creep this value is set at 0.5.

Table 3 SOLID65 Miscellaneous Element Output

Description	Names of Items Output	O	R
Nodal Stress Solution	TEMP, S(X, Y, Z, XY, YZ, XZ), SINT, SEQV	*1*	-

1. Output at each node, if KEYOPT(5) = 2

Table 4 SOLID65 Element Status Table

Status	Status in Direction 1	Status in Direction 2	Status in Direction 3
1	Crushed	Crushed	Crushed
2	Open	Neither	Neither
3	Closed	Neither	Neither
4	Open	Open	Neither
5	Open	Open	Open
6	Closed	Open	Open
7	Closed	Open	Neither
8	Open	Closed	Open
9	Closed	Closed	Open
10	Open	Closed	Neither
11	Open	Open	Closed
12	Closed	Open	Closed
13	Closed	Closed	Neither
14	Open	Closed	Closed
15	Closed	Closed	Closed
16	Neither	Neither	Neither

Table 5: SOLID65 Item and Sequence Numbers (p. 291) lists output available through the **ETABLE** command using the Sequence Number method. See The General Postprocessor (POST1) in the *Basic Analysis Guide* and *The Item and Sequence Number Table* (p. 52) in this manual for more information. The following notation is used in *Table 5: SOLID65 Item and Sequence Numbers* (p. 291):

Name
output quantity as defined in the *Table 2: SOLID65 Element Output Definitions* (p. 288)

Item
predetermined Item label for **ETABLE** command

I,J,...,P
sequence number for data at nodes I,J,...,P

IP
sequence number for Integration Point solution items

Table 5 SOLID65 Item and Sequence Numbers

Output Quantity Name	ETABLE and ESOL Command Input			
	Item	Rebar 1	Rebar 2	Rebar 3
EPEL	SMISC	1	3	5
SIG	SMISC	2	4	6
EPPL	NMISC	41	45	49
EPCR	NMISC	42	46	50
SEPL	NMISC	43	47	51
SRAT	NMISC	44	48	52

Output Quantity Name	ETABLE and ESOL Command Input								
	Item	I	J	K	L	M	N	O	P
P1	SMISC	8	7	10	9	-	-	-	-
P2	SMISC	11	12	-	-	14	13	-	-
P3	SMISC	-	15	16	-	-	18	17	-
P4	SMISC	-	-	19	20	-	-	22	21
P5	SMISC	24	-	-	23	25	-	-	26
P6	SMISC	-	-	-	-	27	28	29	30
S:1	NMISC	1	6	11	16	21	26	31	36
S:2	NMISC	2	7	12	17	22	27	32	37
S:3	NMISC	3	8	13	18	23	28	33	38
S:INT	NMISC	4	9	14	19	24	29	34	39
S:EQV	NMISC	5	10	15	20	25	30	35	40
FLUEN	NMISC	109	110	111	112	113	114	115	116

	Output Quantity Name	ETABLE and ESOL Command Input								
		Item	Integration Point							
			1	2	3	4	5	6	7	8
	STATUS	NMISC	53	60	67	74	81	88	95	102

	Output Quantity Name	ETABLE and ESOL Command Input								
		Item	Integration Point							
			1	2	3	4	5	6	7	8
Dir 1	THETCR	NMISC	54	61	68	75	82	89	96	103
	PHICR	NMISC	55	62	69	76	83	90	97	104
Dir 2	THETCR	NMISC	56	63	70	77	84	91	98	105
	PHICR	NMISC	57	64	71	78	85	92	99	106
Dir 3	THETCR	NMISC	58	65	72	79	86	93	100	107
	PHICR	NMISC	59	66	73	80	87	94	101	108

SOLID65 Assumptions and Restrictions

- Zero volume elements are not allowed.
- Elements may be numbered either as shown in *Figure 1* (p. 283) or may have the planes IJKL and MNOP interchanged. Also, the element may not be twisted such that the element has two separate volumes. This occurs most frequently when the elements are not numbered properly.
- All elements must have eight nodes.
- A prism-shaped element may be formed by defining duplicate K and L and duplicate O and P node numbers (see *Degenerated Shape Elements* (p. 39)). A tetrahedron shape is also available. The extra shapes are automatically deleted for tetrahedron elements.
- Whenever the rebar capability of the element is used, the rebar are assumed to be "smeared" throughout the element. The sum of the volume ratios for all rebar must not be greater than 1.0.
- The element is nonlinear and requires an iterative solution.
- When both cracking and crushing are used together, care must be taken to apply the load slowly to prevent possible fictitious crushing of the concrete before proper load transfer can occur through a closed crack. This usually happens when excessive cracking strains are coupled to the orthogonal uncracked directions through Poisson's effect. Also, at those integration points where crushing has occurred, the output plastic and creep strains are from the previous converged substep. Furthermore, when cracking has occurred, the elastic strain output includes the cracking strain. The lost shear resistance of cracked and/or crushed elements cannot be transferred to the rebar, which have no shear stiffness.
- The following two options are not recommended if cracking or crushing nonlinearities are present:
  - Stress-stiffening effects.
  - Large strain and large deflection. Results may not converge or may be incorrect, especially if significantly large rotation is involved.

SOLID65 Product Restrictions

There are no product-specific restrictions for this element.

Appendix B

ANSYS Mechanical APDL Element Reference: LINK180

Source: ANSYS Mechanical APDL Element Reference, pages 823-827,
Release 14.0,
November 2011.

LINK180

3-D Spar (or Truss)

MP ME ST PR PRN <> <> <> <> <> <> PP VT EME MFS
Product Restrictions

LINK180 Element Description

LINK180 is a 3-D spar that is useful in a variety of engineering applications. The element can be used to model trusses, sagging cables, links, springs, and so on. The element is a uniaxial tension-compression element with three degrees of freedom at each node: translations in the nodal x, y, and z directions. Tension-only (cable) and compression-only (gap) options are supported. As in a pin-jointed structure, no bending of the element is considered. Plasticity, creep, rotation, large deflection, and large strain capabilities are included.

By default, LINK180 includes stress-stiffness terms in any analysis that includes large-deflection effects. Elasticity, isotropic hardening plasticity, kinematic hardening plasticity, Hill anisotropic plasticity, Chaboche nonlinear hardening plasticity, and creep are supported. To simulate the tension-/compression-only options, a nonlinear iterative solution approach is necessary; therefore, large-deflection effects must be activated (**NLGEOM**,ON) prior to the solution phase of the analysis.

See LINK180 in the *Mechanical APDL Theory Reference* for more details about this element.

Figure 1 LINK180 Geometry

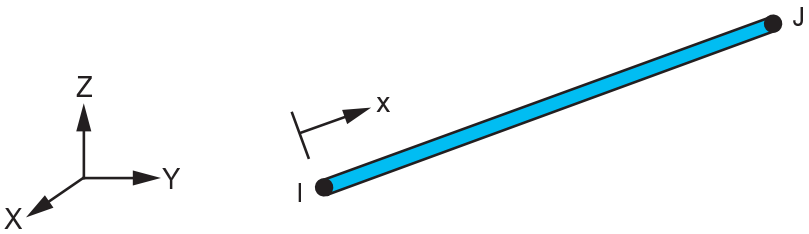

LINK180 Input Data

The geometry, node locations, and the coordinate system for this element are shown in *Figure 1* (p. 823). The element is defined by two nodes, the cross-sectional area (AREA), added mass per unit length (ADDMAS), and the material properties. The element X-axis is oriented along the length of the element from node I toward node J.

Element loads are described in *Nodal Loading* (p. 49). Temperatures may be input as element body loads at the nodes. The node I temperature T(I) defaults to TUNIF. The node J temperature T(J) defaults to T(I).

LINK180 allows a change in cross-sectional area as a function of axial elongation. By default, the cross-sectional area changes such that the volume of the element is preserved, even after deformation. The default is suitable for elastoplastic applications. By using KEYOPT(2), you may choose to keep the cross section constant or rigid.

LINK180 offers tension-only or compression-only options. You can specify the desired behavior via the third real constant. (See *"LINK180 Input Summary"* (p. 824) for details.) A nonlinear solution procedure is

necessary for these options; for more information, see the documentation for the **SOLCONTROL** command.

You can apply an initial stress state to this element via the **INISTATE** command. For more information, see "Initial State" in the *Basic Analysis Guide*.

The *"LINK180 Input Summary"* (p. 824) table summarizes the element input. *Element Input* (p. 43) gives a general description of element input.

LINK180 Input Summary

Nodes
I, J

Degrees of Freedom
UX, UY, UZ

Real Constants

AREA - Cross-sectional area
ADDMAS - Added mass (mass/length)
TENSKEY - Tension- or compression-only option:
0 -- Tension *and* compression (default)
1 -- Tension only
-1 -- Compression only

Material Properties
EX, (PRXY or NUXY), ALPX (or CTEX *or* THSX), DENS, GXY, ALPD, BETD

Surface Loads
None

Body Loads

Temperatures --
T(I), T(J)

Special Features

Birth and death
Initial state
Large deflection
Large strain
Linear perturbation
Nonlinear stabilization
Plasticity
Stress stiffening
User-defined material
Viscoelasticity
Viscoplasticity / Creep

KEYOPT(2)
Cross-section scaling (applies only if large-deflection effects [**NLGEOM**,ON] apply):

0 --
Enforce incompressibility; cross section is scaled as a function of axial stretch. (default).

1 --
Section is assumed to be rigid.

LINK180 Output Data

The solution output associated with the element is in two forms:

- Nodal displacements included in the overall nodal solution
- Additional element output as shown in *Table 1: LINK180 Element Output Definitions* (p. 825).

Several items are illustrated in *Figure 2* (p. 825). A general description of solution output is given in *Solution Output* (p. 50). Element results can be viewed in POST1 with **PRESOL**,ELEM. See the *Basic Analysis Guide* for details.

Figure 2 LINK180 Stress Output

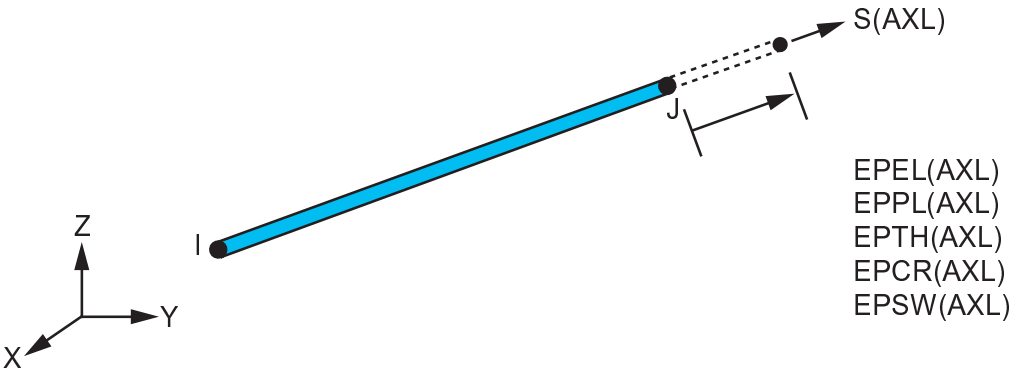

The Element Output Definitions table uses the following notation:

A colon (:) in the Name column indicates that the item can be accessed by the Component Name method (**ETABLE**, **ESOL**). The O column indicates the availability of the items in the file `Jobname.OUT`. The R column indicates the availability of the items in the results file.

In either the O or R columns, "Y" indicates that the item is *always* available, a number refers to a table footnote that describes when the item is *conditionally* available, and "-" indicates that the item is *not* available.

Table 1 LINK180 Element Output Definitions

Name	Definition	O	R
EL	Element number	Y	Y
NODES	Nodes - I, J	Y	Y
MAT	Material number	Y	Y
REAL	Real constant number	Y	Y
XC, YC, ZC	Center location	Y	*1*
TEMP	Temperatures T(I), T(J)	Y	Y
AREA	Cross-sectional area	Y	Y
FORCE	Member force in the element coordinate system	Y	Y

Name	Definition	O	R
Sxx	Axial stress	Y	Y
EPELxx	Axial elastic strain	Y	Y
EPTOxx	Total strain	Y	Y
EPEQ	Plastic equivalent strain	*2*	*2*
Cur.Yld.Flag	Current yield flag	*2*	*2*
Plwk	Plastic strain energy density	*2*	*2*
Pressure	Hydrostatic pressure	*2*	*2*
Creq	Creep equivalent strain	*2*	*2*
Crwk_Creep	Creep strain energy density	*2*	*2*
EPPLxx	Axial plastic strain	*2*	*2*
EPCRxx	Axial creep strain	*2*	*2*
EPTHxx	Axial thermal strain	*3*	*3*

1. Available only at the centroid as a ***GET** item.
2. Available only if the element has an appropriate nonlinear material.
3. Available only if the element temperatures differ from the reference temperature.

The element printout also includes 'INT, SEC PTS' (which are always '1, Y Z' where Y and Z both have values of 0.0). These values are printed to maintain formatting consistency with the output printouts of the BEAM188, BEAM189, PIPE288, and PIPE289 elements.

Table 2: LINK180 Item and Sequence Numbers (p. 826) lists output available through **ETABLE** using the Sequence Number method. See The General Postprocessor (POST1) in the *Basic Analysis Guide* and *The Item and Sequence Number Table* (p. 52) in this manual for more information. The following notation is used in *Table 2: LINK180 Item and Sequence Numbers* (p. 826):

Name
output quantity as defined in *Table 1: LINK180 Element Output Definitions* (p. 825)

Item
predetermined Item label for **ETABLE** and

ESOL

E
sequence number for single-valued or constant element data

I,J
sequence number for data at nodes I and J

Table 2 LINK180 Item and Sequence Numbers

Output Quantity Name	ETABLE and ESOL Command Input			
	Item	E	I	J
Sxx	LS	-	1	2

Output Quantity Name	ETABLE and ESOL Command Input			
	Item	E	I	J
EPELxx	LEPEL	-	1	2
EPTOxx	LEPTO	-	1	2
EPTHxx	LEPTH	-	1	2
EPPLxx	LEPPL	-	1	2
EPCRxx	LEPCR	-	1	2
FORCE	SMISC	1	-	-
AREA	SMISC	2	-	-
TEMP	LBFE	-	1	2

LINK180 Assumptions and Restrictions

- The spar element assumes a straight bar, axially loaded at its ends, and of uniform properties from end to end.
- The length of the spar must be greater than zero, so nodes I and J must not be coincident.
- The cross-sectional area must be greater than zero.
- The temperature is assumed to vary linearly along the length of the spar.
- The displacement shape function implies a uniform stress in the spar.
- Stress stiffening is always included in geometrically nonlinear analyses (**NLGEOM**,ON). Prestress effects can be activated by the **PSTRES** command.
- To simulate the tension-/compression-only options, a nonlinear iterative solution approach is necessary.

LINK180 Product Restrictions

There are no product-specific restrictions for this element.